Modelling temperature dependence in the *Arabidopsis thaliana* circadian clock

Paula Andrea Avello Fernández

PhD

University of York

Mathematics

July 2019

To my grandmother Iris

Abstract

The circadian clock is the mechanism responsible for generating and controlling the biological rhythms that occur with 24 h periodicity in most living organisms. This clock allows organisms to anticipate the environmental variation caused by the rotation of the Earth such as the daily light and temperature cycles, providing them adaptive advantages. The circadian clock is a complex network of genes interacting with each other in regulatory processes which have been represented by mathematical models. In the plant *Arabidopsis thaliana*, the mechanisms by which light regulates the circadian clock have been widely modelled mathematically and implemented computationally permitting to explain experimental observations and to generate hypotheses, which have led experimental investigation. However, the role of temperature and the mechanisms of adaptation to temperature variation are poorly understood, and especially in the scenario of global climate change, modelling a temperature responsive plant clock is of increasing importance. Here we present a framework of temperature dependence for the *Arabidopsis* circadian clock by applying Arrhenius equations to the most predominant models for the plant system and we additionally propose three minimal models via random parameterisations to explore design principles underlying temperature compensation. By numerical investigation, we conclude that temperature compensation is especially sensitive to degradation processes, and that the combined effect of light and temperature favors the robustness of the clock. We also propose to analyse the plant clock as a whole system and under that perspective we suggest that context graph-theoretic approaches could be a powerful tool to uncover the design principles for temperature mechanisms.

Contents

List of Tables

List of Figures

Acknowledgements

First and foremost, I would like to express my deepest gratitude to my supervisor Dr Jonathan W Pitchford for his encouragement, for all his great advice, immense expertise, knowledge, criticism, assertiveness and invaluable support even when things were wrong. It would not be possible to learn so much and to improve in so many aspects without his supervision. He is the best supervisor that I could have imagined having. I am also deeply grateful to Professor Seth Davis for introducing me to this fantastic world of modelling circadian rhythms. The opportunity to join his Lab Group and presenting the progress of my research has been crucial in developing this thesis. His insightful suggestions, knowledge and support have been immensely helpful to grow up as a researcher.

I wish to show my sincere gratitude to the members of my Training Advisory Panel, Professor Martin Bees and Dr Marina Knight for all constructive criticism, advice, helpful guidance, and encouragement. A special thank goes to Professor Martin Bees for critically examining this thesis. His comments have helped indubitably to improve this work. I would also like to recognize the precious support that Professor Paul Bush provided me when I undertook this research topic.

I also wish to thank everyone at the Departments of Mathematics and Biology, they have been a wonderful community for research. I wish to thank Dr Stephen Connor for being my first point of contact in this PhD journey and for the opportunity to teach. To Professor Victoria Gould for supportive conversations. To Nicolas Page and to all support staff for their assistance during the whole period of my studies.

To all my PhD fellows in Mathematics for such good social meetings and weekly seminars. I would like to thank my officemate Wenfeng for support and long conversations. I also wish to thank all my officemates in the Department of Biology for many wonderful moments. I would like to extend this gratitude to all members of Davis Lab Group for helpful discussion and making me feel welcome, especially James, Kayla, Jack, and Manuela.

A special thank you to my housemates, Tom, Sky, Phil, Dean and Vidas for their friendship and unforgettable good times. A great thank goes to Helena Seget for the invaluable support and friendship since I arrived in the UK. A big thank you to all my friends that I made through these past years for making my stay in York such a unique and enjoyable experience: Ben, Carmen, Dina, Dora, Estelia, Joe, Kathy, Lilia, Marina, Miriam, Paulina, Verónica G. C., Verónica G. T. and more.

My sincere thanks also goes to Cristina Arancibia for her great support since I started to embark on this dream. My deep thanks to Dr Manuel Galea for encouraging me to

pursue PhD studies and for wonderful conversations with Natalia, Lorena and Carla. To Dr Soledad Torres for her great support throughout my career.

I wish acknowledge Henry Rice for meticulous proofreading. I also want to thank my officemates Josie and Eleanor for answering my continuous English language questions.

This work was funded by the CONICYT PFCHA/DOCTORADO BECAS CHILE/2013 72140562. I would like to acknowledge CONICYT for financial support.

Last but not least, I wish to thank my family for their unconditional love and support. To my parents for their care and being good examples of hard working people. To my brothers, Luis and Danny for their endless love and our stimulating discussions about science since we all started our various undergraduate studies; without their support this personal achievement would not have been possible.

Declaration

I declare that this thesis is a presentation of original work and I am the sole author under the supervision of Dr Jonathan W Pitchford, except where work which has formed part of a jointly-authored publication has been included. This work has not previously been presented for an award at this, or any other, University. All sources are acknowledged as References.

Chapter 2 has been published in a peer-reviewed journal. Details on the journal are: Avello, P.A., Davis, S.J., Ronald, J. and Pitchford, J.W., 2019. Heat the Clock: Entrainment and Compensation in Arabidopsis Circadian Rhythms. Journal of Circadian Rhythms, 17(1), p.5. DOI: http://doi.org/10.5334/jcr.179

The experimental results shown in chapter 3 were obtained and reproduced in the Figures 3.3, 3.4, 3.5, and 3.6 by the Davis Lab (Department of Biology, University of York). I acknowledge Prof Seth Davis for sharing this.

General Introduction

The circadian clock is a molecular system that generates and controls biological rhythms that occur in cycles of around 24 h. This system consists of genes interacting with each other to regulate their expression. External cues such as light and temperature interact with this system, therefore gene expression is also affected by environmental changes caused by the rotation of the earth [1]. The process by which the clock synchronizes with the external cycle is known as entrainment [2]. After entrainment, circadian rhythms are able to persist with a periodicity of 24 h in the absence of environmental cues, which is known as free-running conditions [3]. The clock is also able to face fluctuations in temperature, which means, biological rhythms are able to oscillate with a periodicity of approx. 24 h over the physiologically relevant range of temperatures, a mechanism known as temperature compensation [4].

The circadian clock is found in most living organisms, examples include bacteria, fungi, flies, plants and mammals [5, 6, 7, 8, 9] and its correct performance improves the health, fitness and well-being of the organisms [10, 11].

Circadian rhythms are the result of positive and negative feedback in a network of transcription factors, which regulate the mRNA and thus protein levels of each other. These complex systems have been modelled in diverse organisms [12, 13, 14] by mathematical approaches in order to understand the crucial factors driving the circadian oscillations, and to determine whether the structure of these clocks can determine functionality [15, 16]. While elucidation of the design principles behind the clock structure has been a major focus, there is also consideration of how far clock complexity reflects environmental variation [17].

In *Arabidopsis*, the use of mathematical modelling has its genesis in the ODE-based model presented by [18] in 2005 to characterise the interaction between *CIRCADIAN CLOCK ASSOCIATED 1 (CCA1)*, *LATE ELONGATED HYPOCOTYL (LHY)* and *TIMING OF CAB EXPRESSION 1 (TOC1)*. Because of their similarities, *CCA1* and *LHY* were considered as a single variable within the model so that the *Arabidopsis* clock was represented as a two-node negative loop between *CCA1/LHY* and *TOC1*. This work launched the recurrent use of mathematical modelling with experimental efforts to generate hypotheses, which have elucidated the structure and function of the plant circadian system [19]. In addition to the ODE-based approach, Boolean [20] and linear time invariante (LTI) [21, 22, 23] models have been used. However, the ODE-based approach remains the most widely used (see Chapter 4 for a description of the development of the predominant ODE-based models for *Arabidopsis*).

The rapid and invaluable progress in the understanding of the plant system, thanks to joint modelling-experimental efforts, has resulted in an increase in the complexity of the models (i.e. increased number of equations governing the system with a large number of parameters) and therefore a decrease in the computational tractability of their implementations. A recent model [24] proposes a compact characterization of the plant system with a reduced number of equations and parameters compared with prior models, granting a more tractable mathematical alternative for modifications and computational implementation. Published works based on extensions of this model include study of the effect of sucrose in the plant circadian system [25] and the work presented in Chapter 2 of this thesis [26].

Three recent mathematical approaches have been developed to enrich modelling techniques for the *Arabidopsis* circadian clock. The first addresses the optimization problem caused by the increased number of parameters present in the latest models for *Arabidopsis* [27]. This approach suggests applying the method of distributed delays in order to simplify existing models, thus yielding a reduced number of parameters to fit. The second is a minimal approach to investigate the potential role of functional structures found in other biological networks (called motifs), specifically in Arabidopsis [28]. Finally, a stochastic dynamical model for biochemical oscillators has been presented as an alternative to the traditional ODE-based approach, to model the inherent stochasticity of biological systems [29].

In *Arabidopsis*, mathematical models have focused mainly on characterizing the plant clock in response to light. However, while being an important stimuli, temperature has received less attention. This gap in the literature is necessary to fill because in the context of climate change, characterization of temperature in the plant model system is of increasing importance. Mathematical work on temperature dependence in circadian systems has used the Arrhenius equation to characterise temperature sensitivity of the rates of the circadian models [30, 31, 32, 33], and by choosing proper activation energy values to make a compensated model. However, little has been done to explore the design principles, which may explain temperature compensation. The aim of this thesis is therefore to address this gap in the literature and explore the design principles with the focus on temperature sensitivity.

Thesis structure

This thesis is organized in four chapters. Each chapter begins with an abstract summarizing its main contents. Each chapter has also an Introduction, which links the research to key background literature and which specifies the aims and objectives of the chapter.

For this reason, and to avoid repetition, this general introductory chapter for this thesis does not present details of models and methods where these are contained elsewhere in the thesis. Following the introduction, a Methods section in each chapter specifies the procedures by which the analyses were carried out. Next, the key findings of the analyses are shown in the Results section. Each chapter ends with a Discussion section, followed by Supplementary Material as appropriate. A general conclusion is given at the end of this thesis.

In Chapter 1, a numerical approach is outlined, with the aim of understanding temperature dependence in the *Arabidopsis* circadian clock within the context of a recent ODE-based model of the plant network by De Caluwé et al. (2016). We firstly explore the robustness of this model to incorporate other forms of light forcing functions, rather than being limited to the binary forcing used in the original model. We next incorporated temperature dependence into the system by applying Arrhenius equations to the translation rates of the model, and assessing the influence of temperature on the plant system by analysing its transient and periodic behaviour.

In Chapter 2, we extend the analysis of Chapter 1 by applying Arrhenius equations to all parameters of the De Caluwé et al. (2016) model in order to study which processes within the plant clock may drive compensation and entrainment. The combined effect of thermal and photic forcing in more realistic scenarios, including those motivated by possible future climate change, are also analysed.

In Chapter 3, we incorporate temperature dependence into a recent light-dependent model, to investigate the possible functions of the protein HSP90 in the plant circadian clock. To elucidate the role of HSP90 in entrainment, we simulate the effect of Geldanamycin, which is known as inhibitor of the function of HSP90. Moreover, we adapt the original model to exhibit *PRR9* and *PRR7* as functionally independent responses and compare the outputs of these revised models with experimental results generated by the Davis Lab (Department of Biology, University of York). Numerical investigations lead us to propose that HSP90 inhibits *CCA1/LHY* transcription, promotes *ELF4/LUX* translation, and inhibits the translation of *PRR9* and *PRR7*. Our numerical results support the hypothesis, suggested from experiments, that HSP90 influences the morning loop and is required for proper thermal entrainment but not for light entrainment.

In Chapter 4, we explore the more general design principles of the plant clock, using methods originally inspired by systems biology, by reviewing the most predominant models of *Arabidopsis* in order to discern regulatory patterns that may explain clock function and temperature compensation. We incorporate temperature dependence into several ODE-based models by applying Arrhenius equations to their translation rates. Additionally,

we propose three minimal models and explore what key features govern their function via a series of random parameterisations and simulations, to enrich the analysis. Results show that the highly repressive interactions between the components of the plant clock, together with autoregulation patterns and three-node feedback loops, tend to contribute to the function of the clock in general and to its robustness to variation in temperature in particular. However, the fact that the networks governing clock function vary with time, due to light and temperature forcing, reinforces the importance of studying the functionality of the plant clock as a dynamic entirety rather than as a set of discrete static motifs.

1 Incorporation of temperature and analysis of transient effects in the De Caluwé et al. 2016 model

Abstract

The circadian clock is a biological mechanism that permits living organisms to anticipate daily changes in environment such as light and temperature. This chronological system is made up of genes which interact together to generate biological rhythms of 24 hour periodicity. In the *Arabidopsis* circadian system these interactions play mostly a repressive role within the network, and forcing by light is considered an important ingredient to induce the expression of several clock genes. However, it is known that the plant circadian clock also responds to changes in temperature; knowledge of this phenomenon is especially important in the context of global food security and climate change. Complex mathematical models have been used to characterize the key features of the plant oscillator and its responses to changes in light. A recent model [24] offers a simple alternative to reproduce a wide range of behaviors in a variety of day-night cycles. This model maintains the simplicity of the earliest mathematical approaches, and incorporates recent structural findings regarding the plant circadian system. Here we extend the model of [24] to incorporate temperature dependent responses by applying Arrhenius equations to the parameters governing translation rates of the model. To assess the influence of temperature on the plant system, we analyse the model's transient behaviour. We also simulate several time scales for data collection in order to understand whether the timing of the experimental sampling affects the results. In addition, we further adapt the model to allow for more realistic smooth transitions between light and dark phases. This work is a starting point for more sophisticated implementations of temperature dependent circadian clocks with the ability to describe temperature dependence over a wider range of parameters, and to provide insights into the biological mechanisms involved in temperature-dependent behaviour.

1.1 Introduction

The circadian clock is made up of a complex network of genes which, interacting together, allow organisms to anticipate daily environmental variations, thereby contributing to their welfare. For example, the ability of the clock to track variation in light contributes to human health by preventing incidence of cancers [34]. In plants, it grants advantages in growth and development processes [35, 36], and in mice this clock intervenes in the aging process [37] and cardiovascular disease [38].

The circadian clock generates molecular rhythms, and these have been modelled using mathematical approaches so as to provide a better understanding of these rhythms. In *Arabidopsis*, the first mathematical model [18] was built to characterize the first feedback

loop identified from experiments [39]. This model [18] described a simple negative feedback between the morning genes *CIRCADIAN CLOCK ASSOCIATED 1* (*CCA1*) and *LATE ELONGATED HYPOCOTYL LHY*, and the evening gene *TIME OF CAB EXPRESSION 1* (*TOC1*). Explicitly, *TOC1* promoted *CCA1* and *LHY* expression, and reciprocally *CCA1* and *LHY* repressed *TOC1* expression. Because *CCA1* and *LHY* were found to have similar temporal dynamics, they were modelled as a single variable resulting in a plant model governed by a system of seven ordinary differential equations (ODEs) involving 29 parameters. Six ordinary differential equations (ODEs) formalized the evolution in time of mRNA levels, or protein levels in the cytoplasm or nucleus, and an additional equation formalized a light sensitive protein P via which light forcing was incorporated into the model to promote *CCA1/LHY* gene expression.

Motivated by the simple model of [18], subsequent interactive mathematical-experimental work discovered new clock components which further reformulated and refined the roles of genes and proteins within the plant network. As a result, mathematical models increased in complexity and their computational implementation became less tractable. For example, in the following year, [40] considered a clock model of 16 ODEs with 60 parameters, in 2012 [41] built a model of 28 ODEs with 107 parameters, and [42] in 2014 modelled 35 variables and 119 parameters for the plant system. This increased number of components and parameters was necessary because these models attempted a more quantitative fitting to experimental data and a more detailed description of molecular processes, and thereby providing useful insights on the underlying mechanisms regulated by light.

1.1.1 A compact model

A recent model [24] proposes a minimal approach to describe the mechanism of the plant oscillator. The model presents a reduced number of equations and parameters compared to the previous models, without excluding recent discoveries of the plant network structure, and it claims to capture the same features of the previous models by accounting for a more qualitative (rather than quantitative) fitting, providing a useful mathematical tool of easy implementation for numerical investigation of the plant system. The model consists of nine coupled ordinary differential equations (ODEs) describing changing protein and mRNA levels, with 34 parameters characterizing transcription, translation, and mRNA and protein degradation rates. This model, in common with previous clock models, combines similar genes into a single variable, admitting a total of four clock components that represent eight clock genes. These four components are: *CIRCADIAN CLOCK ASSOCIATED 1* and *LATE ELONGATED HYPOCOTYL* (*CCA1/LHY*), the *PSEUDO-RESPONSE REGULATOR* 7 and 9 genes *(PRR9/PRR7)*, the evening genes *EARLY FLOWERING* 4

and *LUX* (*ELF4/LUX*), and *PSEUDO-RESPONSE REGULATOR 5* with *TIMING OF CAB EXPRESSION 1*(*PRR5/TOC1*). For each clock component, mRNA and protein levels are modelled separately and are considered to be regulated by light. The effect of light is parametrized in a binary manner: light forcing variables L and D take values $L = 1$ and $D = 0$ in light phases, and $L = 0$ and $D = 1$ in darkness. In the *CCA1/LHY* and *PRR9/PRR7* components, the effect of light at the transcription level is characterised via a dark-accumulating protein P, which represents the proteins PHYTOCHROME INTERACTING FACTOR 3 (PIF3) and PHYTOCHROME INTERACTING FACTOR 3-LIKE 1 (PIL1). This protein P is also affected by light, resulting in a transient induction effect on the components regulated by interaction with this protein.

The interactions between the clock components in the model [24] are described by a network, where each edge represents transcription factors affecting the transcription rates of their target genes. For activation or inhibition effects, Hill functions are used to model the increase or decrease (respectively) in transcription rate (see Chapter 4 for details). Except regulation of *PRR9/PRR7* by *CCA1/LHY*, all interactions involve negative regulations. Figure 1.1, from Figure 1 of [24], depicts the structure of the network and shows how the modelled interactions result in a clock structure composed by several positive and negative feedbacks.

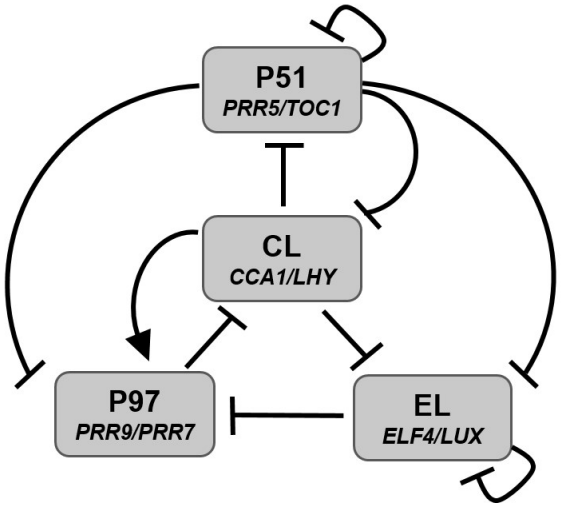

Figure 1.1: **Clock network model.** In the model [24], similar genes were merged into the single variables CL, P97, P51, and EL, which represent the pair of genes *CCA1/LHY*, *PRR9/PRR7*, *PRR5/TOC1*, and *ELF4/LUX*, respectively. The unique positive interaction of the model is depicted by an arrow, whereas blocked arrows represent negative interactions, i.e. inhibition of a component by a transcription factor.

In agreement with the formatting convention for *Arabidopsis* studies, gene names are written in italic and protein names in roman font. The nomenclature for the variables of the ODE system is preserved as it is in the original model of [24]. That is, variables are shown in square brackets and have an attached subscript m or p representing mRNA and protein concentrations, respectively. For example, $[CL]_m$ denotes mRNA levels of the variable CL, which itself represents *CCA1/LHY* genes, whereas $[CL]_p$ means protein levels of those corresponding genes.

The model is summarised by the following system of ODEs,

$$\frac{d[CL]_m}{dt} = (v_1 + v_{1L} * L * [P]) * \frac{1}{1 + (\frac{[P97]_p}{K_1})^2 + (\frac{[P51]_p}{K_2})^2} - (k_{1L} * L + k_{1D} * D) * [CL]_m$$

$$\frac{d[CL]_p}{dt} = (p_1 + p_{1L} * L) * [CL]_m - d_1 * [CL]_p$$

$$\frac{d[P97]_m}{dt} = (v_{2L} * L * [P] + v_{2A} + v_{2B} * \frac{[CL]_p^2}{K_3^2 + [CL]_p^2}) * \frac{1}{1 + (\frac{[P51]_p}{K_4})^2 + (\frac{[EL]_p}{K_5})^2} - k_2 * [P97]_m$$

$$\frac{d[P97]_p}{dt} = p_2 * [P97]_m - (d_{2D} * D + d_{2L} * L) * [P97]_p$$

$$\frac{d[P51]_m}{dt} = v_3 * \frac{1}{1 + (\frac{[CL]_p}{K_6})^2 + (\frac{[P51]_p}{K_7})^2} - k_3 * [P51]_m$$

$$\frac{d[P51]_p}{dt} = p_3 * [P51]_m - (d_{3D} * D + d_{3L} * L) * [P51]_p$$

$$\frac{d[EL]_m}{dt} = L * v_4 * \frac{1}{1 + (\frac{[CL]_p}{K_8})^2 + (\frac{[P51]_p}{K_9})^2 + (\frac{[EL]_p}{K_{10}})^2} - k_4 * [EL]_m$$

$$\frac{d[EL]_p}{dt} = p_4 * [EL]_m - (d_{4D} * D + d_{4L} * L) * [EL]_p$$

$$\frac{d[P]}{dt} = 0.3 * (1 - [P]) * D - [P] * L$$

The parameter values are those fitted to experimental observations in [24] for a qualitative dynamics matching, summarised in the following table.

Parameter description	Name	Value	Units
CL transcription	v_1	4.6	$\mathrm{nM.h^{-1}}$
CL light-induced transcription	v_{1L}	3.0	$\mathrm{nM.h^{-1}}$
P97 transcription	v_{2A}	1.3	$\mathrm{nM.h^{-1}}$
P97 CL-induced transcription	v_{2B}	1.5	$\mathrm{nM.h^{-1}}$
P97 light-induced transcription	v_{2L}	5.0	$\mathrm{nM.h^{-1}}$
P51 transcription	v_3	1.0	$\mathrm{nM.h^{-1}}$
EL transcription	v_4	1.5	$\mathrm{nM.h^{-1}}$
CL mRNA degradation (light)	k_{1L}	0.5	$\mathrm{h^{-1}}$
CL mRNA degradation (dark)	k_{1D}	0.2	$\mathrm{h^{-1}}$
P97 mRNA degradation	k_2	0.4	$\mathrm{h^{-1}}$
P51 mRNA degradation	k_3	0.6	$\mathrm{h^{-1}}$
EL mRNA degradation	k_4	0.6	$\mathrm{h^{-1}}$
CL translation	p_1	0.8	$\mathrm{h^{-1}}$
CL light light-induced translation	p_{1L}	0.4	$\mathrm{h^{-1}}$
P97 translation	p_2	1.0	$\mathrm{h^{-1}}$
P51 translation	p_3	0.6	$\mathrm{h^{-1}}$
EL translation	p_4	1.0	$\mathrm{h^{-1}}$
CL degradation	d_1	0.7	$\mathrm{h^{-1}}$
P97 degradation (dark)	d_{2D}	0.5	$\mathrm{h^{-1}}$
P97 degradation (light)	d_{2L}	0.3	$\mathrm{h^{-1}}$
P51 degradation (dark)	d_{3D}	0.5	$\mathrm{h^{-1}}$
P51 degradation (light)	d_{3L}	0.8	$\mathrm{h^{-1}}$
EL degradation (dark)	d_{4D}	1.2	$\mathrm{h^{-1}}$
EL degradation (light)	d_{4L}	0.4	$\mathrm{h^{-1}}$
Inhibition: CL by P97	K_1	0.2	nM
Inhibition: CL by P51	K_2	1.2	nM
Activation: P97 by CL	K_3	0.2	nM
Inhibition: P97 by P51	K_4	0.2	nM
Inhibition: P97 by EL	K_5	0.3	nM
Inhibition: P51 by CL	K_6	0.5	nM
Inhibition: P51 by itself	K_7	2.0	nM
Inhibition: EL by CL	K_8	0.4	nM
Inhibition: EL by P51	K_9	1.9	nM
Inhibition: EL by EL	K_{10}	1.9	nM

Table 1: Parameter values.

1.1.2 The Arrhenius approach for temperature dependence

Although light is an important stimulus, it is not the only signal regulating circadian rhythms; temperature is also an important stimulus to regulatory factor [43]. In *Arabidopsis*, there is evidence that a small difference of 4°C in temperature is able to reset the clock [44]. However, the effect of temperature is less well studied than that of light, and its incorporation within mathematical models is not fully developed.

Theoretical work on temperature dependence within the context of circadian rhythms, has mainly used the assumption that parameters of clock models can be described by the Arrhenius equation [45]. This equation describes a temperature dependent reaction rate via the concept of an activation energy, defined as the minimum amount of energy needed for a reaction to occur (see Figure 1.2).

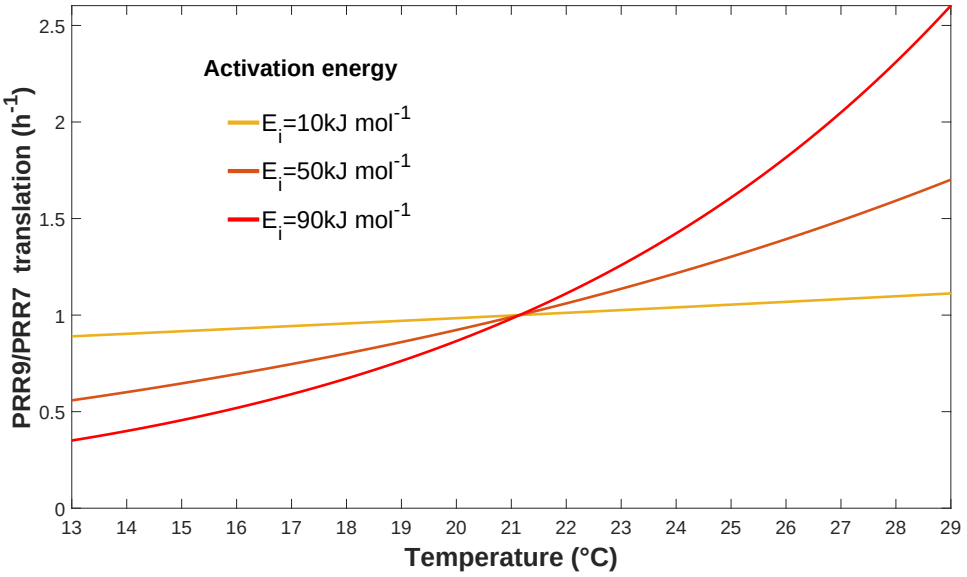

Figure 1.2: **The larger activation energy, the higher the dependence of the reaction rate on the temperature**. Modelled Arrhenius temperature dependence of translation rate of *PRR9/PRR7* for different activation energies.

Explicitly, for a given rate k_i, temperature dependence is characterised as follows,

$$k_i = A_i \exp\left(\frac{-E_i}{RT}\right), \tag{1}$$

where the parameters A_i and E_i are physical constants, respectively a rate constant and an activation energy for that particular reaction, and R is the universal gas constant (8.3145×10^{-3}kJ mol^{-1} K^{-1}) and T is temperature (in Kelvin).

A closely related concept to the notion of activation energy is the Q_{10} coefficient. Q_{10} is defined as the ratio of the reaction rates measured at two temperatures differing by 10°C [46]. This coefficient can also be calculated for an arbitrary range of temperatures by [47],

$$Q_{10} = \left(\frac{k_i^{T_2}}{k_i^{T_1}}\right)^{\frac{10^\circ}{T_2 - T_1}}, \quad T_2 > T_1, \tag{2}$$

where $k_i^{T_1}$ and $k_i^{T_2}$ represent rates of the process i at the temperatures T_1 and T_2, respectively.

Biochemical processes usually present reaction rates that double or triple in response to an increase in temperature of 10°C. This is quantified by equation 2 from which Q_{10} values between 2 and 3 are obtained. The Arrhenius equation allows us to predict a reaction rate with an observed Q_{10} value by the activation energy term E_i. Explicitly, an expression for activation energy can be determined from equation 1,

$$E_i = \frac{R \times \log\left(\frac{k_i^{T_2}}{k_i^{T_1}}\right)}{\frac{1}{T_1} - \frac{1}{T_2}}, \tag{3}$$

where the numerator in equation 3 is a function that depends on the ratio of reaction rates obtained at two temperatures, T_1 and T_2. Note that knowing the rate k_i of each reaction at a reference temperature allows us to invert equation 1 to calculate each A_i term at a variable temperature T according to,

$$A_i = k_i \exp\left(\frac{E_i}{RT}\right). \tag{4}$$

Based on the Arrhenius relationship, mathematical work has been elaborated mostly in the frame of the temperature compensation mechanism. Examples of organisms in which temperature effects have been modelled by this equation include *Neurospora* [32, 48], *Chlamydomonas* [49], and *Drosophila* [50]. In particular, temperature compensation is explicitly introduced into mathematical models by choosing suitable values for the parameters E_i [48]. The assumption involved in this is that temperature compensation is achieved by the trade off between reactions that lead to an increase in period and reactions that lead to a decrease in period as temperature rises [51], so that the period p of a circadian oscillator is invariant over a range of physiological temperatures (i.e. $\frac{dp}{dT} \approx 0$). The

mathematical expression for the change in period with respect to a change in temperature is given by [48],

$$\frac{dp}{dT} = \frac{p}{RT^2}\sum_{i=1}^{m} c_i E_i, \tag{5}$$

where the coefficients $c_i = \frac{d\log p}{d\log k_i}$ [32] determine whether a process contributes to increase or decrease the period of the system as temperature varies. These coefficients can be calculated numerically by solving the equations of a given clock model [52] for a small change in the parameter k_i while the other parameters remain fixed [32].

Note that the period p can therefore be expressed as a function of temperature through the rate constants k_i as $p = p(k_1(T), k_2(T), ..., k_m(T))$. Thus, equation 5 is easily deduced by applying the chain rule. Specifically, one obtains,

$$\frac{dp}{dT} = \sum_{i=1}^{m} \frac{dp}{dk_i}\frac{dk_i}{dT}. \tag{6}$$

If k_i in the term $\frac{dk_i}{dT}$ of equation 6 is substituted by equation 1, then

$$\frac{dp}{dT} = \sum_{i=1}^{m} \frac{dp}{dk_i}\frac{E_i}{RT^2}k_i. \tag{7}$$

Multiplying equation 7 by the factor $\frac{p}{p}$ (a convenient factor to rewrite the terms of the equation in form of derivatives of logarithmic functions), one finally has,

$$\frac{dp}{dT} = \frac{p}{RT^2}\sum_{i=1}^{m} \frac{d\log p}{d\log k_i}E_i. \tag{8}$$

Alternatively, equation 5 can be rewritten by the following expression [48],

$$\frac{d\ln p}{dT} = \frac{1}{RT^2}\sum_{i=1}^{m} c_i E_i, \tag{9}$$

therefore, by setting $\frac{1}{RT^2}\sum_{i=1}^{m} c_i E_i = 0$ and calculating the control coefficients c_i, we just need to find suitable E_i values that fulfill this condition in order to obtain a compensated model.

Although this approach for temperature compensation has been widely used, very little has been done regarding modelling the temperature entrainment mechanism. In [52], the authors incorporated temperature compensation into the Goodwin model, a generic oscillator proposed to model processes at molecular level in cells [53], and they showed that the modified model could be entrained by sinusoidal temperature cycles, yet, for a limited forcing period only. Activation energy values were allowed to vary on the range 0-150 kJ mol^{-1}. In [49], authors proposed a model for *Chlamydomonas*, where temperature compensation and entrainment by square and sinusoidal temperature waves were achieved

for activation energies ranging from 40 to 84 kJ mol^{-1}; however, entrainment also was subject to a limited forcing period. Unlike the results in [52], the model for *Chlamydomonas* in [49] required different activation energy values to be entrained than the needed to obtain compensation. In both models, the ability of entrainment was assessed by comparing the period of the external cycle with the period of the system.

In *Arabidopsis*, the use of the Arrhenius equation is less frequent, or is restricted to certain narrow cases. For example, [33] incorporated temperature dependence into [54] model by making light-dependent parameters sensitive to temperature. Activation energy values used ranging from 1.02 to 40.59 kJ mol^{-1}. They modified this model to be temperature compensated following [32] ideas, so that they could fit experimental data with the results supporting the hypothesis that light signalling is required for temperature compensation.

Unlike the [33] approach, in this thesis we looked for a more qualitative setting in order to understand the elemental principles behind temperature dependence in the plant circadian clock. Our goal is to determine what structural design is needed for clock function, allowing plants to adapt daily to temperature changes. Thus, as a starting point, in this chapter we evaluated the robustness of the model [24], firstly by modifying the model to allow smoother transitions between light and dark phases, and secondly incorporating a temperature response by applying the Arrhenius equation into the parameters of the model's translation rates. We then explored whether this simple change, namely including the influence of temperature, is sufficient to entrain rhythmic dynamics. Different entrainment regimes were simulated to analyse the role of transient behaviour, with relevence both to future modelling studies and to the interpretation of experimental data. Finally, we studied the rhythmicity of the clock across several simulated time scales for insights on the effect of the sampling frequency in experimental results.

1.2 Methods

1.2.1 The model

The mathematical model under investigation is that introduced in [24], a highly interconnected model with multiple light input, which has been showed to be effective in modelling the light entrainment of the plant clock [55] (see Introduction section for details).

1.2.2 Adapting the model for changes in light

In the model [24], environmental light conditions are considered as binary phases so that light-dark cycles are modelled unrealistically as square waves. Therefore we adapted the

model to allow for continuous changes in light levels. Explicitly, we considered two descriptions of continuously varying illumination; a simple sinusoidal function, and a function using a tanh function to smooth transitions between light and dark as advocated in [41, 54]. The equation for tanh forcing is defined by

$$\begin{aligned} L(t)_{tanh} = 0.5 * ((1 + \tanh((t - per * floor(t/per) - dawn)/Tw)) \\ - (1 + \tanh((t - per * floor(t/per) - dusk)/Tw)) \\ + (1 + \tanh((t - per * floor(t/per) - per)/Tw))), \end{aligned} \quad (10)$$

where Tw is the parameter of "twilight" duration, that is, the time taken by the system to transit between light and dark phases; *dawn* and *dusk* are phase parameters with values $dawn = 0$ and $dusk = per/2$ for a 24 h cycle (i.e. *per*, the period, is equal to 24); tanh is the typical hyperbolic tangent function, and floor is a function of rounding operation.

The equation for *sin* forcing is given by,

$$L(t)_{sin} = A \sin\left(2\pi\left(\frac{1}{p}\right)t\right) + 0.5, \quad (11)$$

where A is the amplitude set to be equal to 0.5, and p is the period (in hours).

1.2.3 Including temperature dependence

The original model of [24] includes light as the only external stimulus, thereby limiting any entrainment response to be purely driven by light. In order to incorporate temperature entrainment, we introduce temperature dependence by assuming that each rate can be described by an Arrhenius equation [30, 52, 45].

The parameter values of the model are chosen so that the model exactly matches that of [24] at the reference temperature 21°C (Table 1). All translation rates of the model were allowed to vary with temperature, i.e. the parameters p_1, p_{1L}, p_2, p_3, and p_4. Each value of each translation rate was fixed to the corresponding temperature reference of 21°C and constrained to an arbitrary activation energy value. Then, the equation 1 was solved to predict the values of those parameters at a temperature of 17°C after calculation of the A_i terms from equation 4.

1.2.4 Identifying transients and quantifying rhythmic behaviour

In each of the simulations, the procedure is that the system is started with all dynamic variables initialised to independent uniform random values between 0 and 0.1. The system is then run forward in time for a fixed number of days under a periodic environmental

regime (see the model equations in Introduction section) in the expectation that rhythmic behaviour will manifest itself (entrainment). After this entrainment stage, the environmental parameters are fixed to some prescribed level (free-running) and the systems behaviour is monitored. These simulations thereby mirror the experimental approaches common in the circadian literature.

Initial investigations asked how many days of entrainment need to be imposed for all systems to synchronize i.e. for any transients induced by the random initial conditions to die out. Simulations involved up to 287 days of entrainment, with typical cycles of 12 hours at 21°C (warm) and 12 hours at 17°C (cold). To allow some initial investigation, we set the activation energy E_i to 90 kJ mol^{-1}, which is broadly consistent with published estimates [32, 52].

Another important consideration involves the question of when to measure the period of the resulting free-running oscillations. To develop reliable estimates, the periodicity of *CCA1/LHY* expression was assessed by evaluating the period based on changes in the first and second day of free-running following thermal entrainment, then between the third and fourth days (the method used in experiments), and finally the eighteenth and nineteenth days. Note that the equation 1 has two free parameters, A_i and E_i, and one constraint. For this reason simulation results are presented for activation energies taking the values E_i=10, 50 and 90 kJ mol^{-1}. To account for any influence of initial conditions, 100 replicates of each simulation were carried out. We also carried out simulations where each activation energy was chosen at random, independently, from a U[10,90] distribution. In these random cases, 400 independent replications were used (Figure 1.10).

Similarly, we used three methods to calculate the period. The first method involved observing the mRNA level at the initiation of free running, and then computing how long it takes to reach the same amount of mRNA. The period was also calculated by measuring the time difference between consecutive troughs, and between consecutive peaks. Because measures were very similar (not to say identical), results shown here were obtained by the trough method.

Simulations and analysis were perfomed in MATLAB. The integration of the system of ODEs was computed using the ODE45 solver. Solutions were verified by other solvers such as ODE23s.

1.3 Results

1.3.1 Adapting the model for continuous changes in light

In order to model a more "realistic" light-dark cycle, we implemented a tanh and a simple sinusoidal function (see equations 10 and 11) for continuous changes in light levels (see Figure 1.3). The results show that the model [24] is robust against perturbations in light forcing; outputs from "realistic" light functions were very similar compared to the original square waves. Figure 1.4 provides an illustrative example of the model's output under different light forcing regimes. A wide variety of similar simulations were carried out for similar forcing regimes, constrained only to be practical biologically and practically, and in no cases was any important difference in output observed. In other words, the [24] model is robust to different choices of light forcing functions, and the constraint of strict light-dark dynamics in the original model is unlikely to introduce any artefacts.

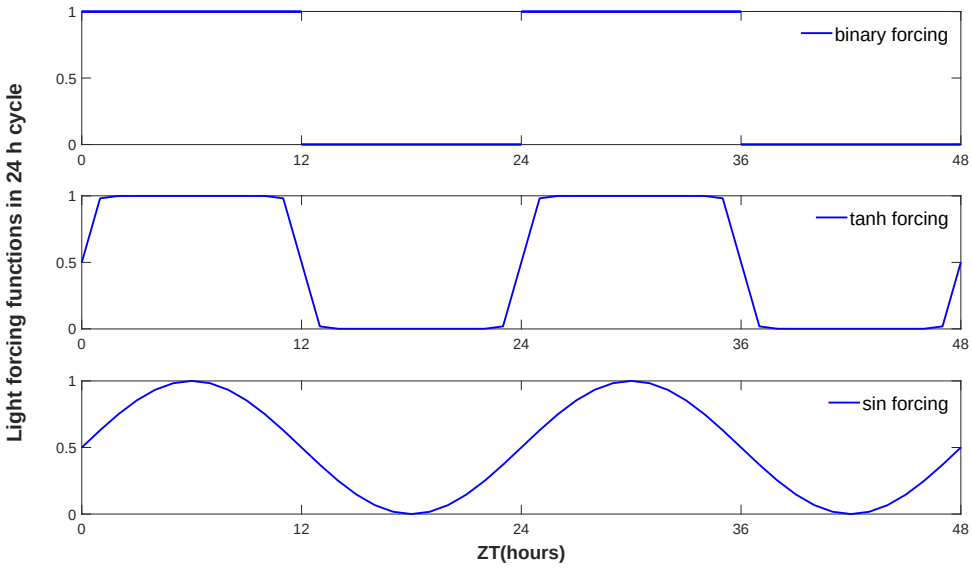

Figure 1.3: **Forcing functions for light variability**. The top subplot shows the binary model of [24] for light variability. We adapt this model to allow smooth transitions between light and dark using a tanh function as advocated in [54]. We also consider a simple sinusoidal function to allow continuous changes in light levels. The Zeitgeber time (ZT) is given for a notional unit of an hour, where the phases ZT0 and ZT24 indicate when light is on (i.e. dawn), and ZT12 and ZT36 when light switches off (i.e. dusk) in a 24 h cycle.

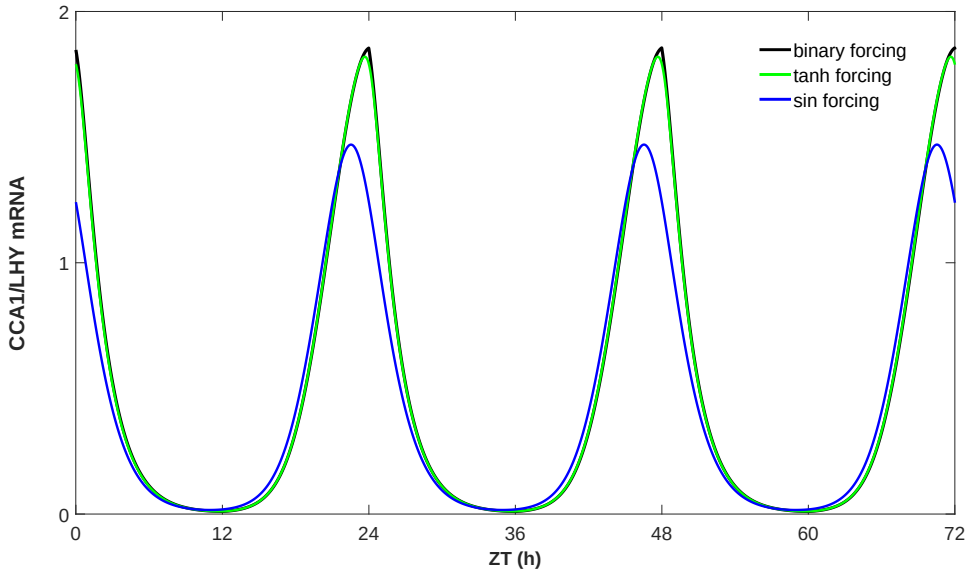

Figure 1.4: **The clock model behaviour is robust when the equations of [24] are forced with different models for light variability.** In all cases a qualitative agreement of model outputs is observed, but with a small decrease in amplitude in the case of sinusoidal light forcing. Similary to [54], the parameter of twilight of the tanh function (see equation 10) was set to be equal to a 0.5 h duration. For the sinusoidal function (see equation 11), the parameters of amplitude and phase were set to 0.5. The Zeitgeber time (ZT) is given for a notional unit of an hour, where the phases ZT0, ZT24 and ZT48 indicate the beginning of the light forcing (i.e. dawn), and ZT12, ZT36 and ZT60 when light forcing switches off (i.e. dusk) in a 24 h cycle

.

1.3.2 Adapting the model for changes in temperature: transient effects

The clock model (see the model equations in Introduction section) was implemented to simulate standard experimental conditions, i.e. entrainment of 12 hours in warm conditions and 12 hours in cold conditions under constant light, for a 21°C/17°C thermal cycle. The general behaviour of the system was assessed by observing periodicity and phase of the last entrainment cycle peak, and also the phase of the first peak after the clock is released into free-running conditions (constant warm and light).

Figure 1.5 depicts the period calculated over a range of entrainment durations. Results show that when the clock was entrained for less than a hundred cycles, the system continually varied in rhythmicity in both entrained and initial free-running conditions. In contrast, after two hundred entrainment cycles the periodicity was well defined and the system reached its final state of regular periodic oscillations. Consistent with this, the

initial free-running period was closer to the value observed in the last thermal cycle when seven days of entrainment were implemented. The emergence of stable oscillations as a result of a long entrainment process can also be observed in Figure 1.6. Outputs of the peak phase of *CCA1/LHY* confirm the transient state of the system when it is forced for a few thermal cycles; differences in phase between the first free-running peak and the last peak under entrainment are minimal. However, the peak phase of *CCA1/LHY* remains stable in entrained and free-running conditions.

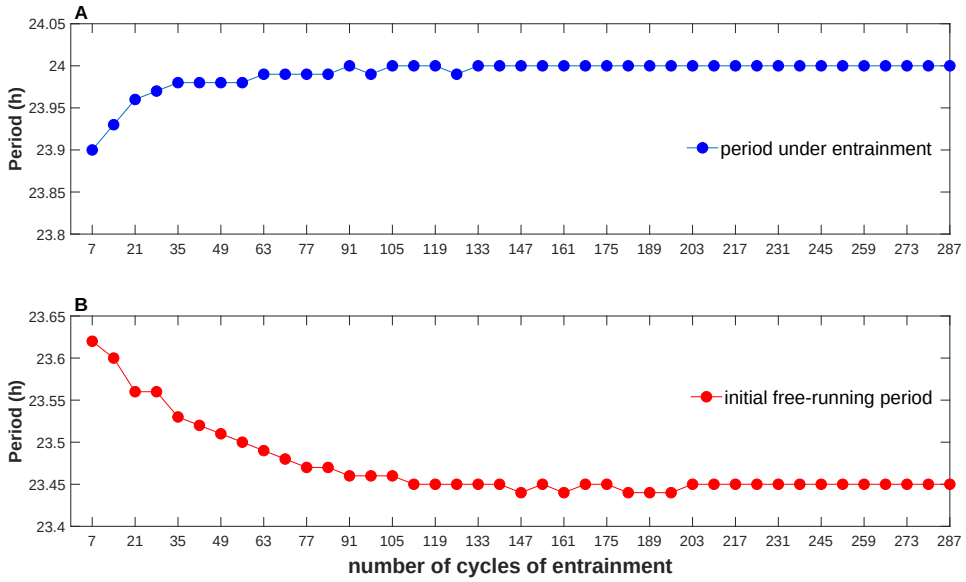

Figure 1.5: **More than a hundred days of entrainment are needed by the model to reach its final oscillatory state, but stable oscillations emerge with approximately the correct period after seven days of entrainment. The initial free running period decreases slightly as the length of the entrainment process increases.** Results show outputs for thermal cycles of 12 h in warm and 12 h in cold ranging from 7 to 287 days of entrainment. A) depicts the period observed in the last cycle under entrainment and B) shows how long the clock takes to oscillate once immediately after the release into constant warm conditions.

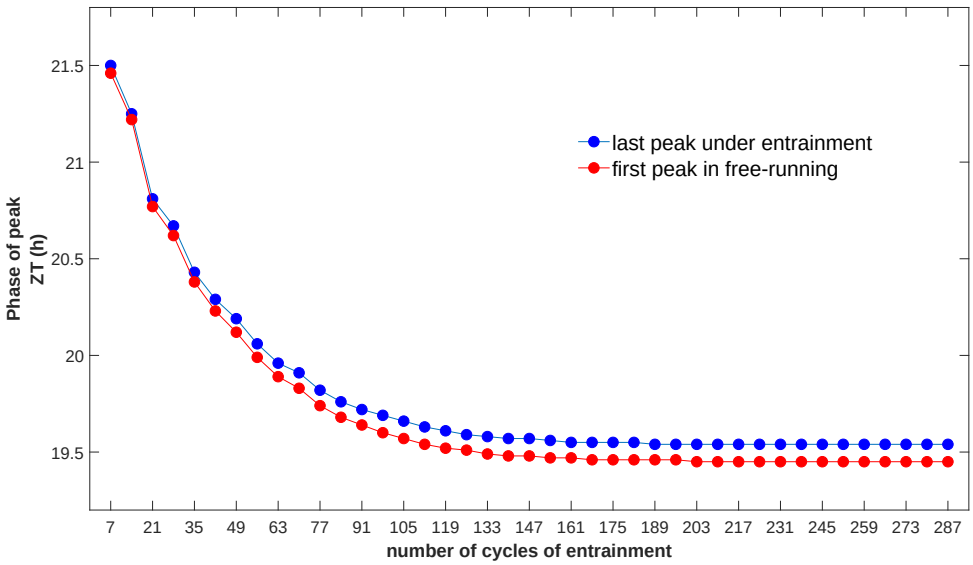

Figure 1.6: **The phase of the *CCA1/LHY* mRNA follows a similar pattern to that observed for period in Figure 1.5.** Phase of the peak of *CCA1/LHY* mRNA levels for thermal cycles of 12 h in warm and 12 h in cold ranging from 7 to 287 days of entrainment. Results show the ZT hour notation of the phase of peak observed in the last day of entrainment and the first day in free-running conditions.

Figure 1.7 presents the same information described in Figures 1.5 and 1.6, but illustrated as a time series. The plot shows the last 10 cycles of 182 thermal cycles of entrainment and contrasts those results with outputs from seven thermal cycles. In both cases the clock was released into free-running conditions after entrainment. Although in short and long entrainment processes the clock can be thermally entrained (i.e. it oscillates approximately once per cycle), in 182 cycles case the period matches exactly the external rhythm and remains stable. In contrast, for seven cycles of entrainment, the system still slightly shifts at the end of the process and is not able to perfectly achieve the rhythmicity of the external forcing. In (Figure 1.8), these trajectories (under entrainment) are shown in the *CCA1/LHY PRR5/TOC1* phase plane, highlighting the stability in limit cycle reached by the long entrainment process.

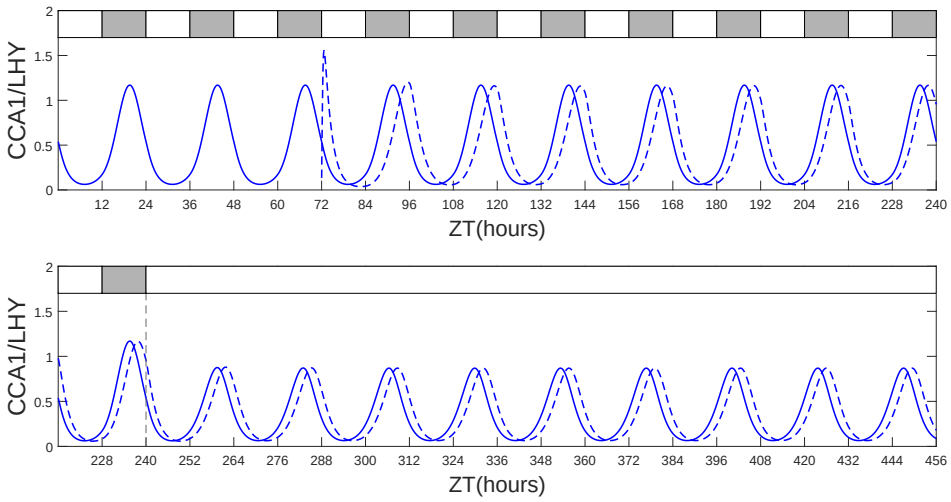

Figure 1.7: **Hundreds of thermal cycles of entrainment are needed by the model to reach the final state**. Comparison of the standard entrainment length (seven days of entrainment) and a long process of entrainment (182 days). The solid line depicts simulated mRNA levels over time in the last 10 days following 172 days of entrainment (top panel) before the clock is released into free-running conditions (bottom panel). The dashed line depicts simulated mRNA level for seven days of entrainment (top panel) and those under free-running conditions (bottom panel). The clock model was forced at 12 h at warm (21°C) and 12 h at cold (17°C) in a 24 h thermal cycle under constant light. The conditions of free-running are constant warm and light. The Zeitgeber time (ZT) is given for a notional unit of an hour, where the phase ZT0 (and consecutively every 24 hours) indicates the beginning of the temperature forcing (i.e. dawn), and ZT12 (followed by phases every 24 hours from ZT12) indicates when temperature forcing switches off (i.e. dusk).

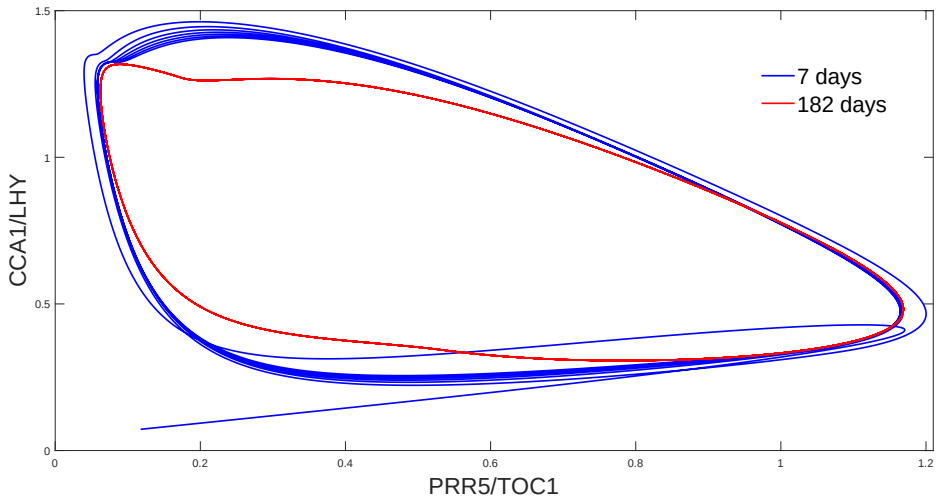

Figure 1.8: **More than seven days of thermal entrainment are needed for the model to reach a stable limit cycle**. Trajectories of the system in phase plane of *PRR5/TOC1* against *CCA1/LHY* mRNA levels. The dynamic of seven days of entrainment in limit cycle (blue line) is compared to a longer process of 182 days of entrainment (red line), where the last seven days of entrainment following 175 days of a forced clock are shown. A 24 h 21°C/17°C thermal cycle was simulated.

1.3.3 Periodic behavior at different time scales

In order to understand whether the timing of the experimental data collection influences the results, we simulated several time scales for data collection and evaluated the periodicity of the system. Simulations were carried out for seven days with 12 hours in warm and 12 hours in cold, as done in standard experiments. A 21°C/17°C thermal cycle was used. To be precise in our estimates we implemented three methods to calculate the period and compared them. The first method implemented consisted of calculating the time taken by the system to return to the initial free-running state; some limitations were found. For example, the method was not compatible with cases when the amplitude of the free-running oscillations was lower than the value observed when the clock is released, as this level no longer is obtained (see Figure 1.7 for an example). In the other two methods, the time differences between troughs and peaks (respectively) were calculated. The results obtained were practically indistinguishable. However, because in this study the expression of *CCA1/LHY* is considered for the analysis, and because *CCA1/LHY* slightly overanticipates dawn and its mRNA levels rapidly decrease, we chose the trough method for all subsequent numerical calculations. This method allowed us to obtain reliable estimates, in particular for the initial free-running period, as the first trough phase of *CCA1/LHY* occurs earlier than the first peak phase.

Figure 1.9 shows the distribution of the period after 100 replications for three activation energy values (E_i=10, 50 and 90 kJ mol^{-1}) at four time scales: the closest cycles before and after the release of the clock, and the $3^{rd} - 4^{th}$ and $18^{th} - 19^{th}$ days forward in free-running. As expected for entrained conditions, differences in distribution are observed between activation energy values, and a larger variability in periodicity emerges when the values E_i=50 and 90 kJ mol^{-1} are used to parametrise the influence of temperature on the system. This is explained by the Arrhenius law, as higher activation energy values imply higher sensitivity of the rates to a change in temperature. For this reason, in the opposite case of low temperature sensitivity (i.e. E_i=10 kJ mol^{-1}), the variability of the distribution of the period is smaller as the clock is less strongly forced. In agreement with the previous results, transient behaviour was observed in the initial free-running period.

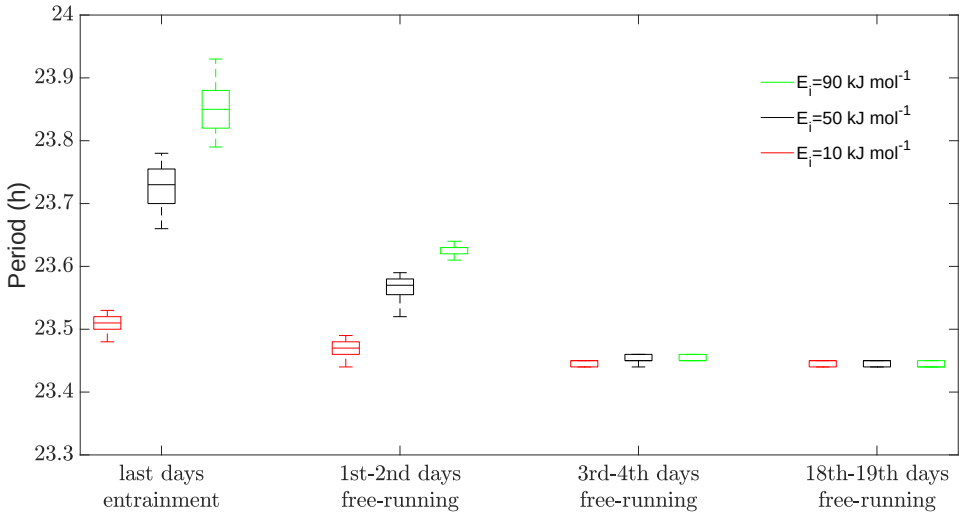

Figure 1.9: **Period estimates derived from the 1^{st} and 2^{nd} days in free-running conditions are very unreliable**. Distribution of the clock period for different activation energy values (red, black and green boxes represent E_i=10, 50 and 90 kJ mol^{-1}, respectively) in four times scales: from the last two days of entrainment following five days of those conditions to $18^{th} - 19^{th}$ days in constant temperature and light. 100 independent replications were used. Transient behaviour is observed on the 1^{st} and 2^{nd} days in free-running conditions. The higher influence of temperature on the translation rates of the model, the higher variation in periodicity when the clock is forced.

Results from random activation energy values (see Figure 1.10) are consistent with those shown in Figure 1.9. When the Arrhenius parameters E_i were allowed to vary uniformly at random on the range 10 kJ mol^{-1} and 90 kJ mol^{-1}, modelled outcomes on the 1^{st} and 2^{nd} days after the release of the clock also showed presence of transient behaviour, which supports the idea that these time scales are very unreliable for data collection.

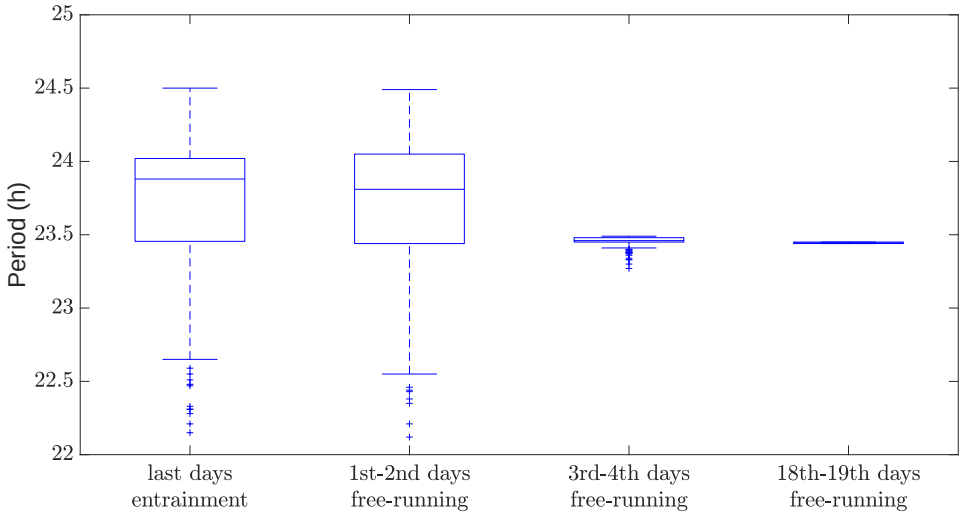

Figure 1.10: **Observations on the 1^{st} and 2^{nd} days in free-running conditions are very unreliable**. Distribution of the period length when random activation energy values are assigned to translation rates. Each distribution corresponds to a different time scale. Observations in entrainment conditions come following five days of entrainment. All modelled outcomes in free-running were obtained under constant temperature and light. 400 independent replications were used from uniformly distributed random numbers between 10 and 90. Similarly to results in Figure 1.9, transient behaviour is observed on the 1^{st} and 2^{nd} days in free-running conditions.

To test the temperature results, the distribution of the period in different time scales for light entrainment was also analysed (Figure 1.11). Similar to the temperature analysis, we measured the period around the transition from photo cycles to free-running conditions followed by measurements on $3^{rd} - 4^{th}$ and $18^{th} - 19^{th}$ days in continuous light. Seven days of entrainment for 12 hours in light and 12 hours in dark for 100 replications were simulated. Consistent with temperature results, observations on the 1^{st} and 2^{nd} days of free-running are very unreliable. In contrast, there is minimal variability in the period calculated under light forcing, which indicates that the temperature-dependent model requires more time to reach its final state.

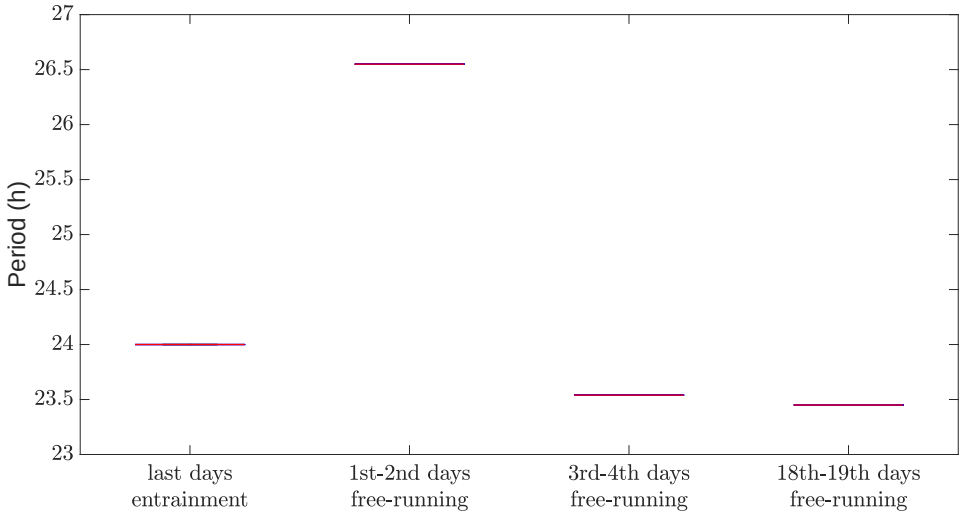

Figure 1.11: **Period estimates based on the 1^{st} and 2^{nd} days in free-running conditions may be unreliable**. Distribution of the clock period in four times scales. Modelled outcomes under entrained conditions corresponds to the last two days following five days of entrainment by photo cycles of 12 h in light and 12 h in dark. 100 independent replications were used. The rhythmicity of the system did not vary in any time scales analysed. It is also observed that the outputs obtained match exactly published results [55]. This confirms that the trough method is efficient at quantifying periodicity.

1.4 Discussion

With the aim to discuss the effect of temperature in the context of the model [24], in this chapter we present the model from [24], and show how it can be extended to account for continuous variation of light. We develop a framework by which temperature dependence can be added to the model, and we implement this by hypothesizing temperature sensitivity on translation rates following the established Arrhenius law. This produces some useful preliminary results concerning the clock's period at various time scales. This chapter is best regarded as the first step in a research process which will involve interactive mathematical and experimental efforts that together will lead to a better understanding of how the clock is reset to match the environmental changes.

Transient analysis showed that more than a hundred thermal cycles are required to allow the system to reach its final state. In contrast, results for periodicity of the clock system at different time scales were obtained from simulations performed similarly to standard experimental conditions. That is, numerical outputs for entrainment cycles of 12 hours in warm and 12 hours in cold during seven days followed free-running conditions at constant light and warm. Results in both light and temperature forcing showed that data obtained on the 1^{st} and 2^{nd} days of continuous conditions are very unreliable. Moreover, the variability in rhythmicity of the system was dependent on the influence of temperature, which was characterized by three different activation energy values. Together, this reaffirms the fact that the dynamics of the plant system varies due to intrinsic/extrinsic events.

For preliminary results, we arbitrarily assumed temperature-dependent changes on the translation rates of the model, and excluded transcription and degradation processes, which have been proven to be temperature sensitive [56]. This simplification was enough to provide helpful insights into how long of entrainment is needed by the plant clock model to avoid transient behaviour. However, in the follow-up chapter we incorporate temperature dependence in all rates of the model, which govern transcription, mRNA and protein degradation, and translation processes, in order to identify what processes are important in the current clock model for temperature mechanisms [26].

We have shown that temperature-dependent changes in the translation rates of the model can entrain the system; after removing transients, the clock's period matches exactly the external rhythm, a stable phase is also observed, and sustained oscillations are possible in the absence of the temperature forcing, which are elemental properties to demonstrate entrainment [2]. Additionally, testing these properties on cycles different than 24 h length is considered an accurate way to demonstrate the capability of a model to be entrained by

an external cue [2]. The model [24] has been shown to possess a wide entrainment range, being able to oscillate once per light-dark cycle in cycles with length between 17 and 32 hours, and for different hours of exposure to light and dark within a cycle (photoperiod) [55]. In the next chapter we address these ideas in order to analyse the combined effects of varying light and temperature in the adaptation to changing environmental conditions.

2 Heat the clock: Entrainment and Compensation in *Arabidopsis* Circadian Rhythms

Abstract

The circadian clock is a biological mechanism that permits some organisms to anticipate daily environmental variations. This clock generates biological rhythms, which can be reset by environmental cues such as cycles of light or temperature, a process known as entrainment. After entrainment, circadian rhythms typically persist with approximately 24 hours periodicity in free-running conditions, *i.e.* in the absence of environmental cues. Experimental evidence also shows that a free-running period close to 24 hours is maintained across a range of temperatures, a process known as temperature compensation. In the plant *Arabidopsis*, the effect of light on the circadian system has been widely studied and successfully modelled mathematically. However, the role of temperature in periodicity, and the relationships between entrainment and compensation, are not fully understood. Here we adapt recent models to incorporate temperature dependence by applying Arrhenius equations to the parameters of the models that characterize transcription, translation, and degradation rates. We show that the resulting models can exhibit thermal entrainment and temperature compensation, but that these phenomena emerge from physiologically different sets of processes. Further simulations combining thermal and photic forcing in more realistic scenarios clearly distinguish between the processes of entrainment and compensation, and reveal temperature compensation as an emergent property which can arise as a result of multiple temperature-dependent interactions. Our results consistently point to the thermal sensitivity of degradation rates as driving compensation and entrainment across a range of conditions.

2.1 Introduction

The circadian clock is an interconnected network of biological processes needed for some organisms to anticipate daily environmental variations. The synchronization of the clock with the night/day cycle grants advantages such as growth and development in plants [57, 58, 59, 11, 60, 61], energy balance in mammals [62], conidium development in Neurospora [63], sleep modulation in Drosophila [64] and starvation response in Cyanobacteria [65]. This biological system generates rhythmic gene expression, and mathematical models have helped to uncover the crucial molecular mechanisms of diverse living organisms [24, 42, 66, 67, 68, 69, 14, 70, 71, 72, 73]. For an overview of insights into the complexity of circadian systems using mathematical and biological techniques, see [13, 8, 19, 74, 9].

In plants, mathematical models based on ordinary differential equations (ODEs) were built in order to characterize the first feedback loop indentified by experimental observa-

tions. Subsequenty, mathematical models have continued describing the key mechanisms driving the plant oscillator [24, 42, 66, 41, 54, 22, 75, 76, 40, 77, 18]. These models have motivated hypotheses which, in parallel with experimental validation, have helped to establish not just the components of the network, but also to elucidate their role [19, 78].

Light and temperature are important stimuli to regulate circadian rhythms [79, 2]. However, most modelling efforts have only focused on incorporating the effect of light in the plant circadian system. The influence of temperature is less clear, and is less well studied. A better understanding of temperature dependence in the circadian clock, and its relation to light, is needed for several reasons. While experiments necessarily concentrate on controlled and idealised scenarios, the real physiological challenges faced by plants are more varied. In the simplest case, global climate warming will require plants to maintain a 24 hour rhythm at an increased average temperature. Alternatively, a local environmental warming might require a plant to disperse toward a higher latitude to maintain an optimal temperature range. Such a latitudinal change will necessarily involve a change in the associated light-dark cycle, with higher latitudes being subject to (in summer) longer days and shorter nights. Similarly, for crop plants, it may be the case that potentially productive cultivars have evolved at different latitudes or temperatures; an understanding of how a plant's clock will function when translocated to a new environment could be crucial in assessing its suitability [80, 81].

An important property of many circadian clocks is that the free-running period, *i.e.* the frequency of the oscillator in the absence of changing external stimuli, varies minimally over a range of temperatures, a phenomenon known as temperature compensation. A small number of studies consider the role of temperature in the Arabidopsis circadian clock, seeking to combine experimental results with numerical simulations. [82] simulated the role of *GIGANTEA (GI)* in temperature compensation using the model of [77]. By modifying the transcription rates of the genes *CIRCADIAN CLOCK ASSOCIATED 1 (CCA1)* and *LATE ELONGATED HYPOCOTYL (LHY)* along with the hypothetical gene Y, they were able to fit the experimental data and to propose that GI is a component of Y. Also, [83] used the model [77] to test the contribution of *FLOWERING LOCUS C (FLC)* on compensation observed in experiments. They could fit experimental observations by increasing the maximum transcription rate of the hypothetical gene X in the model. This simulated the *LUX ARRHYTHMO (LUX)* gene effects on the clock, which is known to play a role in temperature compensation [84]. [33] built a temperature compensated model by incorporating temperature dependence into the model [54]. The authors thereby explained temperature compensation as a consequence of the architecture of the clock network, where rates of transcription, translation and, mRNA and protein degradation

were hypothesised to change with temperature.

Explanations of temperature compensation are centred around two hypotheses [33, 85]. The first proposes that the structure of the clock gene network, together with simple temperature dependence of its control coefficients, have evolved in order to produce an overall balance. The alternative hypothesis is that separate specific molecular mechanisms have evolved in order to ensure compensation, as argued in the case of the Neurospora circadian clock [32]. It is notable, however, that [32] hypothesised temperature dependence of two key translation rates using idealised hyperbolic tangent functions. This is in contrast to the Arrhenius formulation used in [33]. The latter approach, which allows for a simple parameterisation and which can be derived from the laws of statistical mechanics, forms the basis of this investigation.

The ability to maintain a 24 hour free-running period across a range of temperatures may not be a property subject to evolutionary selection; of more practical ecological relevance is an ability to maintain a circadian rhythm under a range of varying, and perhaps unpredictable, light and temperature stimuli. In this sense, although the mechanisms driving them may be related, the ability of a clock to be entrained must be separated from the phenomenon of temperature compensation. Mathematical models allow precisely this separation to be achieved.

Here we aimed to gain insight into clock mechanisms involved in adaptation to changing environmental conditions. To this end, we modified a recent model [24] by hypothesising temperature-induced changes in reaction rates, distinguishing the roles of transcription, translation and degradation. We conducted a simulation study across a wide range of light-dark and warm-cold regimes, and we explored the ability of our model to be thermally entrained and to show temperature compensation. Our results generally supported the holistic network-driven hypothesis for compensation, but they emphasised the importance of the thermal dependence of degradation on the clock's function. These conclusions were generally supported when the results were challenged by allowing greater uncertainty in the thermally sensitive parameters, and when results were compared to those from an earlier, more complex, mathematical model [41].

2.2 Methods

2.2.1 The model

The mathematical model presented here is based on [24]. The model is considerably simpler than earlier models [42, 66, 41, 54], but is known to replicate many key features of the plant circadian system. Figure 2.1, adapted from Figure 1 of [24], depicts the structure

of the network model and shows how its components interact via positive and negative feedbacks.

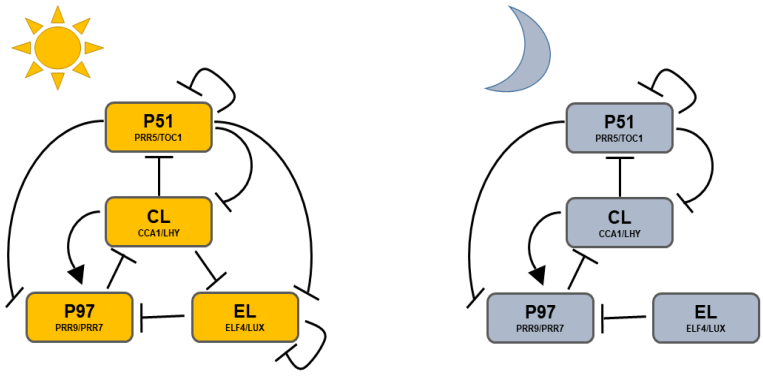

Figure 2.1: **Schematic diagram illustrating main features of the [24] model in light and dark phases.** In the model, similar genes were merged into the single variables CL, P97, P51, and EL, which represent the pair of genes *CCA1/LHY*, *PRR9/PRR7*, *PRR5/TOC1*, and *ELF4/LUX*, respectively. Edges represent transcription factors affecting the transcription rates of a gene in the network.

As explained in [24], the parameter values of the model are based on a fit to qualitative dynamics, based on matching amplitude, phase and period with experimental observation. Details of the model and its parameter values are in Chapter 1, Introduction Section.

All simulations and analysis were performed in MATLAB. The integration of the system of ODEs was performed using the ODE23s solver, and numerical accuracy was verified by comparing to the outputs of alternative solvers such as ODE45.

2.2.2 Including temperature dependence

We introduce temperature dependence into the model [24] by assuming that each rate can be described by the Arrhenius equation (see Chapter 1, Introduction Section for details). This formulation appears to introduce a further two unknown parameters for each temperature dependent reaction. However, by requiring that the model parameters match those fitted by [24] at their reference temperature of 21 °C, and by defining a realistic Q_{10} value for each reaction, this apparent uncertainty is ameliorated. Equation 3 in Chapter 1 immediately allows an indicative value of E_i to be calculated: assuming a reference

temperature of $T_1 = 21°C$, and a Q_{10} of 2 (commonly accepted value for biochemical reactions), substituting into Equation 3 gives an approximate value of $E_i = 50$ kJ mol^{-1}. This value of the activation energy is used as a starting point in the following numerical study. The role of the uncertainty in the values of E_i for each reaction i can be investigated via Monte Carlo simulations spanning a range of plausible values, see Figure 2.7 in Results Section.

In order to assess entrainment, we observe the agreement between the length of the external temperature cycle and the modelled outputs [49, 52]. We expect the system to oscillate once per thermal cycle. To assess temperature compensation, we evaluate the system in terms of the temperature coefficient Q_{10} of the period length p [47],

$$Q_{10} = \left(\frac{p_{T_1}}{p_{T_2}}\right)^{\frac{10°}{T_2 - T_1}}, \quad T_2 > T_1. \tag{12}$$

Therefore, overcompensation is reflected for $Q_{10} < 1$, (i.e. period length increases as temperature rises). In contrast, for undercompensation cases, a $Q_{10} > 1$ is observed (i.e. period length shortens with increasing temperature).

2.2.3 Combining light and temperature variation

The preceding mathematics allows simultaneous changes in both temperature and light to be simulated in the model, and their roles to be quantified. The structure of the numerical investigation is as follows. Initially, the behaviour of the temperature dependent model is studied in two general contexts: temperature entrainment (i.e. can meaningful 24 h cycles be induced by realistic daily variation in temperature) and temperature compensation (i.e. how sensitive to temperature is the free-running period of the clock). Thereafter, simultaneous changes in light and temperature are imposed, to investigate under what environmental conditions a circadian rhythm is predicted to remain viable.

2.3 Results

2.3.1 Temperature entrainment

Simulations were carried out to replicate standard experimental conditions [22, 86]. These were the model was entrained for 7 days under 12h warm/12h cold temperature cycles (a diurnal temperature range of 4°C was simulated (4°C difference between warm and cold)) under constant light before release into free-running conditions (constant light and warm temperature).

Figure 2.2 shows the predicted gene expression (mRNA levels) of *CCA1/LHY* in the last two thermal cycles, and for the four days following the release of the clock into free-running conditions. The key features of the output can be divided into two regions, referring to behaviour under thermal entrainment (up to ZT48 in the figure), and then to subsequent free-running behaviour (after ZT48).

The second row of outputs, depicting a moderate thermal forcing of 12h at 21°C followed by 12h at 17°C, shows that the clock can be thermally entrained; the clock oscillates approximately once per thermo-cycle. However, thermal entrainment to a 24h period was not observed in cooler scenarios (first row: at 17°C/13°C the observed period is 34.3h), and nor was it observed under warmer scenarios sharing the same 4°C variation (third row: at 25°C/21°C the clock's period is significantly shorter than 24h; fourth row: at 29°C/25°C the thermally entrained rhythm is approximately 15h).

A similar pattern emerges when examining the behaviour of the entrained (or otherwise) clock under subsequent free-running conditions. After ZT48, the clock held at 21°C displays an approximately 24h period (second row), but systems held at cooler and warmer temperatures display large variation from this circadian behaviour, with periods in excess of 30h at 17°C and shorter than 14h at 29°C.

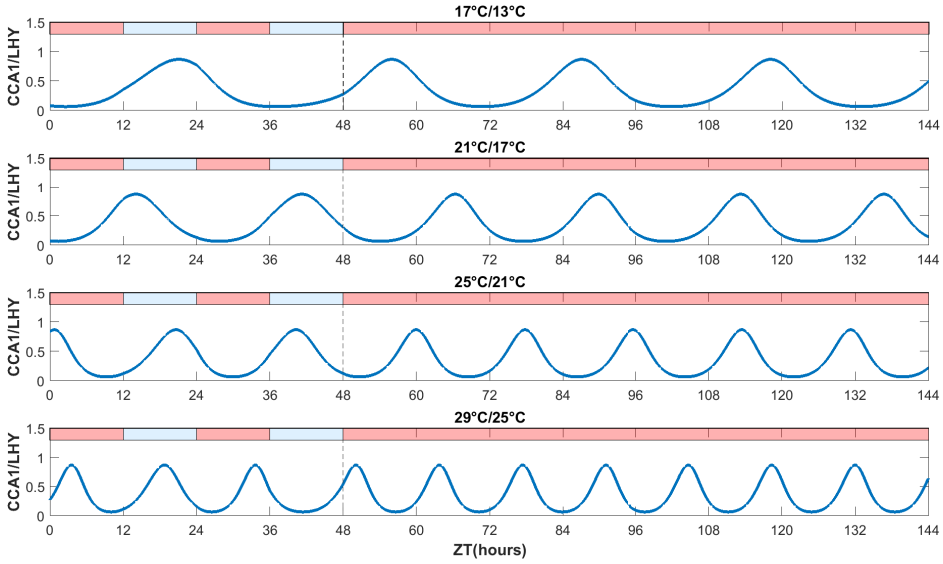

Figure 2.2: **Incorporating the Arrhenius law allows thermal entrainment, but only within a limited temperature range**. A 24 hour 21°C/17°C thermal cycle induces a functional clock, as shown by the rhythmic expression of *CCA1/LHY* mRNA. However, a 17°C/13°C thermal cycle induces a markedly increased period while warmer temperatures cause faster oscillations and ultradian rhythms.

This behaviour is not unique for *CCA1/LHY*; similar results were observed for *ELF4/LUX*, *PRR9/PRR7*, and *PRR5/TOC1* (See Figures 2.3, 2.4, and 2.5).

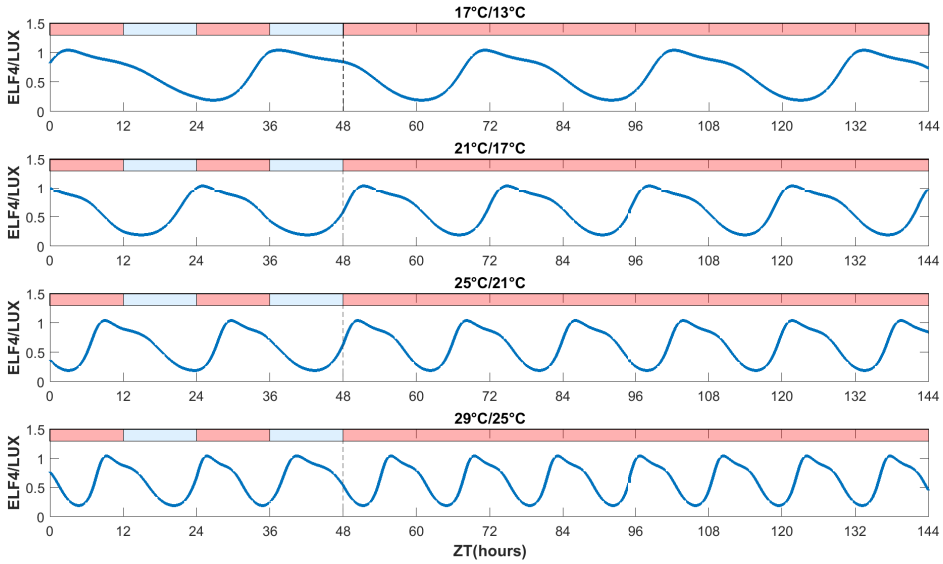

Figure 2.3: **Incorporating the Arrhenius law allows thermal entrainment, but only within a limited temperature range**. Periodicity of *ELF4/LUX* expression behaves similarly to the other components of the clock model under thermal conditions. A 24 h 21°C/17°C thermal cycle induces a functional clock. However, faster oscillations and ultradian rhythms are observed as temperature increases. In contrast, a 17°C/13°C thermal cycle causes notably slower oscillations.

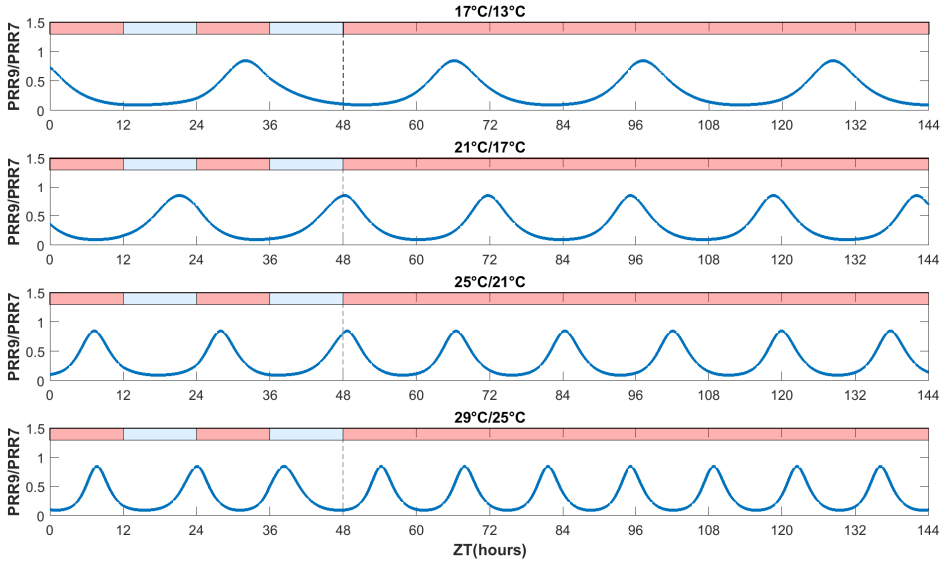

Figure 2.4: **Incorporating the Arrhenius law allows thermal entrainment, but only within a limited temperature range**. Periodicity of *PRR9/PRR7* expression performs comparably to the other clock components under thermal conditions. A functional clock is observed in a 24 h 21°C/17°C thermal cycle. However, faster oscillations and ultradian rhythms are obtained as temperature increases, and clearly slower oscillations are induced at 17°C/13°C thermal cycle.

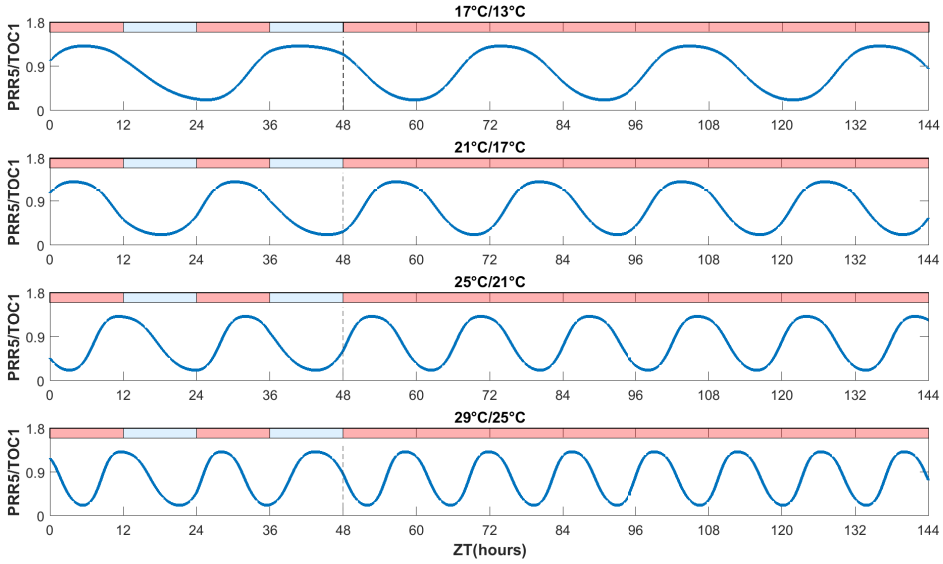

Figure 2.5: **Incorporating the Arrhenius law allows thermal entrainment, but only within a limited temperature range**. mRNA level periodicity of *PRR5/TOC1* agrees with the other clock component results under thermal conditions. A 24 h 21°C/17°C thermal cycle induces a functional clock. A 17°C/13°C thermal cycle causes markedly slower oscillations. However, the warmer temperature, the faster oscillations are observed.

To further test the applicability of the model, its behaviour under severe temperature stress conditions in constant light was also analysed. Consistent with results in Figure 2.2, at 24 hour 5°C/1°C thermal cycle (freezing stress) the clock showed a pronounced increased period, while at 39°C/35°C thermal cycle (heat stress) the clock displayed substantially higher frequency oscillations (Figure 2.6).

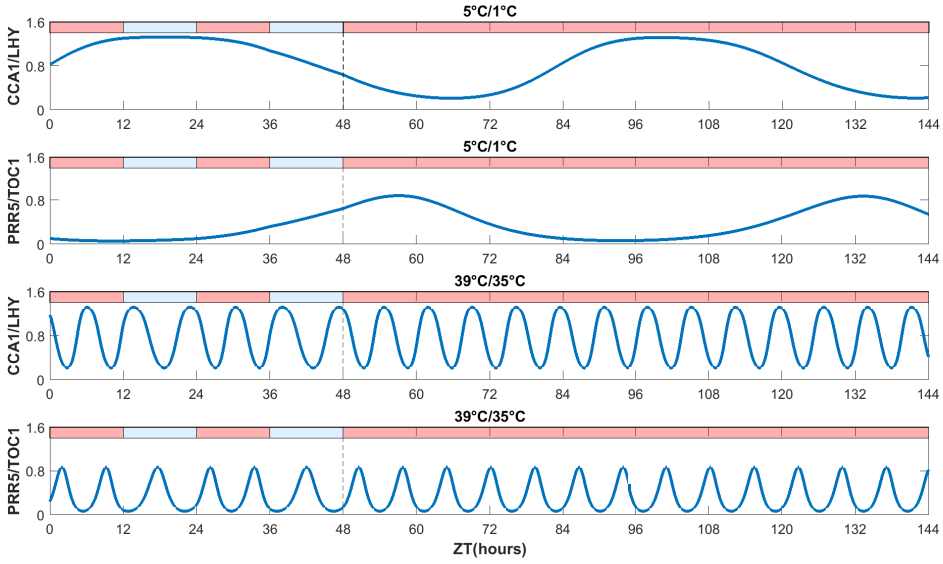

Figure 2.6: **Temperature stress under constant light conditions can cause a defective clock**. *CCA1/LHY* and *PRR5/TOC1* expression responses to freezing and heat stress conditions are consistent with results in Figure 2.2. Faster oscillations are strongly induced by heat while a freezing thermal cycle results in a heavily decreased period.

The consistent story which emerges is that thermal entrainment may be possible in the absence of light-dark forcing, but only within a limited temperature range (where the free-running period is approximately 24 h in any case). In other words, it is the interaction between light and temperature, rather than temperature in isolation, which is important in understanding the robustness of circadian rhythms in varying environments. To test that this general conclusion is not sensitive to the exact choice of the activation energies E_i we also carried out simulations where each activation energy was chosen at random, independently, from a U[40,60] distribution (see Figure 2.7); the results supported the conclusion.

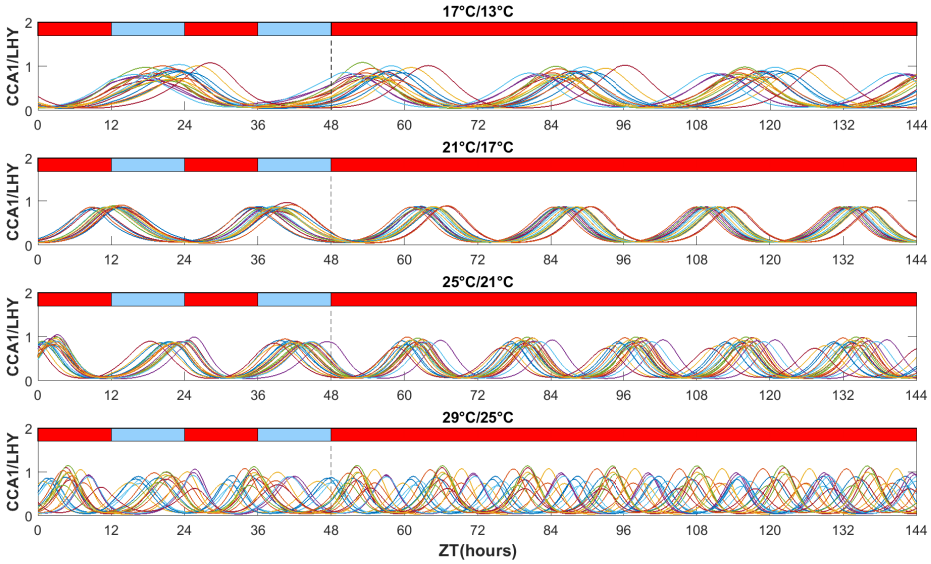

Figure 2.7: **Thermal entrainment is observed in the model across a range of parameter values describing temperature dependence.** Random uniform distributed activation energy values between 40 and 60 were allocated independently to each rate in the model. Results are similar to the outputs obtained when the influence of temperature was parametrized to be equal. A 24 h 21°C/17°C thermal cycle induces a functional clock. However, the warmer temperatures, the faster oscillations and ultradian rhythms are observed. In contrast, colder temperatures induce slower oscillations.

2.3.2 Temperature compensation

Temperature compensation has been explained as an emergent property, happening via a balance of network reactions each of which is not necessarily compensated[31]. That the [24] model can in principle display temperature compensation, but that this is not the case in general, is illustrated in Figure 2.8. Figure 2.8D shows that when each constituent reaction in the network is allowed to vary with temperature with $Q_{10} = 2$, the resulting clock has free-running period which declines markedly with temperature (undercompensation). The resultant Q_{10} of period value is around 2.

The reasons for this lack of overall compensation can be elucidated by running a modified model allowing temperature dependence (with $Q_{10} = 2$) in only one rate in any given simulation [45]. Figure 2.8A-C summarises this, where the resultant free-running periods from allowing thermal dependence of each of the 20 parameters in isolation is plotted. The outputs are grouped into thermal dependence of (A) translation rates, (B) transcription rates, and (C) mRNA and protein degradation rates. Figure 2.8A and B show that translation and transcription rates can have both positive and negative effects on period. For

example, in Figure 2.8A an increase in the translation rate of *PRR9/PRR7* shortens the period with increasing temperature, whereas the period increases with temperature for all other represented genes. This indicates that any overall temperature compensation model must emerge from a balance between these processes. Indeed, if the model is implemented with thermal variation in all translation rates, or in all transcription rates, the emergent clock is thermally compensated with a Q_{10} of period approximately equal to 0.97 in both cases.

Figure 2.8C shows that, in contrast, thermal dependence of degradation rates results in consistent reductions of period with increasing temperature, and that the influence of these degradation rates exceeds that of the translation and transcription rates. In other words, the overall failure of compensation in Figure 2.8D can be attributed to the thermal dependence of degradation rates.

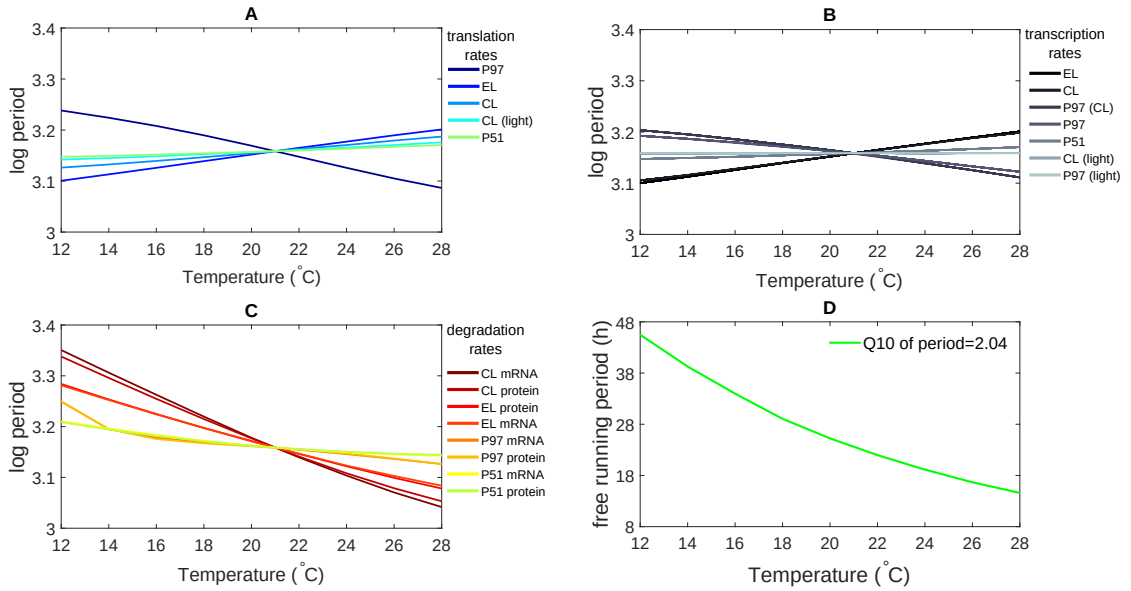

Figure 2.8: **The model is not temperature compensated, and this failure to compensate is driven by degradation rates**. Experimental protocols of [82] and [4] were simulated. A-C show the log period across a range of temperature, where only one parameter is subject to temperature variation for each output. Results are grouped to show thermal dependence of (A) translation, (B) transcription, and (C) mRNA and protein degradation rates. Labels are in order of the size of effect and they show how the parameter's effects are induced (in brackets). The resultant free-running period when all rates vary with temperature is shown in (D). Note that thermal dependence in translation or transcription may either increase or decrease period, whereas changing degradation rates causes a consistent decrease.

2.3.3 Simultaneous effects of light and temperature

We then simulated the clock in more realistic environmental conditions by simultaneously changing light and temperature. Explicitly, simulations were carried out using a 24 h cycle length, with this 24h divided into (light and warm) and (cold and dark) regimes of variable durations, where the cold temperature is (respectively) 4°C, 8°C and 12°C lower than the warm temperature. As in Figure 2.2, all rates were allowed to vary with temperature using an assumption that $E_i = 50$ kJ mol^{-1} for each reaction.

Figure 2.9 summarises the results. The central row of the second column depicts a circadian clock under "standard" conditions with 12h in light at 21 °C followed by 12h dark at cold temperatures cycles, the system is entrained to a predictable 24h rhythm. This rhythm persists, with increased amplitude, at 25°C, and also at 17°C provided the temperature range does not exceed 8 °C. However, at 29°C the circadian functionality of the clock is lost. Interestingly, when the temperature variation is at its largest (12°C) this has the effect of preventing entrainment at low temperatures (where a 48h period is induced), but conversely of restoring circadian rhythmicity at 29°C.

In contrast, the relative consistency of outputs in the second column indicates that, even at extreme durations ranging from 6h to 21h light, the clock can be successfully thermally and photically entrained at this temperature. The circadian rhythm is disrupted only at the shortest light duration of 3h. The system can respond to wide changes in light-dark cycles so long as the temperature remains close to 21°C.

The clock was again relatively entrainable at a base temperature of 25°C, but with diminishing amplitude (and eventual failure of the circadian rhythm) at the extremes of simulated light duration (3h or 21h). However, at the warmest (29°C, final column) temperatures the circadian clock behaved erratically, with a general decline in amplitude and increase in period as temperature increases. There are signs of erratic ultradian rhythms when the light duration exceeds 12 h, but also of circadian rhythms which display a large phase shift for the shorter light durations.

At cooler temperatures (17°C, first column), the amplitude of oscillations decreased. In short days (3h, 6h and 9h of warm-light) the clock showed long-period oscilliations, with a transition to circadian dynamics with low amplitude as light duration increases.

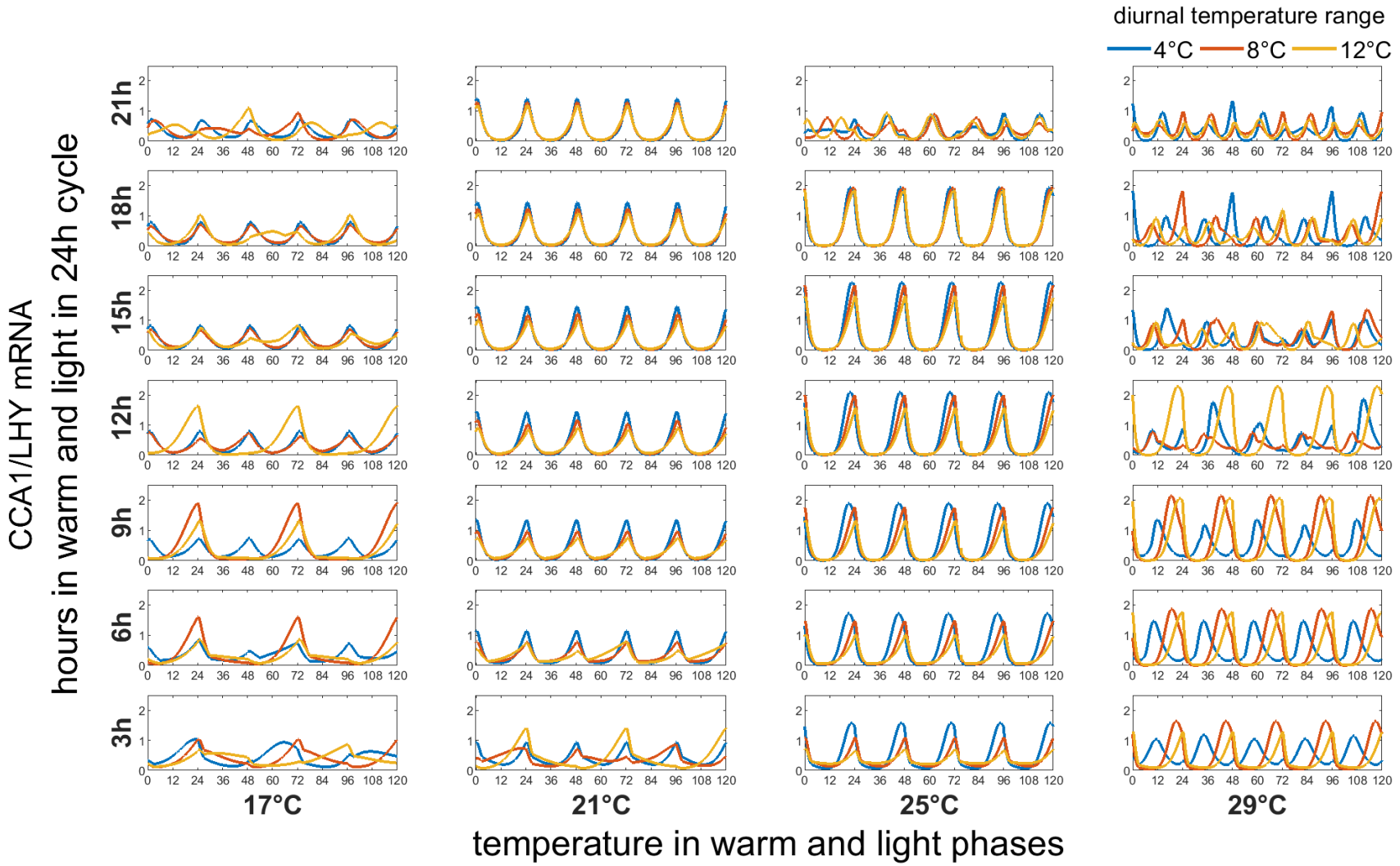

Figure 2.9: **The combined effect of photic and temperature forcing can induce entrainment across a wide range of light-dark durations, but only within narrow temperature limits**. At 21°C the clock is correctly entrained even for large diurnal temperature ranges and uneven light-dark cycles (central columns). At lower (first column) or higher (final column) temperatures, non-circadian rhythms may emerge. Further, there is a general increase in amplitude as temperature increases.

2.4 Discussion

Using numerical investigations, we studied how the [24] model clock responds to the combined effects of light and temperature. The results demonstrate that dynamics in both of these environmental processes are instrumental in resultant clock dynamics, and that any theoretical or empirical assessment of the robustness of the clock to these changes needs to be viewed in an ecological context. Moreover, the results clearly distinguish between the processes of entrainment and compensation, and they point to the key elements in the circadian clock which drive both phenomena.

One broad conclusion is that temperature compensation cannot be explained as the result of a balance between a set of temperature dependent reactions within the clock, and that the reason for this is closely linked to temperature dependence of mRNA and protein degradation rates. Note that we have assigned the same value to the Arrhenius parameters E_i for all rate constants k_i, namely, a constant $E = 50$ kJ mol^{-1}. This implies that the condition for temperature compensation from Equation 9 (Chapter 1, Introduction Section) can be written as,

$$\sum_{i=1}^{m} c_i E_i = E \sum_{i=1}^{m} c_i = 0, \tag{13}$$

therefore, temperature compensation attribute lies on the control coefficients only, which gives a clear indication of what processes in the network are important for period variation (see Figure 2.8). Because each rate constant is perturbed with the same size of change, i.e. same activation energy value, the sensitivity coefficient c_i of the period faithfully reflects the magnitude of period control of the relevant parameter compared to the other parameters that govern the network. This would not be the case if we allowed the parameters E_i to vary so as to achieve temperature compensation. Moreover, this would result in unrealistic Q_{10} of rates. For example, very small activation energy values should be assigned to degradation rates, which means modelling those to be practically insensitive to temperature. If degradation rates were relatively insensitive to temperature, then the interaction between temperature dependent rates of translation and/or transcription would be sufficient to explain temperature compensation, supporting the network hypothesis of [33]. However, because there is substantial evidence that degradation rates are temperature sensitive [56], temperature compensation must be achieved by more complex processes (see, for example, [87]) which are beyond the scope of this model.

Because our purpose was not incorporate explicitly temperature compensation, we have not computed the control coefficients c_i nor to impose any constraint to them. Rather we simply aimed to detect the processes responsible for period variation; therefore, our

discussion is based on the coefficient Q_{10} instead.

For the clock to be functional it needs to interact with both light and temperature. From our numerical results, we hypothesise that in nature, the function of the plant's circadian clock might be adversely affected by long periods of exposure to warm and light conditions. Evidence that temperature compensation in the Arabidopsis clock results from the interaction of light and temperature have been published [33]. Moreover, in our approach *PRR9/PRR7* is essential for temperature compensation, which agrees with experimental results [4]. Notably, our approach allows us to present a theoretical climatic tolerance range resulting from entraining the clock for more realistic environmental cues involving light and temperature cycles simultaneously.

To further test whether our outputs from simultaneous photic and thermal cycles were consistent with experimental results, we simulated the clock for a total of 15 days under both 24 h light/warm and dark/cold cycles, and compared these to dark/warm and light/cold cycles, following the experimental ideas of [88] and [89] (Figure 2.10). Although there are some differences in quantitative details, our model predictions generally matched those results. A circadian rhythm was maintained, and a higher peak expression was observed when the clock was entrained under 25°C in light and 15°C in dark conditions, compared to 15°C in light and 25°C in dark. Furthermore, in 25°C light and 15°C dark the mRNA levels accumulated more rapidly in dark phases, and this increase was slightly advanced, compared with 15°C in light and 25°C in dark entrainment cycles.

The model on which this is study based, while being based on established biological and physical mechanisms, necessarily relies on several assumptions. Perhaps the most restrictive of these are firstly, that each individual component reaction is subject to thermal variation following an identical Q_{10} of 2, and secondly, that the underlying model of [24] may be an over-simplification of the true biological system.

The first of these concerns can be addressed via Monte Carlo simulation. Explicitly, in Figures 2 - 5 which are calculated under the $Q_{10} = 2$ assumption, each of the activation energies E_i in equation 1 is assumed to take a value of 50 kJ mol^{-1}. While this is reasonable as a first assumption, it is likely to be an over-simplification; for example there is evidence of Q_{10} coefficients for degradation rates taking values around 3 [56]. This assumption can be relaxed by choosing each E_i independently and at random, for example from a uniform distribution between 40 kJ mol^{-1} and 60 kJ mol^{-1}. Figure 2.7 summarises example trajectories for 20 such randomisations from a total of 200 realizations. The Q_{10} of rate and Q_{10} of period distributions of those 200 random parametrizations are provided in Figures 2.11; it is clear that, although there are differences in detail between the outputs arising from random parameter sets, the overall qualitative story is unchanged. Naturally,

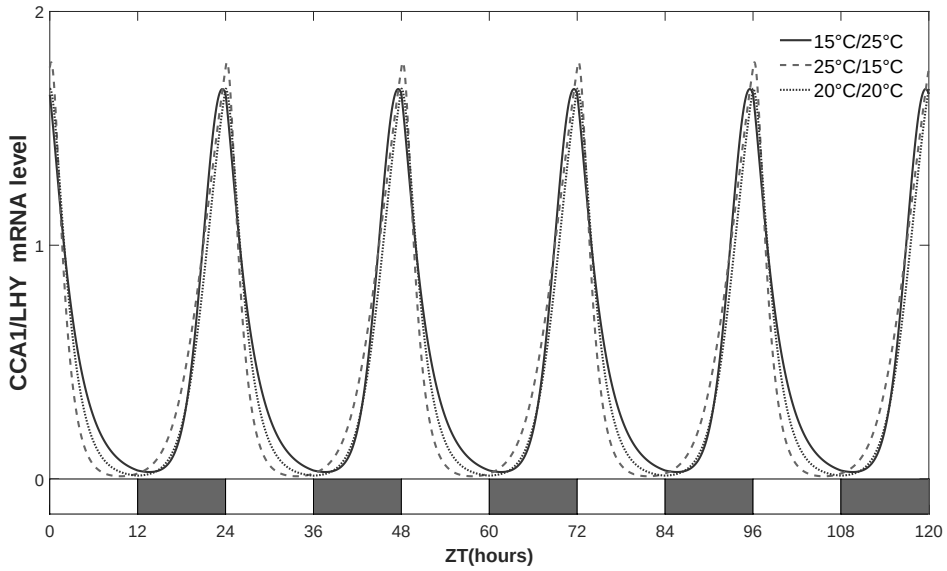

Figure 2.10: **Simulated *CCA1/LHY* expression qualitatively mirrors experimental data contrasting warm/light and cold/dark with cold/light and warm/dark cycles**. Simulations were carried out using a 24 h cycle combining light and temperature forcing. Light and warm, and dark and cold phases were studied in contrast with dark and warm, and light and cold conditions. These combined entraining cycles were designed to compare our results with experimental observations in [88]. Similarly to protocols used for the analysis of LHY expression in Figure 7 of [88], our results correspond to 5 days under a forced clock after 10 days of entrainment.

simulating greater variation in activation energies induces a greater range in modelled outputs. While it is impractical to demand empirical work to estimate Arrhenius parameters governing each interation, theoretical results are useful in emphasising which elements of the circadian clock might be most relevant in driving the overall dynamics. In this case, degradation rates play a surprisingly consistent role in the temperature dependence of the free-running period (Figure 2.8), and these might form the basis for further useful experimental scrutiny.

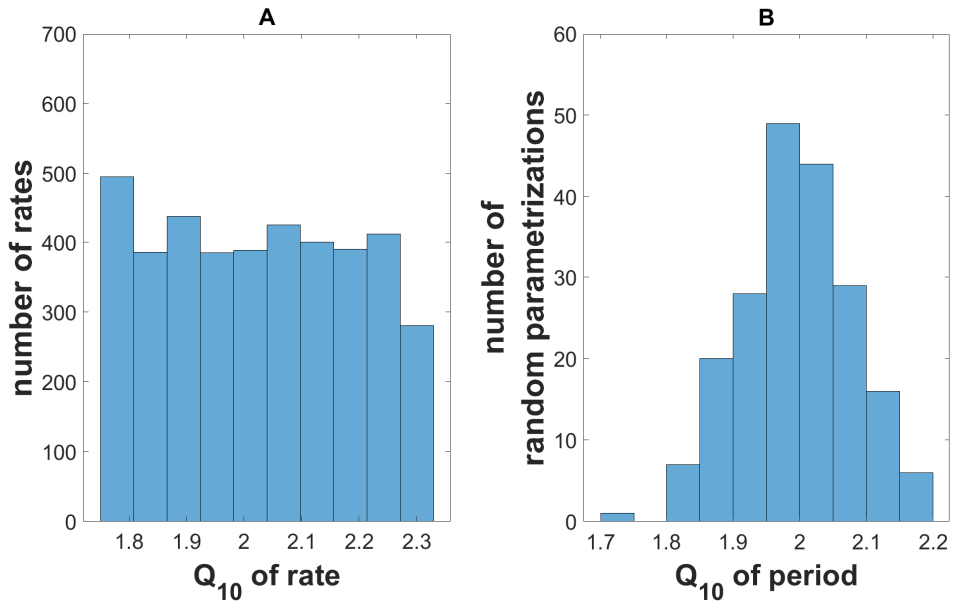

Figure 2.11: **A Q_{10} of period of around 2 is obtained when random activation energy values between 40 kJ mol^{-1} and 60 kJ mol^{-1} are used**. Figure **(A)** shows the distribution of the modelled inputs for 200 trajectories when random parametrizations were implemented. **(B)** displays the distribution of the modelled outputs of those trajectories.

The simple model studied here is based on that of [24], and it is known that this relatively simple model is in principle susceptible to non-trivial resonance and chaotic regimes in its response to regular parametric forcing [55]; these may influence the erratic outcomes observed in, for examples, the extreme temperatures in Figure 2.9. Therefore, to investigate whether the choice of model is critical to the conclusions, we implemented the same theoretical approach to include temperature in the more complex model of [41] (Figure 2.12, 2.13, and 2.14). Again, although differing in some details, very similar results emerge. As with the [24] model, mRNA levels decrease as temperature decreases. Importantly, degradation rates are also key in undercompensation. This supports the importance of interactive work needed between modelling and experiments for future investigation. Efforts should be focused on buillding a model that is able to show temperature compensation by including the recent experimental findings, for example, the placement of HSP90 within the clock for temperature behaviour [90] along with ambient temperature effects on degradation rates [56].

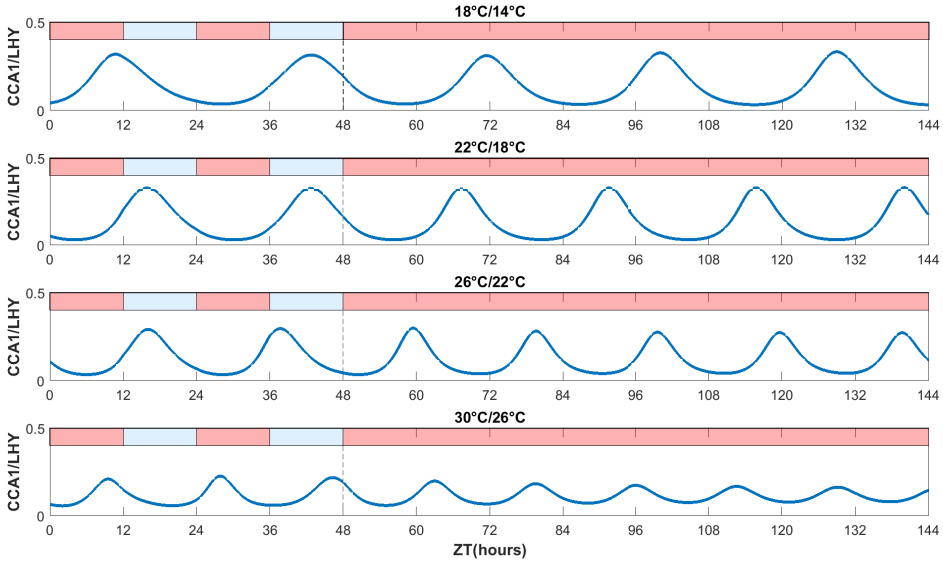

Figure 2.12: **Incorporating temperature dependence in a more complex model [41] supports the conclusions obtained using the [24] model.** A 24 hour 22°C/18°C thermal cycle induces a functional clock. However, colder temperatures (18°C/14°C thermal cycle) cause an increased period while warmer temperatures occasion faster oscillations and a decreased amplitude of the gene expression. To allow model comparison, temperature dependence in [41] was added to the same set of transcription, translation, and degradation parameters as those in the simpler model [24] using the same activation energies.

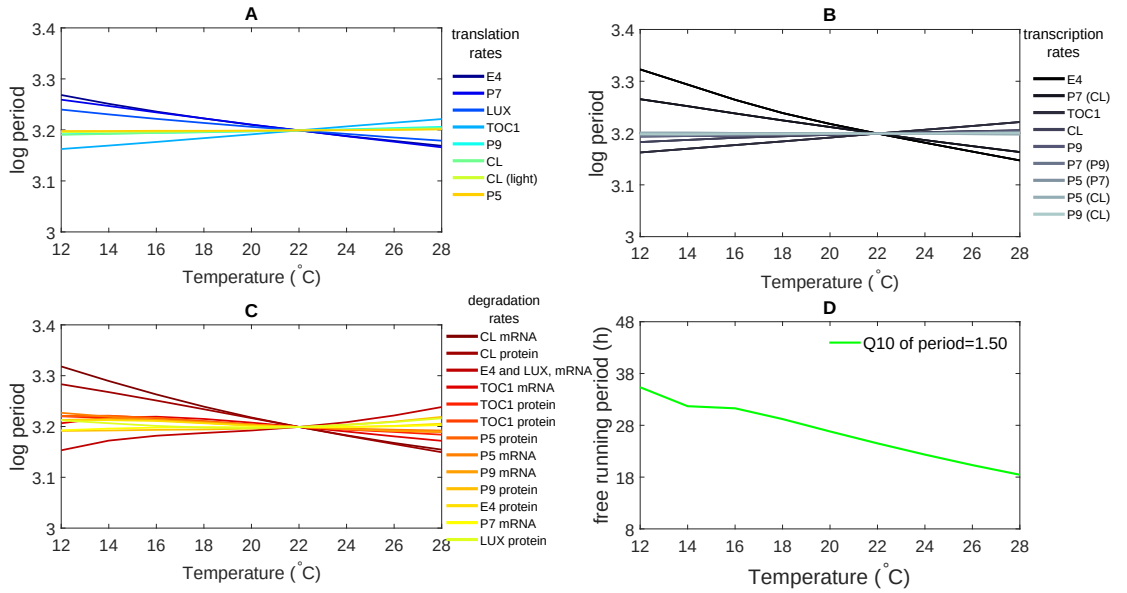

Figure 2.13: **The [41] model is not temperature compensated, and this failure to compensate is driven by degradation rates**. Experimental protocols of [82] and [4] were simulated. A-C show the log period across a range of temperature, where only one parameter is subject to temperature variation for each output. Results are grouped to show thermal dependence of (A) translation, (B) transcription, and (C) mRNA and protein degradation rates. Labels are in order of the size of effect and they show how the parameters' effects are induced (in brackets). The resultant free-running period when all rates vary with temperature is shown in (D). The results are qualitatively similar to those from the [24] model; thermal dependence in translation or transcription rates may either increase or decrease period. This results in a Q_{10} of period lying in the range considered for compensation. However, the effect of changing degradation rates is an overall loss of compensation.

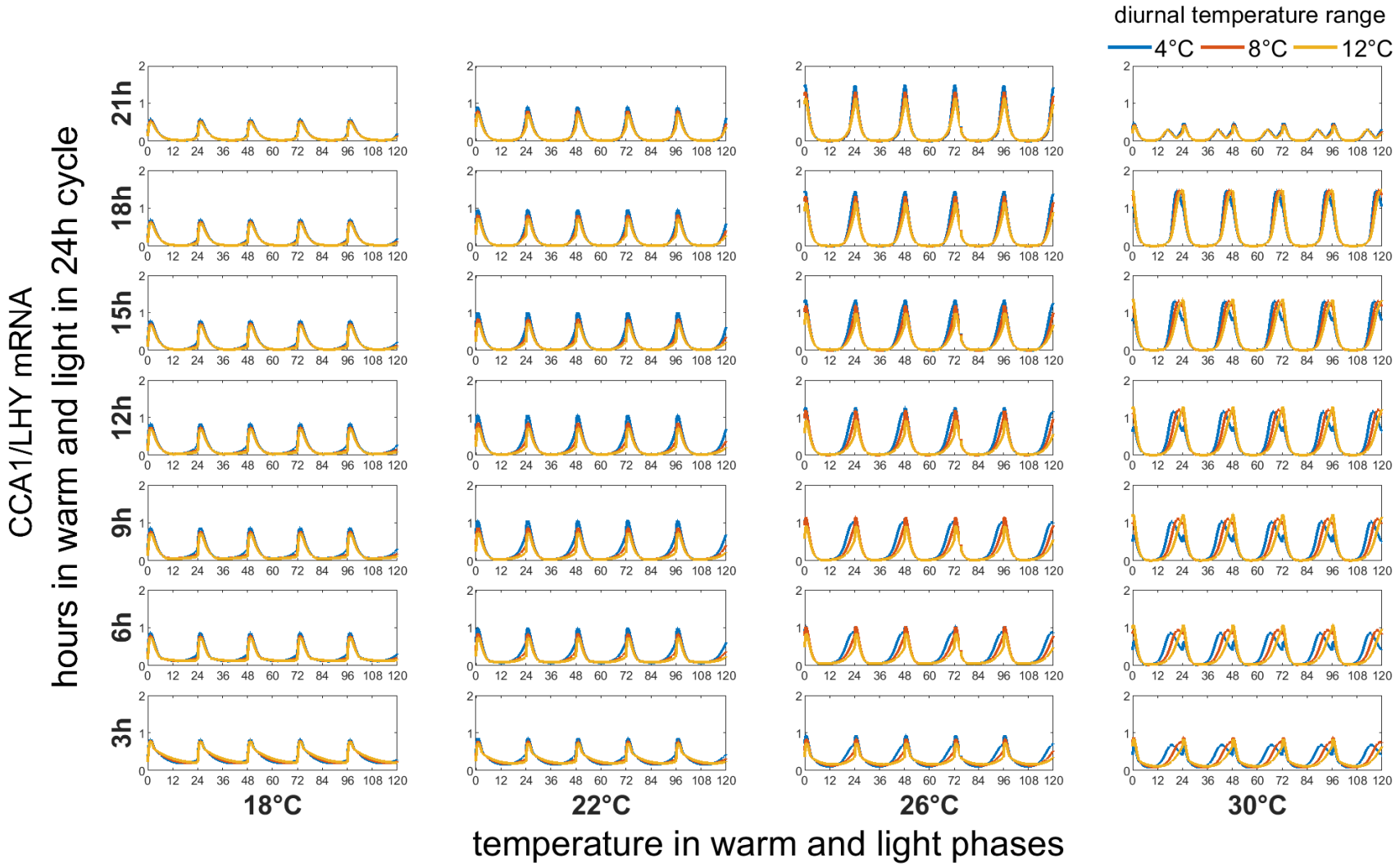

Figure 2.14: **The combined effect of photic and temperature forcing can induce entrainment across a wide range of light-dark durations, but only within narrow temperature limits**. Similarly to the model of [24], at 22°C the clock is correctly entrained. At lower temperatures (first column), a decreased amplitude of the gene expression is observed, and at higher temperatures (final column) there is a general increase in amplitude and non-circadian rhythms might emerge.

Experimental observations for entrainment by temperature cycles have shown that temperature is an important zeitgeber in the plant circadian clock. Even a small change in temperature of 4°C is able to reset the clock [44]. Our results are consistent with this. The simple model presented here has the ability to reproduce sustained oscillations entrained by a relatively small temperature range. Temperature has an important speeding up effect in the entrainment process, and this effect in periodicity is stronger compared to light entrainment [91]. Our clock model mirrors these findings. The free-running period of [24] model (i.e. after photic entrainment) is 23.6 h in constant light [55]. Our model predicts a free-running period of 21.88 h after thermal entrainment when a 24 hour 22°C/16°C thermal cycle is simulated, as observed in [91]. Moreover, results in Figure 2.2 showed that the period observed under entrained conditions is reduced by approximately 10% (on average across the temperatures analysed) when the clock is released into free-running conditions. In contrast, for photic entrainment, the period is reduced by only 2%. Additionally, *PRR9* and *PRR7* clock components have been revealed as necessary for the plant response to thermal cycles [92]. We simulated the clock for the *prr9prr7* double mutant by dividing the relevant transcription rate by a factor of 10 [24], and similar results to [92] were observed (Figure 2.15). *CCA1/LHY* expression clearly oscillated in the *prr9prr7* double mutant, and showed longer period length compared to wild type. A phase delay was also observed in simulations, consistent with [92].

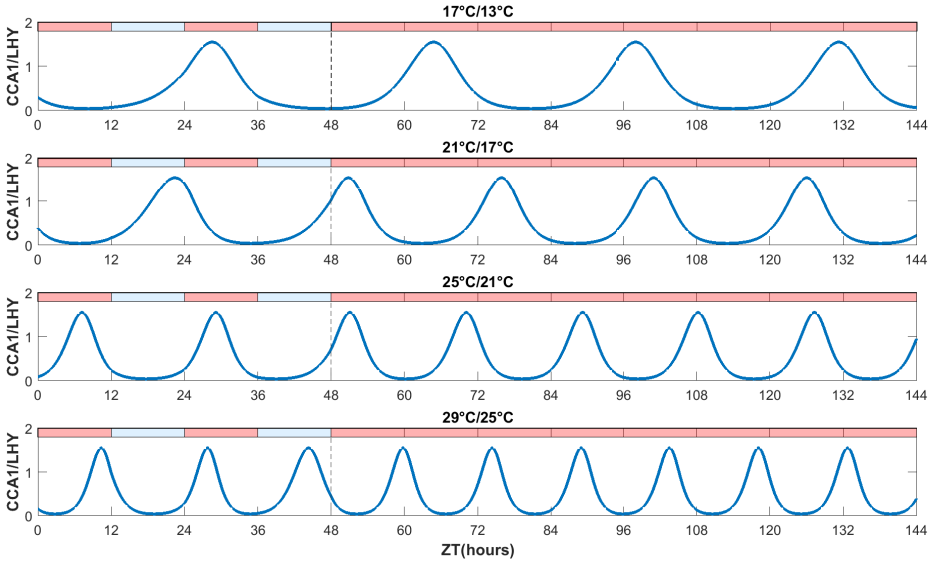

Figure 2.15: ***CCA1/LHY* expression in *prr9prr7* oscillates in response to temperature cycles with a phase shift compared to wild type**. Simulations were carried out similarly to Figure 2.2, in order to compare the outputs with the results obtained for wild type. Results are consistent with [92] observations. Oscillatory behaviour is reproduced in *prr9prr7* with expression levels peaking later than in wild type.

Although our approach gives a pragmatic solution to understand temperature mechanisms in the plant clock, it is not exempt from limitations. It is important to note that, if every rate parameter in a model (complex or otherwise) is affected in the same multiplicative way by changes in temperature, then this is equivalent to a re-scaling of time and no new bifurcational behaviour can emerge. In other words, scaling all rates according to the same Arrhenius relationship is an inappropriate method with which to model the empirically observed entrainment and compensation phenomena.

Explicitly, suppose each rate in a model is scaled by the same factor $f(T)$ which depends on temperature T, and that temperature changes according to some deterministic function of time, $T = g(t)$. One may then write the dynamics of each of the model's dynamic variables x_i as

$$\frac{\mathrm{d}x_i}{\mathrm{d}t} = \sum_{\text{all interactions}} f(T)h_i(\mathbf{x}),$$

where the functions h_i describe the modelled interactions in the absence of any temperature dependence. Trivially, one then has

$$\frac{\mathrm{d}x_i}{\mathrm{d}t} = f(g(t)) \sum_{\text{all interactions}} h_i(\mathbf{x}),$$

so that if one defines a new time, τ, by

$$\tau = \int f(g(t))\mathrm{d}t,$$

then by the chain rule one simply arrives at

$$\frac{\mathrm{d}x_i}{\mathrm{d}\tau} = \frac{\mathrm{d}x_i}{\mathrm{d}t}\frac{\mathrm{d}t}{\mathrm{d}\tau} = h_i(\mathbf{x}),$$

as in the non time- (and temperature-) dependent case. Hence applying the same rate scaling across all parameters corresponds to a (possibly non-uniform) scaling of time, and cannot usefully describe any change in the model's behaviour in response to forcing. Scaling rates with different Arrhenius relationships, or scaling only a subset of rates where this is experimentaly tractable and/or supported by empirical results, is therefore necessary to allow models to display temperature entrainment and compensation.

Previous work based on the Goodwin model for *Neurospora* [52, 48] solved this problem by applying small activation energy values to the degradation rates of the model (making those practically insensitive to temperature) and large values to the production rates. Similarly, [49] in their model for *Chlamydomonas* assigned smaller activation energy values to the degradation rates compared to the values used for production rates in order to achieve temperature compensation. That is, in both cases negative feedback regulation on the transcription of the components of the network is crucial for robustness against temperature changes. Because translation rates play a key role in determining protein levels, which in turn affect transcription, and taking into consideration the results in Chapter 1, where temperature sensitivity in translation rates was effective in entraining the clock, in the remaining chapters we assume that translation rates vary with temperature but that degradation rates are not influenced by temperature. This approach is taken with the aim to obtain qualitative insights on temperature-dependent function of the clock as a whole. However, modelling the influence of temperature in the full range of post-transcriptional and/or post-translational processes is still an open question to answer.

The principal conclusion of this study is to distinguish between the phenomena of entrainment and compensation; robust temperature compensation depends on the interrelationship of a network of temperature-dependent processes and is particularly sensitive to details of temperature-dependent degradation, whereas entrainment to temperature alone operates within a more confined parameter space. In more realistic conditions where both light and temperature fluctuate, the circadian clock is predicted to show a robustness which would be hidden if each varying factor were to be considered alone.

3 Exploring the Role of HSP90 within the Circadian Clock

Abstract

Biological experiments and mathematical models have provided useful understanding of what genes integrate the circadian system, how they interact together and how light affects this complex system. Despite these advances, the importance of temperature in circadian mechanisms, and its role in regulating clock function, is poorly understood. HEAT SHOCK PROTEIN90 (HSP90) is an essential protein that helps in folding, activation, stabilisation and degradation to other proteins. Recently, experimental results showed that HSP90 participates in temperature entrainment of the *Arabidopsis* clock, but the pathway via which it interacts within the clock is not precisely clear. Here we incorporate temperature dependence into a recent light-dependent model, to investigate the possible functions of HSP90 in the plant circadian clock. To elucidate the role of HSP90 in entrainment, we simulate the effect of Geldanamycin, which is known as an inhibitor of the function of HSP90. Moreover, we adapt the original model to exhibit *PRR9* and *PRR7* as functionally independent responses and compare the outputs of these revised models with experimental results generated by the Davis Lab (Department of Biology, University of York). Numerical investigations lead us to propose that HSP90 inhibits *CCA1/LHY* transcription, promotes *ELF4/LUX* translation, and inhibits the translation of *PRR9* and *PRR7*. Our numerical results support the hypothesis, suggested from experiments, that HSP90 influences the morning loop and is required for proper thermal entrainment (but not for light entrainment).

3.1 Introduction

The process of detecting diurnal changes and resetting the circadian clock by external cues such as light and temperature is called entrainment [93, 2]. When the clock is entrained, the biological rhythms generated by this mechanism synchronize with the 24 h day/night cycle. A recent model [24] proposes that regular variation in light inputs, coupled with a majority of negative regulatory interactions between the genes and their mRNA and protein products, can explain light entrainment in the *Arabidopsis thaliana* circadian clock [55]. The effect of light is proposed to act on all components of the clock during the transcription, translation, and mRNA and protein degradation processes of the system. This recent model not only reproduces wild type responses to light over a wide range of regimes but is also able to reproduce clock features observed for a range of plant mutants.

Despite the enormous advances in the understanding of the inner mechanisms underpinning light sensitive behaviour [24, 42, 66], the underlying system that explains temperature behaviour remains poorly established. Experimental observations have shown that temperature is an important zeitgeber in maintaining syncronization with diurnal

environmental changes [92]. For instance, an external temperature cue involving temperature changes as small as 4°C can reset the clock [44]. Thus, elucidating this system that controls plant growth and development is crucial in adapting to a changing climate. As an example, in the climate warming scenario, agricultural production could be affected and it might be needed to translocate crop plants to a new optimal environment to facilitate growth and reproduction, making relevant the understanding of the clock mechanism.

Our previous mathematical work [26] has highlighted the importance of mRNA and protein degradation processes on temperature compensation of the plant clock. We have emphasised the need for further interactive work between modelling and experiments to reveal the temperature system. We believe that it is needed to facilitate a more detailed characterization of post-transcriptional and/or post-translational processes. It also provides a framework within which to include new components known to contribute to temperature entrainment, such as HEAT SHOCK PROTEIN90 (HSP90) [90].

HSP90 is an essential protein that helps in folding, activation, stabilization and degradation to other proteins [94]. Diverse roles within the *Arabidopsis* circadian clock have been associated to HSP90 as result of the interaction with *ZEITLUPE* (*ZTL*) and *GIGANTEA* (*GI*). Examples of roles include maturation and accumulation of *ZTL* [95] and thermotolerance to the plant circadian clock [96]. Recently, the Davis group (University of York) has shown that HSP90 plays an important part in circadian periodicity via its interaction with *CCA1*, *LHY* and *PRR7*. They have also shown that inhibition of HSP90 function by Geldanamycin (GDA) affects expression levels of *CCA1* and *LHY*, and that this effect can be observed under temperature entrainment but not under light entrainment (not published). Additionally, their results showed that GDA does not affect transcription of *CCA1* and *LHY* in the *prr9* mutant, disclosing a functional independence between *PRR9* and *PRR7* within the plant clock.

Here we aimed to understand what mechanisms may underpin the influence of HSP90 in entrainment. For this, mathematical simulations were carried out based on the mathematical model of [24], which was developed for light entrainment, and was extended to temperature entrainment by [26]. We systematically explored a range of possible modifications of the original model in [24] in order to ask in which scenarios it is possible to obtain a functional circadian clock that distinguishes *PRR9* and *PRR7* as functionally independent. We proposed a clock structure where *CCA1/LHY* inhibits *PRR9* and promotes *PRR7*, and hypothesised that temperature affects translation rates of the model. By simulating the effect of GDA we were able to reproduce key features observed in experiments. Overall, our simulations support the hypothesis that HSP90 influences the morning loop during thermal entrainment and not under light entrainment.

3.2 Methods

3.2.1 The model

Experimental results of the Davis group (University of York) showed differences between *prr9* and *prr7* mutants when plants were treated by Geldanamycin contrasted to plants with no treatment in both *CCA1* and *LHY* expression, revealing distinct roles of *PRR9* and *PRR7* in clock regulation by temperature. However, the model [24] combines *PRR7* and *PRR9* roles and represents them as a single model variable, named P97. We therefore modified the model to separate the variable P97 in order to reproduce the experimental observations.

The model structures investigated here come from numerical investigation of eight modifications (M1, M2, ..., M8) of the model [24] (see Figure 3.1). Each modification was designed to present *PRR9* and *PRR7* as separate components. The model M1 in Figure 3.1 shows the least modification implemented. That is, *PRR9* and *PRR7* as separate components interact within the network in the same manner than *PRR9/PRR7* does in [24]. In contrast, M6 shows a clock structure where *PRR9* activation by *CCA1/LHY* is replaced by inhibition, and *PRR7* inhibition by *ELF4/LUX* is missed.

The resulting models are composed of 11 ordinary differential equations (ODEs) rather than nine as in the model [24]. Furthermore, because we firstly aimed to investigate a clock structure suitable of having *PRR9* and *PRR7* separate, rather than to investigate the impact of the parameters in the dynamics of the plant system, parameter values were taken from the original model. In cases when *PRR9* and/or *PRR7* were repressed by *CCA1/LHY* (M4 to M8 models), the mean of the original parameter values that go into *P*97 inhibition was used for parameterization and it was named as K_{11} (Table 2, Supplementary Material). That is, K_{11} is the mean between the Hill function parameters K_4 and K_5 for inhibition of *PRR9/PRR7* by *PRR5/TOC1* and *ELF4/LUX* in the original model, respectively. In the case when *CCA1/LHY* was activated by *PRR9* (M3 model), parameter values for *PRR9/PRR7* activation by *CCA1/LHY*, which is the sole positive interaction in the original model, were used, i.e. the Hill function parameter K_3 with the constant rate v_{2B}.

The model chosen for this study is the clock structure presented as M4 (see Section 3.1.1 in Results). This model differs from the original model in the following key respects:

- *PRR9/PRR7* is split into two separate components, *PRR9* and *PRR7*.
- The role of *PRR7* component within the network of interactions, as described by [24], is unchanged.

- Unlike the original model, *CCA1/LHY* inhibits *PRR9*.

The results of the model [24], and the equivalent model where *PRR9* and *PRR7* are split, are indistinguishable (from a practical point of view) when thermal factors are not included in the simulations (Figure 3.2C). This supports the idea of the model [24] being a useful minimal model for light-dark entrainment.

To model the role of HSP90, thermal factors were included via the Arrhenius law. All translation rates of the model were allowed to vary with temperature, i.e. the parameters p_1, p_{1L}, p_2, p_3 and p_4 of the model (Table 2 in Supplementary Material). The activation energy values allocated to those parameters were 50, 50, 70, 50 and 40 kJ mol^{-1}, respectively. These values enabled the reproduction of sustained oscillations of the plant circadian clock and the prediction of the peak phase of *CCA1/LHY* at dawn observed in experiments. *prr9* and *prr7* single mutants were simulated by reducing the respective transcription rate by a factor of 10. For double mutants, both *PRR9* and *PRR7* transcription rates were divided by 10. The fitting of the GDA effect observed in these experiments was explained by the interaction of *CCA1/LHY*, *PRR9*, *PRR7* and *ELF4/LUX* components. GDA treatment was simulated by increasing the transcription rate of *CCA1/LHY* by a factor of 10 and by increasing the translation rates of PRR9 and PRR7 by a factor of 2.5. It was also required to divide the translation rate of *ELF4/LUX* by 3 to observe GDA effects. When the transcription rate of *CCA1/LHY* goes faster, lengthening of periodicity is observe immediately due to overexpression of *CCA1/LHY*. This effect also requires altering the translation processes of *PRR9*, *PRR7* and *ELF4/LUX*.

All clock structures were implemented in MATLAB. Simulations were performed using the ODE23s solver to obtain the numerical solutions of each system of ODEs.

3.2.2 Simulations vs experiments

We present experimental results of the Davis group (not published) and compare our simulation outputs with those observations. For Figures 3.3–3.6, *Arabidopsis* seedlings were grown for 7 days under warm-cold and light-dark conditions respectively. On day 6, seedlings were transferred to plates containing dimethyl sulfoxide (DMSO), an organic solvent used as the control, and geldanamycin-treated plants were exposed to the drug. All samples were collected every 2 hours. In wild type cases, from ZT20 to ZT12 next morning, whereas in mutant plants, from ZT0 to ZT12. The Zeitgeber time (ZT) is given for a unit of an hour. The phases ZT0 and ZT24 indicate the beginning of the light or warm temperature phases (i.e. dawn), and ZT12 and ZT36 the beginning of the dark or cold temperature phases (i.e. dusk) in a 24 h cycle. We have omitted details of the

material used in experiments as it is beyond the core of this work.

To simulate GDA treatment, parameter values were changed at day 6 under entrained conditions (in both light and temperature entrainment), and its effect was observed on day 7.

3.3 Results

3.3.1 *PRR9* and *PRR7* as separate components

With the aim to find a functional clock structure which was best able to reproduce the experimental observations, and yet remained faithful to plausible biological mechanisms, we simulated the clock for eight modifications of [24] model under light-dark conditions (Figure 3.1). Each clock structure was run for seven days in cycles of 12 h light and 12 h dark, followed by release into free-running conditions (continuous light), using the methods and tests developed in Chaper 1. We found three general classes of clock responses in this scenario, as illustrated in Figure 3.2. These outputs show the simulated mRNA levels of *CCA1/LHY* in the last two days under entrainment and five days after release into continuous light.

Figure 3.2A displays *CCA1/LHY* gene expression for the models M2, M3, M6 and M7. A dysfunctional clock is obtained in all cases. Although circadian oscillations are possible when the clock is forced, they are not sustained in continuous light. The reason for this may be the absence of *ELF4/LUX* repressing *PRR7*, a feature shared for these clock structures. In all these models, the lost of this interaction implies that the clock system misses at least a negative feedback loop, which is known to be essential for oscillatory behaviour.

Figure 3.2B shows outputs for M5 and M8, which also reproduced dysfunctional clocks. Similar to cases in Figure 3.2A, no oscillations are observed in continuous light and a 24 h period is obtained under entrained conditions. By contrast, the clock response to light-dark cycle is nontrivial. Simulated mRNA levels show an amplitude roughly seven-fold higher. They accumulated much faster immediately after light off, resulting in high levels during the entire dark phase. In these cases, no positive interactions between genes were modelled, which implied an increase in the number of positive feedback loops within the clock networks.

Unlike previous cases, models M1 and M4 allow for functional clocks. In both models, the clock entrains to a 24 h cycle and oscillations are maintained after the release of the clock into free-running conditions (Figure 3.2C). Because M4 differentiates the role of *PRR9* and *PRR7* in the clock network and closely matches the outputs of the original

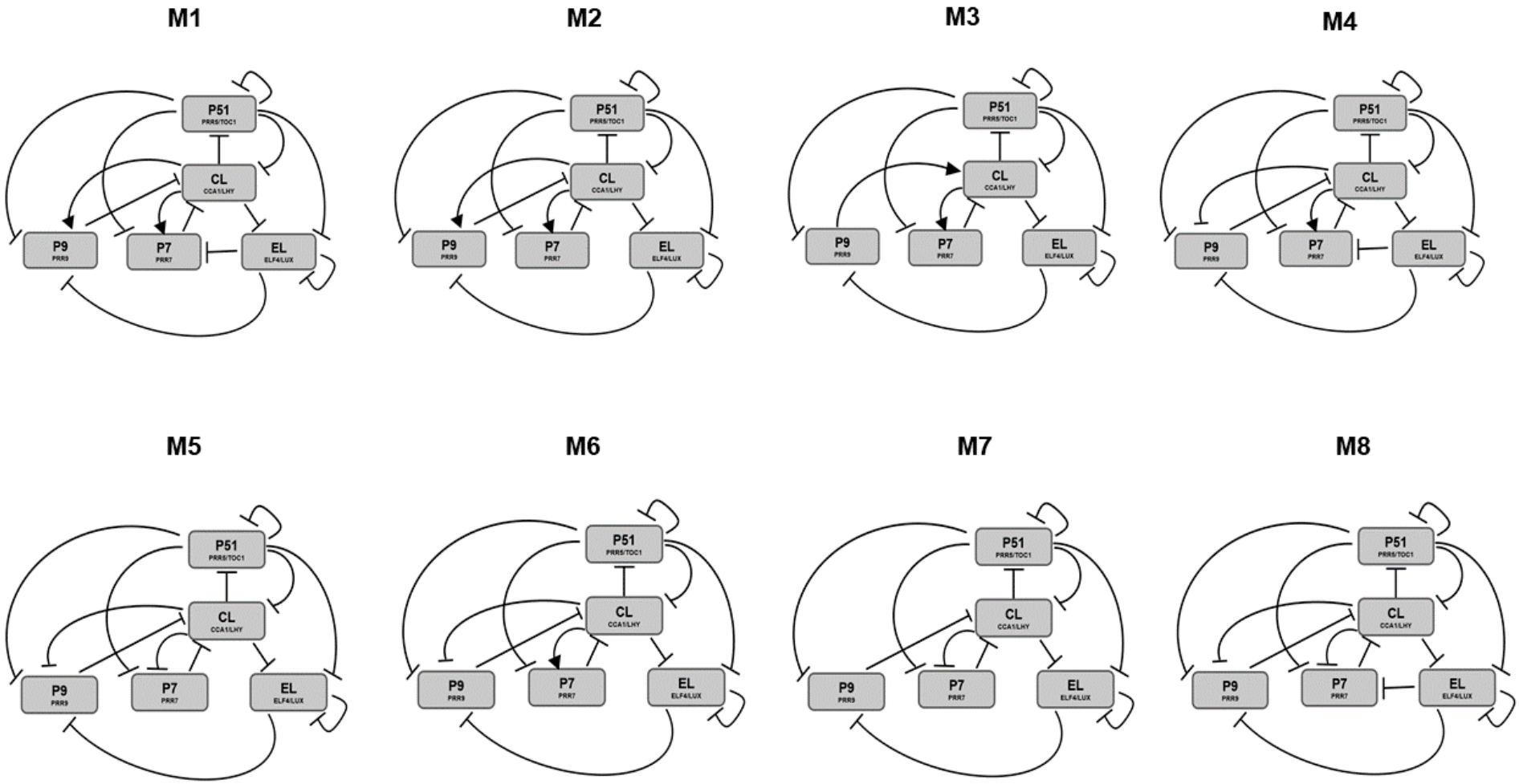

Figure 3.1: **Eight modifications of the model [24], where *PRR9* and *PRR7* are considered as separate components within the circadian oscillator**. Similar genes were merged into the single variables CL, P51, and EL, which represent the pair of genes *CCA1/LHY*, *PRR5/TOC1*, and *ELF4/LUX*, respectively, whereas the variables P9 and P7 represent *PRR9* and *PRR7*, respectively. Interactions that go from P51 component were kept, while interactions between the variables CL, EL, P9 and P7 were defined arbitrary.

model, it will form the basis of this study to analyse the role of HSP90 in entrainment.

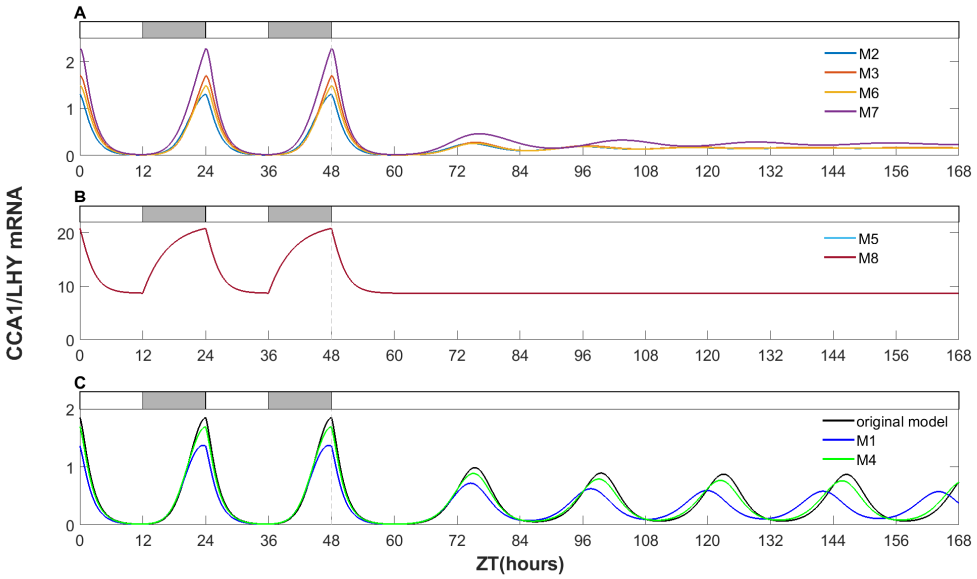

Figure 3.2: **M1 and M4 models allow functional clocks.** Outputs of the proposed models in Figure 3.1 grouped according to their clock responses to change in light conditions. Each panel shows simulated *CCA1/LHY* expression in the last two days of seven days of entrainment under a 24 h light-dark cycle and five days in constant light. A) Similar responses for M2, M3, M6 and M7 models were found. B) shows the simulated gene expression for M5 and M8 models. In neither case A or B there is a viable free-running circadian oscillator, in sharp contrast with biological observation. C) Responses of M1 and M4 are compared with the original model in [24]. Sustained circadian oscillations are clearly preserved in this models, in contrast to cases A and B.

3.3.2 Experimental observations

Figures 3.3 and 3.4 show experimental results by the Davis Lab Group for *CCA1* and *LHY* expression profiles. The experiments contrasted gene expressions of *CCA1* and *LHY* under light-dark and warm-cold conditions in wild type plants treated and non-treated with geldanamycin. The key point observed is that geldanamycin did not change the expression of *CCA1* (Figure 3.3A), and nor did it change *LHY* (Figure 3.4A) under light-dark entrainment. However, *CCA1* and *LHY* levels were affected by the drug under thermal entrainment (Figures 3.3B and 3.4B). In treated plants, lower transcript levels of both genes were observed before ZT4, followed by relatively higher gene expression levels in comparison with non-treated. *CCA1* expression was also phase shifted by geldanamycin,

showing its highest levels between ZT4 and ZT6 rather than peaking at ZT0 (Figure 3.3B).

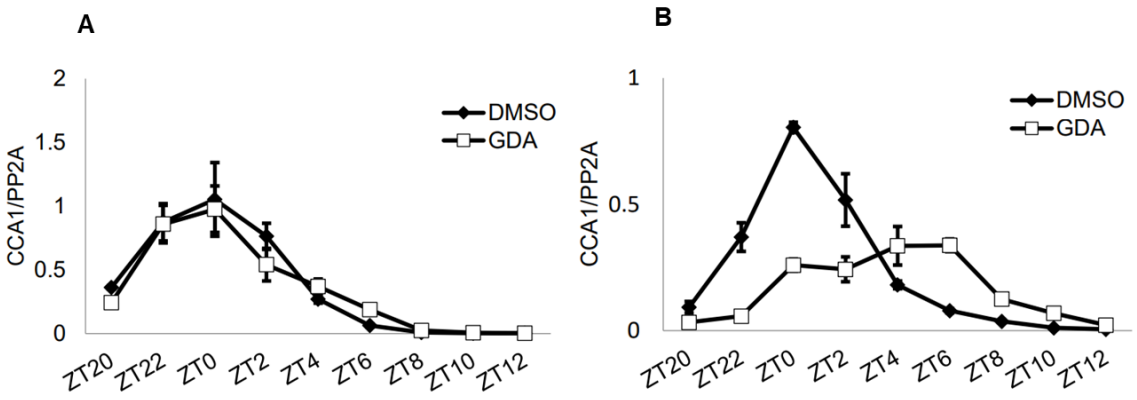

Figure 3.3: ***CCA1* expression in warm-cold, but not light-dark entrained plants is affected by geldanamycin application**. Experimental observations of *CCA1* expression in WT plants treated with DMSO or with 2 μM geldanamycin (GDA). A) shows results for plants under light entrainment, and B) shows results under temperature entrainment. On day six of entrainment (either light or temperature entrainment), plants were exposed to the GDA treatment and were re-entrained for one day. Gene expression is normalised to PROTEIN PHOSPHATASE 2a subunit 3A (PP2A) and represents a mean of three biological replicas. Error bars represent standard deviation.

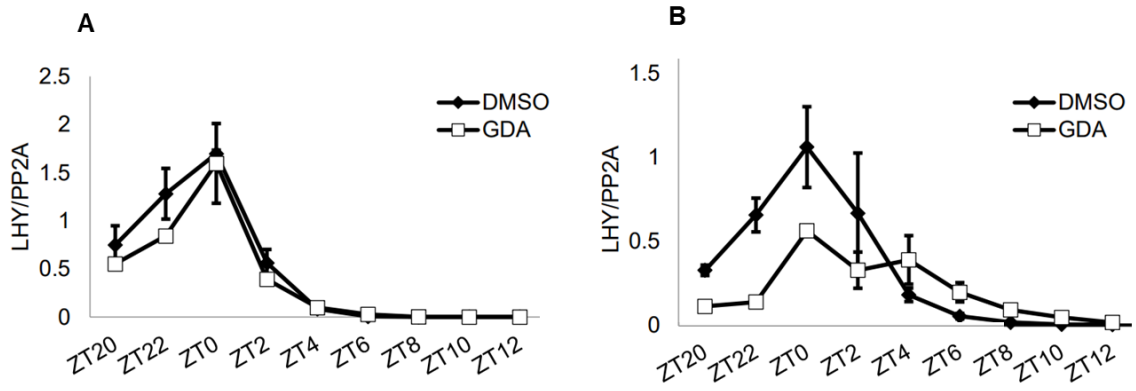

Figure 3.4: ***LHY* expression in warm-cold, but not light-dark entrained plants is affected by geldanamycin**. Experimental observations of *LHY* expression in WT plants treated with DMSO or with 2 μM geldanamycin (GDA). A) shows results for plants under light entrainment, and B) shows results under temperature entrainment. On day six of entrainment (either light or temperature entrainment), plants were exposed to the GDA treatment and were re-entrained for one day. Gene expression is normalised to PROTEIN PHOSPHATASE 2a subunit 3A (PP2A) and represents a mean of three biological replicas. Error bars represent standard deviation.

In order to know whether HSP90 affects both *CCA1* and *LHY* expressions through *PRR7* and *PRR9*, the Davis Group analysed the effect of GDA on *prr9*, *prr7*, and *prr9prr7* mutant plants in the morning. Results for *CCA1* are shown in Figure 3.5. No differences in gene expression were found between treated *prr9* plants and non-treated (Figure 3.5A). The same was observed for *prr9prr7* double mutant plants (Figure 3.5C). However, geldanamycin did affect the expression levels of *CCA1* in *prr7*. After ZT2, treated *prr7* showed higher transcript levels compared to non-treated plants (Figure 3.5B). The same results were found for *LHY* (Figure 3.6).

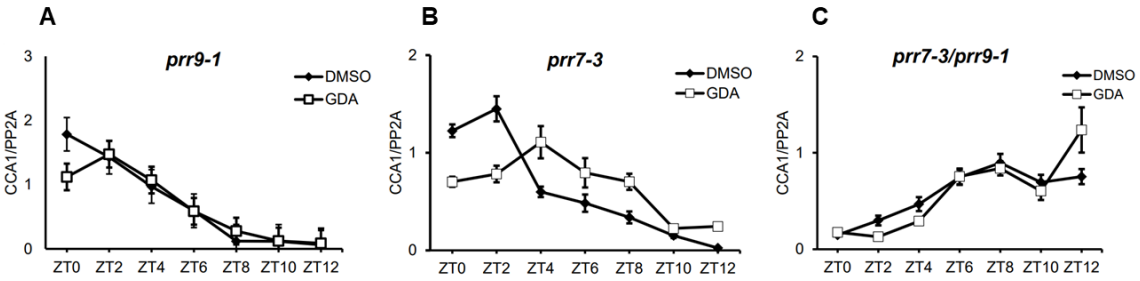

Figure 3.5: **Geldanamycin regulation of *CCA1* is affected in the *prr7* experiments, but not in the *prr9* experiments**. Experimental observations of *CCA1* expression in *prr7* (A), *prr9* (B), and *prr9prr7* (C). Plants were treated with DMSO or with 2 μM geldanamycin (GDA) on day six under temperature entrained conditions, and then were re-entrained for one day. Gene expression is normalised to PROTEIN PHOSPHATASE 2a subunit 3A (PP2A) and represents a mean of three biological replicas. Error bars represent standard deviation.

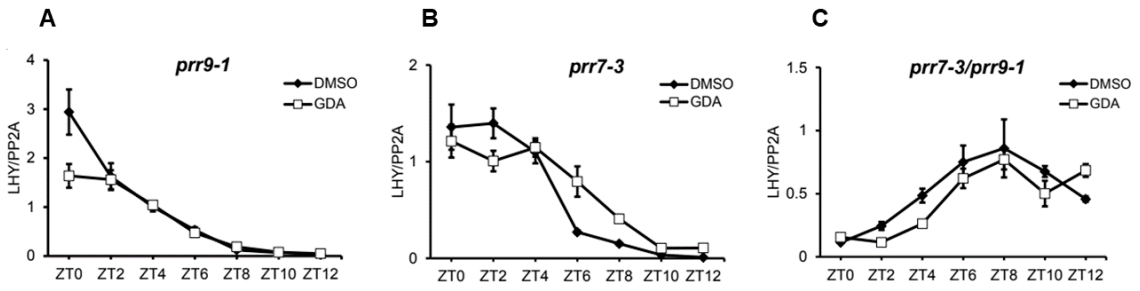

Figure 3.6: **Geldanamycin regulation of *LHY* is affected in the *prr7* but not in the *prr9* background**. Experimental observations of *LHY* expression in *prr7* (A), *prr9* (B), and *prr9prr7* (C). Plants were treated with DMSO or with 2 μM geldanamycin (GDA) on day six under temperature entrained conditions, and then were re-entrained for one day. Gene expression is normalised to PROTEIN PHOSPHATASE 2a subunit 3A (PP2A) and represents a mean of three biological replicas. Error bars represent standard deviation.

3.3.3 Modelling the role of HSP90

The following is all based on model M4 (see equations in Supplementary Material) as results in section 3.1.1 demonstrated that it has the ability of characterising clock responses, having *PRR9* and *PRR7* as functionally independent. The experimental results in Figures 3.3–3.6 showed that HSP90 influences the dynamics of the circadian clock explicitly by contributing to entrainment via the morning loop. Here we have hypothesised that HSP90 inhibits *CCA1/LHY* transcription, promotes *ELF4/LUX* translation, and inhibits the translation of *PRR9* and *PRR7*. The presence of GDA (which inhibits HSP90) had the opposite effect. Simulations based on this hypothesis showed that the M4 model was able to reproduce the key features observed in the data for plants under both light entrainment and temperature entrainment (Figure 3.7). Simulated GDA action did not change the expression of *CCA1/LHY* under light-dark conditions, which agreed with experiments in Figures 3.3A and 3.4A. Remarkably, simulations also agreed with experiments shown for

warm-cold conditions in Figures 3.3B and 3.4B, namely,

- GDA damps the expression of *CCA1/LHY* from before dawn until ZT4.
- GDA increases mRNA levels of *CCA1/LHY* after ZT4 compared to WT.
- *CCA1/LHY* peaks between ZT4 and ZT6 in GDA treatment instead of at dawn.

These results provide mechanistically-based theoretical support for the hypothesis that HSP90 influences the morning loop during thermal entrainment.

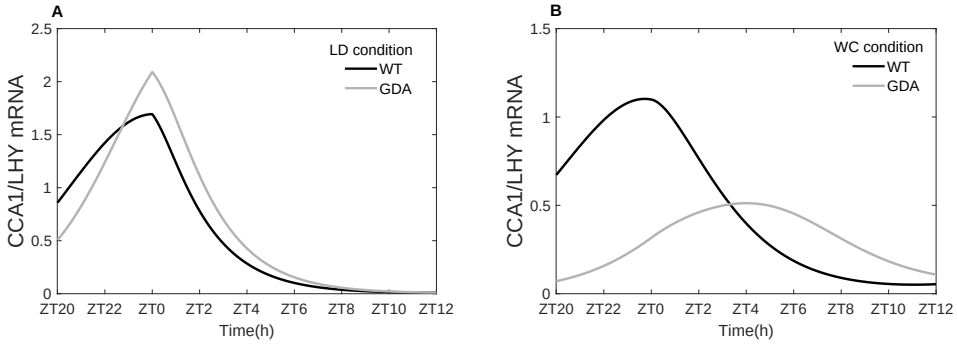

Figure 3.7: ***CCA1/LHY* expression is not affected by GDA in light entrainment, but it is affected in temperature entrainment**. Results from simulations of M4 model during the morning of the day seven of entrainment by a 24 h light cycle in A) (12 h at light and 12 h at dark), and by a 24 h 21°C/17°C thermal cycle in B). In both, ZT0 indicates when light or warm temperature are on. Consistent with observations in Figures 3.3 and 3.4, M4 model supports the hypothesis that HSP90 affects *CCA1/LHY* expression in a temperature dependent manner.

To explore the capability of the model to reproduce observations in mutant plants, we implemented the model for *prr9*, *prr7*, and *prr9prr7* (Figure 3.8). Results from simulations showed that, in the *prr7* mutant, GDA increased mRNA levels of *CCA1/LHY* after ZT6 compared to non GDA treated *prr7* plants. A phase shift is also observed under simulated GDA treatment. These results were again in qualitative agreement with experiments in Figures 3.5B and 3.6B.

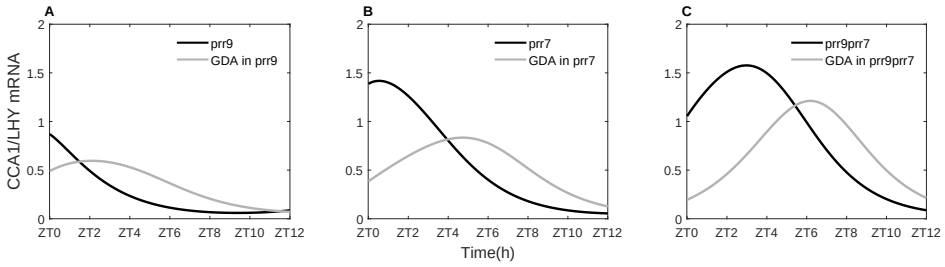

Figure 3.8: ***CCA1/LHY* expression is affected by GDA in *prr7* mutant**. Results from simulations of model M4 during the morning of the day seven of temperature entrainment. A 24 h 21°C/17°C thermal cycle was used. Similarly to experiments in Figures 3.5 and 3.6, M4 model is able to reproduce the effect of GDA in *prr7*, and it partially reproduces the observations in *prr9*. However, it fails to simulate double mutants profile.

It is notable that none of our simulations were able to reproduce the dynamics observed in the *prr9* single and *prr9prr7* double mutants. Numerical results showed that GDA does change the expression of *CCA1/LHY* in these double mutants, but this effect is not observed in experiments. However, the *prr9prr7* simulations show a delay in *CCA1/LHY* expression, and this delay is more noticeable under the simulated application of GDA (Figure 3.8C). The possible reasons for this discrepancy cannot be resolved without further experimental and theoretical work, as alluded to in the Discussion.

3.4 Discussion

The aim of this chapter is to combine experimental observations (mainly from the Davis Lab Group at the University of York) with a range of possible models for the circadian clock, in order to better understand the role of the heat shock protein HSP90. To this end, we extended the simple model of [24] by characterizing *PRR7* and *PRR9* as functionally independent dynamic variables, arriving at a model of the circadian network which is consistent with the existence of an entrainable clock with a free running period close to 24 h. Moreover, we modelled the effect of geldanamycin (GDA) as it is used in experiments, which is known to repress the effect of HSP90. Our results from simulations strongly suggest that one of our models (M4) best describes empirical observations. Our conclusions are consistent with experimental observations, namely that HSP90 acts in the circadian clock through the morning loop in a temperature dependent manner. This mathematical approach has shed light on what processes the current clock models, which are commonly developed to explain behaviour under light-dark conditions without giving consideration to temperature effects, need to be better characterized to explain clock responses to changes in temperature. Overall this work points to the importance of designing a temperature responsive circadian model that includes the latest biological findings to arrive at a better understanding of the complex plant system.

In this analysis, experimental data showed that HSP90 regulates *CCA1* and *LHY* expression and that this was dependent on thermal entrainment. It also revealed that *PRR9* is required to observe the deregulation effects of GDA on *CCA1* and *LHY* expressions but *PRR7* is not required. Interestingly, in [90] it is shown that the *hsp90* mutant exhibits a longer circadian period independent of the entrainment conditions. Moreover, they showed that this effect on period lengthening was lost in *cca1, lhy*, and *prr7*. However, the *prr9* plant mutant did show a longer period. Putting all these together, these results add new evidence supporting the hypothesis that *PRR9* and *PRR7* are functionally independent genes and give insights into a temperature entrainment pathway.

Because the original model of [24] combines the roles of *PRR7* and *PRR9* within a single model variable, whereas the empirical results show that mutations in these clock components have different effects, the model of [24] does not allow the experimental results from mutants to be reproduced. It does, however, provide a modelling framework via which the possible functions of *PRR7* and *PRR9* within the clock can be better understood. We therefore modified this model to include separate *PRR7* and *PRR9* components to test different functions of these genes in the clock system. Some interactions of the [24] model were missed or their roles were changed; for example, in the model M3 the original

repressive interaction of *ELF4/LUX* on *PRR7* is removed and the original repressive role of *PRR9* on *CCA1/LHY* is changed to an activator. These modifications yielded an increase in the number of positive feedback and a decrease in the number of negative feedback loops. Unsurprisingly, in most cases where interactions were missed resulting in a loss of negative feedback, the clock no longer oscillated in free-running conditions. Negative feedback has been formally proved to be necessary for sustained oscillatory behavior, whereas positive feedback has been formally proved to be a requirement for multiple steady states [97, 98, 99]. Furthermore, several works have shown the effect of the number of negative and positive feedback loops in a network and how they correlate to explain the network dynamics [100, 101].

We have used the parameter values published in [24] in our models, rather than attempting to fit or estimate alternative parameterisations. This approach is often used in the literature. For example, [40] took the parameter values from [77] to quantify the interactions between the components that constituted the preceding model, which account for 52 out of the 78 parameters of the model (67%). In [41], the parameters of production (p_7) and degradation (m_{11}) of the light-sensitive activator-protein P were taken from the previous model, [54]. In [42], parameter values of COP1 protein (m_{27}, m_{31}, m_{33}, n_5, n_6, n_{14}, p_6, and p_{15}) and the light-sensitive activator-protein P (p_7), were taken from [41]. Moreover, a large number of parameter values have been constrained to experimental data, making models to be parameterized with a considerable number of values used in predecessor models as they were constrained to the same data.

In our proposed models, the role of some interactions of the [24] were changed. To parameterize the new role (repressor) of *CCA1/LHY* on *PRR7* and/or *PRR9* (M4 to M8 models), the mean of the parameter values of the other interactions (with the same function) as used originally (in [24]) into the *PRR9/PRR7* component was used, namely, the mean between the repressor coefficients K_4 and K_5 in equations (which is termed as parameter K_{11} in the M4 model, see Table 2, Supplementary Material). A comparable approach has been employed previously. In the model [54], *CCA1/LHY* is inhibited by *PRR9*, *PRR7*, and *PRR5* with a common repressor coefficient of the Hill function termed g_1, and a Hill coefficient equal to two; in [41], inhibition by *TOC1* was added into *CCA1/LHY* and this interaction was also parameterized by g_1 with the same previous value of the model [54].

We acknowledge that estimating parameter values is a challenge. To do so successfully, even for relatively simple models such as [24], is likely to require larger datasets and statistical analyses beyond the scope of this thesis. In *Arabidopsis* models, parameter values are commonly taken from previous models, or constrained/fixed to experimental data, or

they are optimized for statistical fitting based on experimental observations. Methods for parameter optimizations have used as a basis the cost function presented in [18] for the first ODE-based model of *Arabidopsis*. This cost function measures the goodness of the model by calculating the difference between elemental characteristics of mRNA levels from experimental data (period, phase, and amplitude), and those characteristics obtained from simulations. Alternatively, [42] presents a cost function where differences between experimental data and simulations are calculated to account for fitting mRNA and protein profiles as a whole, rather than key aspects of oscillations as [18] approach does. However, the question of what is the 'best' fitting method will in general be context- and question-dependent.

The current biological knowledge states that there is a direct repressive effect, which acts alongside an indirect activating effect, of *CCA1* and *LHY* on *PRR9* and *PRR7* [102, 103]. In our attempt to include both *PRR9* and *PRR7* as negative regulatory targets of *CCA1/LHY* (M5 and M8 models), we found non-functional clocks to characterize circadian responses to light. However, we propose a clock structure, summarised by model M4 in Figure 3.1, which includes the direct repressor role of *CCA1/LHY* on *PRR9*, having *PRR7* activated by *CCA1/LHY*. This model is able to reproduce qualitatively the experimental data not just for wild type plants, but also for *prr7*, and partially for *prr9*. These results support the repressive role found of *CCA1* and *LHY* on *PRR9*; however, it also suggests that activation on *PRR7* is needed. This emphasises the need of future investigation to place this positive regulation within the clock.

One of the limitations of the model is its inability to reproduce *prr9prr7* double mutants observations. Figure 3.8C indicates that the model fails to reproduce the observed phase of *CCA1/LHY* in these mutants (Figures 3.5C and 3.6C). Experimental data also shows that *prr9* has a slightly higher dawn peak than *prr7*, but that their expression largely matches up for the rest of the day. This is not observed in any of our simulations. Numerical outputs show a reduced *CCA1/LHY* expression in *prr9* compared to *prr7* mutant, which could explain the phase shift observed in *prr9prr7*. Again, the possibility of a mixture of positive and negative regulation involving *PRR7*, perhaps including other as-yet uncharacterised intermediate proteins, is one which may merit future experimental investigation.

Overall, we have demonstrated that our model is a useful tool to drive important hypothesis: our fundamental theoretical result is that HSP90 assists the plant clock in temperature entrainment via the morning loop, which agrees with biological findings [90]. Moreover, our approach highlights the need of designing a more accurate model oscillator to explain temperature behaviour for the plant system. A re-design of the morning loop

established up to date in most models is indispensable.

In [104], the authors provide four elemental conditions for biochemical oscillators: negative feedback, time delay, sufficient nonlinearity in the reaction rates of the system, and the opposite reaction rates have to be adequately balanced. For *Arabidopsis*, [26] hypothesize how light and temperature affect the robustness of the plant clock and emphasize the need of characterizing post-transcriptional and/or post-translational processes in more details for temperature mechanisms. [28] describe the role of specific interactions of activation and inhibition (called motifs) in the plant network, and give an explanation of how these particular structures may explain the plant clock dynamics. Current biological results suggest that it is possible to incorporate HSP90 as a clock component to regulate *CCA1/LHY* and *PRR7* through an undefined protein [90]. The fact that several temperature coefficient Q_{10} values for mRNA transcription and degradation rates have been published [56] helps to make this ambition a realistic prospect. Although defining a modelling approach to include the recent experimental findings is non-trivial, we can profit from the advances in mathematical modelling along with the recent biological discoveries to lead to an improved knowledge of the underlying clock structure of plants and the complexity of its functions.

The work in this chapter helps to elucidate the design principles of the plant clock, and emphasises the role of interdisciplinary work from biology and mathematical modelling to explain its complex responses to changes in light and temperature. We believe that analyzing and comparing the historical *Arabidopsis* models by incorporating temperature dependence into them will give advantages for the comprehension of the underlying structure of this clock. Because each clock model structure proposed historically differs from others not just in mathematical complexity but also in the way they represent the state of the biological findings in time, a systematic description of this will be beneficial to define modelling strategies for the plant circadian community. These observations provide a natural link to the remaining chapter of this thesis where more general principles of the circadian clock are explored.

3.5 Supplementary Material

The M4 model

The M4 model is summarised by the following system of ordinary differential equations.

$$\frac{d[CL]_m}{dt} = (v_1 + v_{1L} * L * [P]) * \frac{1}{1 + (\frac{[P97]_p}{K_1})^2 + (\frac{[P51]_p}{K_2})^2} - (k_{1L} * L + k_{1D} * D) * [CL]_m$$

$$\frac{d[CL]_p}{dt} = (p_1 + p_{1L} * L) * [CL]_m - d_1 * [CL]_p$$

$$\frac{d[P9]_m}{dt} = (v_{2L} * L * [P] + v_{2A}) * \frac{1}{1 + (\frac{[P51]_p}{K_4})^2 + (\frac{[EL]_p}{K_5})^2 + (\frac{[CL]_p}{K_{11}})^2} - k_2 * [P9]_m$$

$$\frac{d[P9]_p}{dt} = p_2 * [P9]_m - (d_{2D} * D + d_{2L} * L) * [P9]_p$$

$$\frac{d[P7]_m}{dt} = (v_{2L} * L * [P] + v_{2A} + v_{2B} * \frac{[CL]_p^2}{K_3^2 + [CL]_p^2}) * \frac{1}{1 + (\frac{[P51]_p}{K_4})^2 + (\frac{[EL]_p}{K_5})^2} - k_2 * [P7]_m$$

$$\frac{d[P7]_p}{dt} = p_2 * [P7]_m - (d_{2D} * D + d_{2L} * L) * [P7]_p$$

$$\frac{d[P51]_m}{dt} = v_3 * \frac{1}{1 + (\frac{[CL]_p}{K_6})^2 + (\frac{[P51]_p}{K_7})^2} - k_3 * [P51]_m$$

$$\frac{d[P51]_p}{dt} = p_3 * [P51]_m - (d_{3D} * D + d_{3L} * L) * [P51]_p$$

$$\frac{d[EL]_m}{dt} = L * v_4 * \frac{1}{1 + (\frac{[CL]_p}{K_8})^2 + (\frac{[P51]_p}{K_9})^2 + (\frac{[EL]_p}{K_10})^2} - k_4 * [EL]_m$$

$$\frac{d[EL]_p}{dt} = p_4 * [EL]_m - (d_{4D} * D + d_{4L} * L) * [EL]_p$$

$$\frac{d[P]}{dt} = 0.3 * (1 - [P]) * D - [P] * L$$

Parameter values were taken from [24]. The addition of K_{11} is specified in Methods, section 3.2.1.

Parameter description	Name	Value	Units
CL transcription	v_1	4.6	nM.h^{-1}
CL light-induced transcription	v_{1L}	3.0	nM.h^{-1}
P9 and P7 transcription	v_{2A}	1.3	nM.h^{-1}
P7 CL-induced transcription	v_{2B}	1.5	nM.h^{-1}
P9 and P7 light-induced transcription	v_{2L}	5.0	nM.h^{-1}
P51 transcription	v_3	1.0	nM.h^{-1}
EL transcription	v_4	1.5	nM.h^{-1}
CL mRNA degradation (light)	k_{1L}	0.5	h^{-1}
CL mRNA degradation (dark)	k_{1D}	0.2	h^{-1}
P97 mRNA degradation	k_2	0.4	h^{-1}
P51 mRNA degradation	k_3	0.6	h^{-1}
EL mRNA degradation	k_4	0.6	h^{-1}
CL translation	p_1	0.8	h^{-1}
CL light light-induced translation	p_{1L}	0.4	h^{-1}
P97 translation	p_2	1.0	h^{-1}
P51 translation	p_3	0.6	h^{-1}
EL translation	p_4	1.0	h^{-1}
CL degradation	d_1	0.7	h^{-1}
P97 degradation (dark)	d_{2D}	0.5	h^{-1}
P97 degradation (light)	d_{2L}	0.3	h^{-1}
P51 degradation (dark)	d_{3D}	0.5	h^{-1}
P51 degradation (light)	d_{3L}	0.8	h^{-1}
EL degradation (dark)	d_{4D}	1.2	h^{-1}
EL degradation (light)	d_{4L}	0.4	h^{-1}
Inhibition: CL by P97	K_1	0.2	nM
Inhibition: CL by P51	K_2	1.2	nM
Activation: P7 by CL	K_3	0.2	nM
Inhibition: P9 and P7 by P51	K_4	0.2	nM
Inhibition: P9 and P7 by EL	K_5	0.3	nM
Inhibition: P51 by CL	K_6	0.5	nM
Inhibition: P51 by itself	K_7	2.0	nM
Inhibition: EL by CL	K_8	0.4	nM
Inhibition: EL by P51	K_9	1.9	nM
Inhibition: EL by EL	K_{10}	1.9	nM
Inhibition: P9 by CL	K_{11}	0.2650	nM

Table 2: Parameter values of M4 model.

4 Exploring design principles in the *Arabidopsis* circadian clock

Abstract

The biochemical interactions governing the function of the *Arabidopsis* circadian clock have been systematically uncovered and explored by interdisciplinary efforts involving mathematical modelling and biological experiments spanning many decades. This process of developing understanding, which has indisputably contributed practical advances in the understanding of the plant regulatory system, is captured in a series of consecutive mathematical ODE-based models that have been proposed since 2005. These models conceptualize the dynamics of the plant clock in terms of its response to changes in light. However, as demonstrated in the preceding chapters, the interaction of the inner gears of this clock for temperature adaptation is not yet unravelled, and yet the roles of temperature compensation and entrainment are likely to be of increasing importance in the context of global climate change. Moreover, by considering temperature effects, it may be possible to understand the principles governing the structure of the circadian clock's complex biological network. Here we explore these design principles of the plant clock, using methods originally inspired by systems biology, by reviewing the most predominant models of *Arabidopsis* in order to discern regulatory patterns that may explain clock function and temperature compensation. We incorporate temperature dependence into several ODE-based models by applying Arrhenius equations to their translation rates. Additionally, we propose three minimal models and explore what key features govern their function via a series of random parameterisations and simulations, to enrich the analysis. Results show that the highly repressive interactions between the components of the plant clock together with autoregulation patterns and three-node feedback loops, tend to contribute to the function of the clock in general and to its robustness to variation in temperature. However, the fact that the networks governing clock function vary with time, due to light and temperature forcing, reinforces the importance of studying the functionality of the plant clock in its entirety rather than as a set of discrete motifs.

4.1 Introduction

The plant circadian clock is usually conceptualised as a system of interacting genes [19]. These genes typically interact by repressing the expression of other genes in the network, creating feedback loops [18, 41]. Several mathematical models have been built to characterize the structure of the plant system based on biological discoveries [18, 77, 40, 54, 41, 66, 42, 24]. As a result of this, mathematical models have been useful tools to help generate and test hypotheses about the underlying structure of the plant system and to understand its dynamics. In these models light has been proposed to play an impor-

tant role, not just by promoting the expression of some key genes but also by acting at postranscriptional and postranslational levels [77, 40, 54, 41, 66, 24]. The effect of light has been parametrized in a variety of ways in these models, including binary variation [18, 77, 40, 24], smooth transitions from light to dark [54, 41, 66], and via interaction with some hypothesised protein [18, 77, 40, 54, 41, 66, 42, 24]. The result is that the properties of the interaction network vary with time.

The mathematical models proposed to date typically seek to characterize the time evolution of both mRNA and protein levels within plant cells [18, 77, 40, 54, 41, 66, 42, 24]. Equations describe these dynamics as the result of the difference between the production rate and the degradation rate of both gene products. Hill functions are commonly used to characterize the transcription rate terms in the equations [18, 77, 40, 54, 41, 66, 42, 24], and in some cases Michealis-Menten equations have been used to model degradation rates [18, 77, 40]. The models are parametrized with values fitting experimental observations in a qualitative fashion, namely, for a circadian period, amplitude size and phase of gene expression (induced by changes in light). However, details in the description of the molecular basis differ between the models, as do the details of the principles of statistical and qualitative fitting, leading some models to appear to offer a better quantitative fit than others.

In biological networks, oscillatory dynamics have been explained by analysing the feedback loops that form these networks [105, 106]. Feedback loops are believed to play different roles within a network depending on their structure, meaning they have been classified broadly with regards to their shape and functionality. For example, when a transcription factor inhibits its own transcription rate, the response times of the system are faster, and the system is more robust against variations in production rate [106]. The opposite effect is caused when a transcription factor promotes its own transcription rate. The former effect is called negative autoregulation (Figure 4.1A), and the latter positive autoregulation (Figure 4.1B). Another example is the repressilator, originally a synthetic oscillator developed in the study of *E. coli*, consisting of a three-component feedback of inhibitors (Figure 4.1C). This has been shown to be fundamental for oscillatory behaviour. In general, a feedback is defined as positive if the number of negative interactions within the loop is even, or negative if this number is odd, and their basic functionalities can facilitate bistability and promote sustained oscillations, respectively [106].

The feedforward loop is another three-component circuit of interactions found in biological networks, and has been studied in order to understand the dynamics of a whole network. Unlike the repressilator, edges are not restricted to have an inhibitory role; they also can be activators. This circuit is formed by a component that regulates directly and

indirectly (through the another component) a target component. Thus, a total of eight possible classes of feedforward loops can be defined (Figure 4.2). For a description of their dynamical functions, see [107].

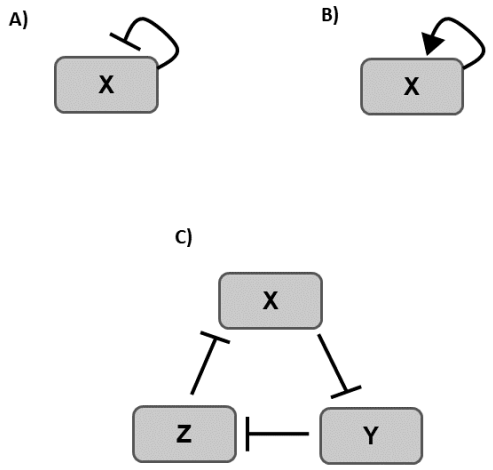

Figure 4.1: **Examples of feedback loops**. A) Negative autoregulation. B) Positive autoregulation. C) the three-node components feedback loop, also termed as the *repressilator*.

Feedback and Feedforward loops as substructures of biological networks can be called network motifs [108]. A network motif is an interaction pattern that is more likely to be found in the real network rather than in random networks of the same size (i.e. the same number of nodes and edges). The principle behind this concept is that, because the network motif has been retained over evolutionary time, it must grant a fitness advantage to the organism. Network motifs were first detected for the *E. coli* transcription network [108], and from then the interest turned on the detection of their dynamical functions in different organisms and different biological networks [106, 108]. In Arabidopsis, motif analysis carried out under simulated constant light conditions has helped to explain the dynamics observed in clock mutants [28]. However, how the plant clock network correlates with temperature behaviour is not yet clarified.

In this chapter, we analysed the structures of a range of clock models proposed over the past 15 years, and added temperature dependence in order to gain insights into temperature behaviour. We centred our analysis in the transcription regulatory interactions

of the plant system. We aimed to know whether network motifs commonly found in other transcription networks are involved in temperature-dependent mechanisms in the plant circadian system. In particular, our analysis considers temperature compensation and numerical results are performed by allowing translation rates in the models to vary with temperature according to the Arrhenius law. To gain a better understanding of the key motifs driving clock function and its robustness to temperature variation, we also performed a large-scale simulation study based on random parameterisations of three simplified models, based on the principles of [28]. Taken together, the results support the idea that the highly repressive role of transcription factors of the plant clock can be related to the robustness of this clock against temperature changes. Our results also suggest that plant clock networks need to be analysed as a whole, as dynamic rather than static networks, and future modelling-experimental efforts could be placed in a network sampling context.

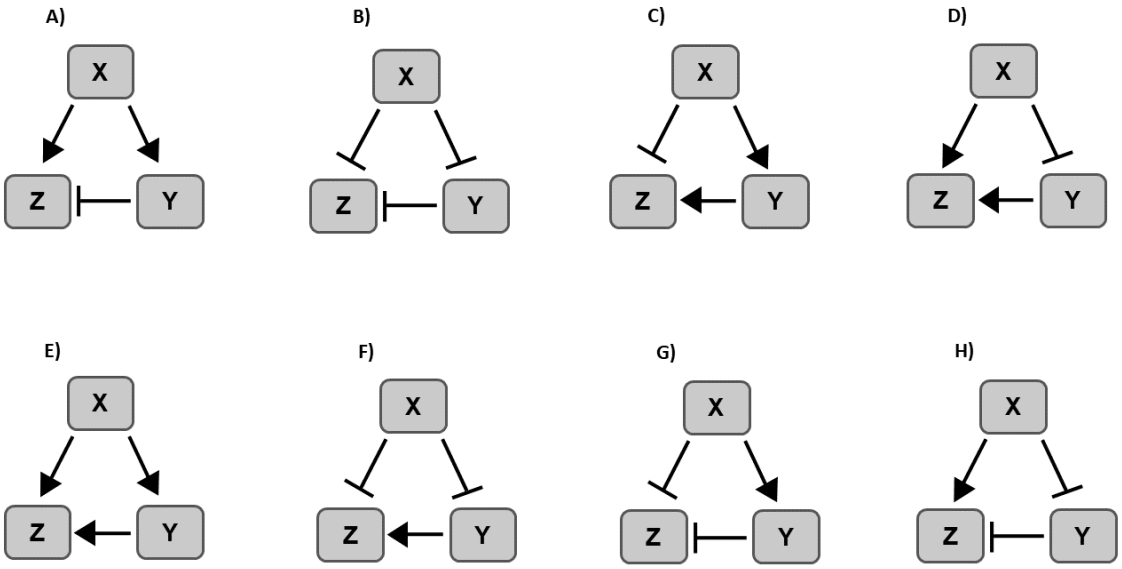

Figure 4.2: **The eight classes of feedforward loops**. Feedforward loops are classified based on their *coherent* or *incoherent* effect of a gene X on its target Z. For example, in figure A) X directly activates Z and indirectly represses it as X promotes Y, which is a repressor of Z. This circuit is called *Incoherent type 1.* In contrast, F) shows a gene X repressing its target Z and *coherently* X represses Y, which has an activator effect on Z. F) is termed as *Coherent type 2.* The top row shows the four types of incoherent feedforward loops; from A to D, *Incoherent type 1, 2, 3, 4*, respectively. The bottom row shows the four types of coherent feedforward loops; from E to H, *Coherent type 1, 2, 3, 4*, respectively.

4.2 Methods

4.2.1 The models

A total of eight ODE-based models of different complexity are analysed. Following nomenclature from previous studies, we refer to these models as: L2005a [18], L2005b [77], L2006 [40], P2010 [54], P2012 [41], P2013 [66], F2014 [42], and DC2016 [24]. Because our goal is to describe these models in terms of their structure rather than to focus on each model's biochemical details, we present them as transcription networks and refer the reader to the original papers for a complete description.

Figure 4.3 depicts the clock structures of the models, including all interactions included in each model. Note that these networks are derived by considering the mathematical equations governing the dynamics in each case, and that this does not necessarily correspond to the network diagrams published in the original papers, which were in some cases simplified. Figure 4.3 allows one to visualize the increase in mathematical complexity of the models as new empirical discoveries have been incorporated into the clock network. Their relative complexity also serves to highlight the difficulty of elucidating the dynamics of the inner transcriptional gears of the plant oscillator. In addition we present the interactions as matrices, which we call *transcription matrices* (for an alternative representation see Supplementary Material). The rows in each matrix display the outgoing interactions from transcription factors in the networks, while columns represent the ingoing effect on the transcription rates of the components of the network; the plus and minus signs mean activation and inhibition, respectively. CL again represents *CCA1* and *LHY* when they are modelled as a single variable, and E34L represents *ELF3*, *ELF4* and *LUX* grouped as the evening complex, consistently with the block effect allocated in the models.

Each edge in each network is modelled by a Hill function, which characterizes the inhibitor or activator effect of a transcription factor on the rate of production of mRNA. The Hill function is defined by [108],

$$Y = \frac{\beta}{1 + \left(\frac{X}{K}\right)^n}, \tag{14}$$

for a repressor, and by

$$Y = \frac{\beta X^n}{K^n + X^n}, \tag{15}$$

for an activator, where Y is the rate of production of mRNA, β is the maximal production rate, X is the inhibitor or activator concentration, K is the inhibition or activation coef-

ficient, and n is the Hill coefficient. In other words, each edge in the network is governed by at least three parameters: the repression (or activation) coefficient, the Hill coefficient and a rate constant of transcription. In cases when the transcription of a gene is regulated by a light transient induction effect via interaction with a protein P, a rate constant is also considered to mediate light input.

4.2.2 Structural description of the plant transcription network

We have carried out a statistical analysis to describe the network structures that have been hypothesised through the mathematical models for the *Arabidopsis* circadian clock: L2005a [18], L2005b [77], L2006 [40], P2010 [54], P2012 [41], P2013 [66], F2014 [42], and DC2016 [24]. This analysis consists of computing network statistics (number of components, number of edges, density, and the average clustering coefficient), and then applying a probabilistic approach to detect frequency of network motifs. In particular, we test the prevalence of autoregulation, feedforward and three-component feedback loops by comparing their occurrences in the hypothesised circadian networks against their occurrences in random networks of the same size, following the methodology of [108].

The average number of autoregulation (N_{auto}), feedforward (N_{FFL}), and feedback (N_{Fback}) loops in random networks can be determined by,

$$N_{auto} = \frac{E}{N}, \tag{16}$$

$$N_{FFL} = \lambda^3 N^{n-e}, \tag{17}$$

$$N_{Fback} = \frac{1}{3}\lambda^3 N^{n-e}, \tag{18}$$

where $\lambda = \frac{E}{N}$ is the *mean connectivity*, N and E are the numbers of nodes and edges in the network, respectively, and n and e the number of nodes and edges of the particular pattern under consideration.

The standard deviations (SD) of these estimations can be calculated by the square root of the equations 16, 17 and 18, and a Z score is used to quantify the significance of the occurrences of these subgraphs. The Z score tells us how many standard deviations the number of the subgraphs observed in the network models exceeds the number expected in random networks.

(Note that, with the exception of the [24] model where $ELF4$ and LUX are merged into a single variable solely, statistical calculations in models including the evening complex

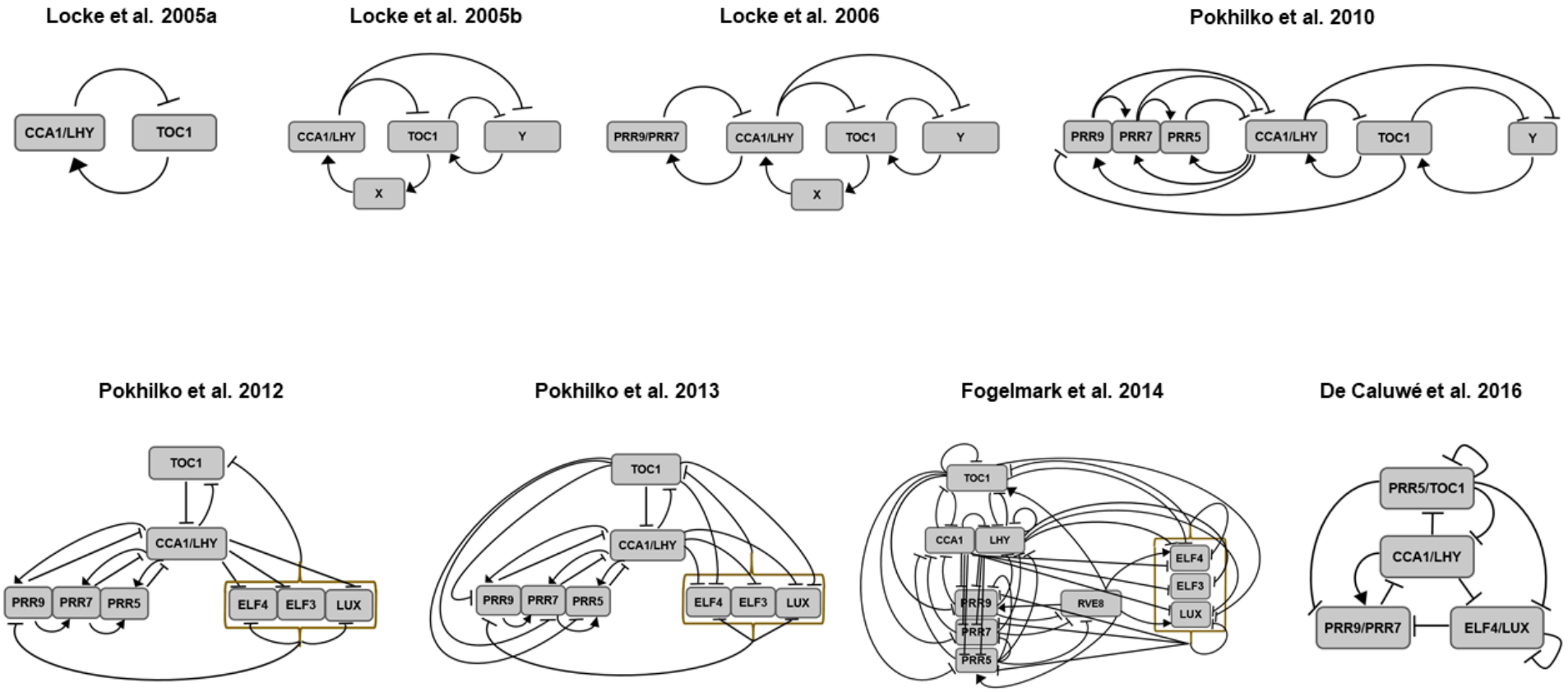

Figure 4.3: **Developments in ODE-based models for the *Arabidopsis* circadian clock**. Transcription networks are illustrated for eight models for the plant clock. The plant oscillator was firstly modelled as a simple negative feedback. As more clock components were discovered, three-node circuits were incorporated, and the wiring of the plant network became more complicated. The most recent clock model structures incorporate autoregulation patterns, and have mainly repressive interactions.

were performed taking $ELF4$, $ELF3$ and LUX into account as individual components.)

4.2.3 Temperature dependence

Following the ideas developed in Chapters 1 and 3, we allowed translation rates only to vary with temperature. Arrhenius equations were applied to the relevant parameters (see Table 5, Supplementary Material) by using a temperature reference of 22°C in all models in order to match their published parameter values corresponding to this temperature. With the aim to assess whether temperature compensation is present, the effect of temperature was modelled by using an activation energy value of 50 kJ mol^{-1} for each rate, and simulations were carried out according to the experimental protocols of [4] and [82]. A model was considered compensated if its Q_{10} of period was in the range between 0.8 and 1.2 [32] (see Section 2.2.2 in Chapter 2). To test whether these conclusions were reliable, we introduced variability into the influence of temperature onto the clock models by randomly choosing each activation energy value from a uniform distribution between 40 kJ mol^{-1} and 60 kJ mol^{-1}. Two hundred replications of those random parameterizations were performed for each model, and temperature compensation was assessed in each case.

Note that in [42], the authors modelled the protein production rate as equal to one copy per mRNA for all transcription factors with the exception of *ELF4* and *ELF3* components. This approach differs from the other models in that protein production is usually characterized by p copies of mRNA that are translated (with the translation rate p not necessarily equal to 1 h^{-1} in most cases). Thus, to incorporate temperature into [42] model, we extended that model by adding parameters p_j, (j representing a component model) in the terms of protein production rates of the dynamical equations labeled by (5), (7), (10), (12), (15), (20), (30), (45) in [42]; p_1, p_2, p_3, p_4, p_5, p_{30}, p_{31}, and p_{32}, respectively. We fixed the p_j values to be equal to 1 at the temperature reference 22°C in order to preserve the original model and allowed them to vary with temperature as described previously.

4.2.4 Numerical Investigation of minimal models via random parameterisation

A recent modelling study by [28] provides an interesting alternative approach towards discovering the design principles of the circadian clock by proposing a number of possible clock structures and investigating their emergent properties by a series of random parameterisations. Motivated by this study, and to complement the results emerging from the more complex models L2005a [18], L2005b [77], L2006 [40], P2010 [54], P2012 [41], P2013 [66], F2014 [42], and DC2016 [24], we additionally proposed three minimal models

with the aim to compare and contrast the results obtained when comparing the historical clock models of *Arabidopsis*. We proposed three simplified clock structures (Figure 4.4) of four repressor components, which represent $CCA1/LHY$, $PRR9/PRR7$, $PRR5/TOC1$ and $ELF4/LUX$, in order to assess changes in the periodicity of the plant clock when the parameters of these models are allowed to vary with temperature under a simulated continuous light condition (as in [28]). Because our goal is to analyse structural patterns that may explain temperature compensation, our models are not expected to faithfully reproduce the detailed behaviour of the plant circadian system. Rather, we ask which structures and parameterisations allow these minimal models to show regular oscillatory behaviour and an empirically justifiable phasing of peak expression levels (i.e. the order of the peak mRNA levels of the clock components should agree with that observed in reality, with *CCA1* and *LHY* peaking at dawn before *PRR9* and *PRR7*, followed by the peak of *PRR5* and *TOC1* before *ELF4* and *LUX*). Consistently with the more complex models, the proposed structures are characterized by systems of ODEs for mRNA and protein levels (see Supplementary Material for equation details). The parameter values were assigned randomly from independently uniformly distributed numbers between 0 and 1. In the same manner, Hill coefficients were assigned from discrete uniform distributions on the range between 2 and 4. The initial conditions of the system were fixed to be equal to 0.1 in all cases. By using a notional unit of time of an hour, the clock was run for 20 days and the first 10 days were discarded in order to avoid transient effects. Next, we searched for parameter sets reproducing oscillatory behaviour. The period of the system was calculated by the trough method as explained in Chapter 1. We then selected from those sets the parameter values that showed a subjective proper phase for the peak of the gene expression.

To compare models, hitting rates were calculated as in [28]. This measure gives us an averaged proportion of the parameter sets that met our criteria of selection with respect to the total number of parameters that were generated at random in the researching scheme. The higher the hitting rate, the more robust the model against parameter combinations. This proportion is defined by,

$$P = \sqrt[n]{\frac{\text{number of obtained parameter sets}}{\text{number of searched parameter sets}}}, \tag{19}$$

where n is the number of independent parameters.

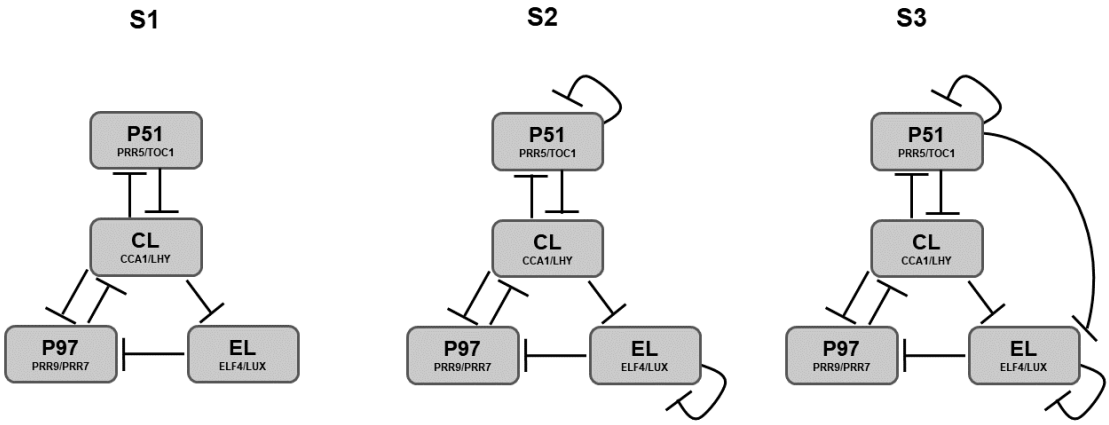

Figure 4.4: **Minimal clock model structures**. Figure S1 includes a three-node feedback loop. In S2 autoregulation patterns were added to end up with S3 structure having a feedforward loop. All clock components are characterized to have a repressive role within the network.

4.3 Results

4.3.1 Description of the hypothesized clock plant structures

Table 3 shows the basic network statistics of the models under consideration. The networks are all much more dense, and more clustered, than the large-scale transcription networks typically observed in systems biology [108]. It should be noted that, as model complexity (number of components) increases, there is no useful trend in the density or clustering coefficient of the networks; the circadian models are all dense well-connected networks. It is also noteworthy that the proportion of negative interactions is much higher in models from 2012, surpassing the number of positive interactions. Table 4 extends this comparison by looking at the frequency of network motifs in comparison to Erdos-Renyi random graphs of the same size and density. No clear story emerges, but it may be notable that the occurrence of three-component feedback loops is much more common in models from 2012; Z scores for L2012, L2013 and F2014 showed that they appear more often than what is expected at random.

	Global properties				
ODE model	number of components	number of edges	density	clustering coefficient	prop. of neg. interactions
L2005a	2	2	0.50	-	0.50
L2005b	4	6	0.38	0.83	0.50
L2006	5	8	0.32	0.75	0.50
P2010	6	14	0.39	0.73	0.50
P2012	8	17	0.27	0.82	0.71
P2013	8	22	0.34	0.87	0.77
F2014	10	46	0.46	0.92	0.89
DC2016	4	10	0.63	1	0.90

Table 3: Network statistics of the *Arabidopsis* circadian models illustrated in Figure 4.3.

Figure 4.5 illustrates the main result from this comparison of models and their behaviour in changing temperatures; when translation rates are allowed to vary with temperature, only the more recent (and more complex) models exhibit temperature compensation. The earliest clock models, L2005a, L2005b and L2006 only function within a narrow temperature range; at lower temperatures the clock is disrupted. Temperature compensation is not observed in these models, the clock slows down, or speeds up, markedly as temperature increases in these early models before all rhythmic behaviour is lost (L2005a, L2005b and L2006). The more complex P2010 model functions across a broader temperature range, but is similarly uncompensated. However, the most complex and most recent models P2012, P2013, F2014 and DC2016 all show temperature compensation to a greater or lesser extent. All simulations were carried out following experimental protocols of [4] and [82]. Figures 4.6 and 4.7 show that this finding is not an artefact of the fixed choice of activation energy in the simulations in Figure 4.5. When activation energies are allowed to vary between 40 kJ mol^{-1} and 60 kJ mol^{-1} the same patterns emerge; only the models P2012, P2013, F2014 and DC2016 exhibit temperature compensation, but this temperature compensation is robust to variability in activation energy.

	Regulation patterns					
ODE model	autoregulation	expected autoregulation	feedforward	expected feedforward	feedback	expected feedback
L2005a	0	1 ± 1	-	-	-	-
L2005b	0	1.5 ± 1.2	2	3.4 ± 1.8	1	1.1 ± 1.1
L2006	0	1.6 ± 1.3	2	4.1 ± 2.0	1	1.4 ± 1.2
P2010	0	2.3 ± 1.5	10	12.7 ± 3.6	4	4.2 ± 2.1
P2012	2	2.1 ± 1.5	13 (Z=1.1)	9.6 ± 3.1	6 (Z=1.6)	3.2 ± 1.8
P2013	2	2.8 ± 1.7	23 (Z=0.5)	20.8 ± 4.6	11 (Z=1.5)	6.9 ± 2.6
F2014	4	4.6 ± 2.1	115 (Z=1.8)	97.3 ± 9.9	50 (Z=3.1)	32.4 ± 5.7
DC2016	2	2.5 ± 1.6	7	15.6 ± 4.0	2	5.2 ± 2.3

Table 4: Comparison of the network motifs found in a range of circadian models, with those expected at random for graphs with the same size and density (mean $\pm$ 1$\times$SD). Z scores are shown in cases when expected values are exceeded.

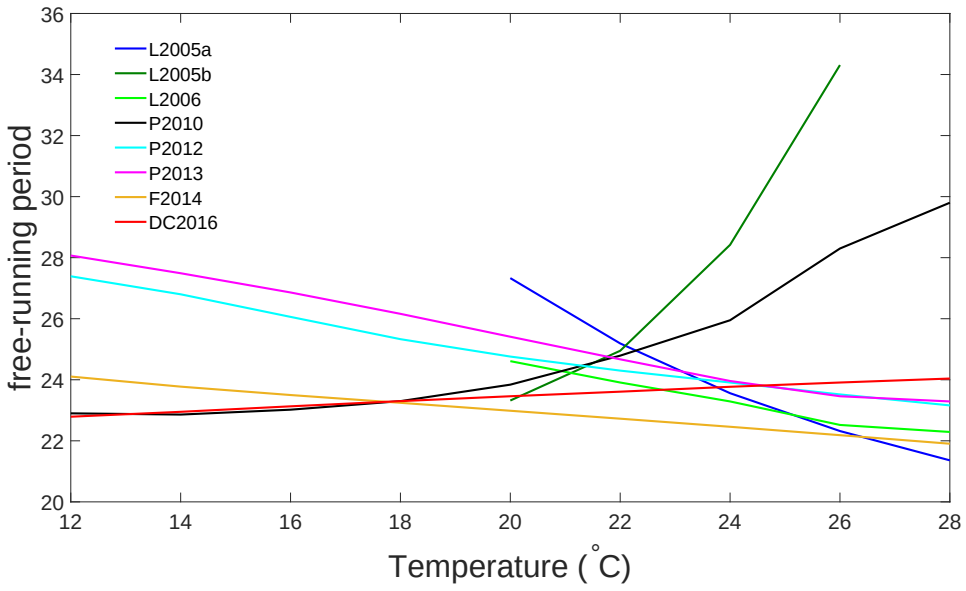

Figure 4.5: **The models P2012, P2013, F2014 and DC2016 exhibit temperature compensation**. Simulations were carried out following experimental protocols of [4] and [82]. The earliest clock models, L2005a, L2005b and L2006 allow incorporation of temperature into the plant clock, but only function within a reduced temperature range; at lower temperatures the clock is disrupted. Temperature compensation is not observed in these models, and nor in P2010; the clock either slows down (L2005b, P2010) or speeds up (L2005a,L2006) markedly as temperature increases in these early models.

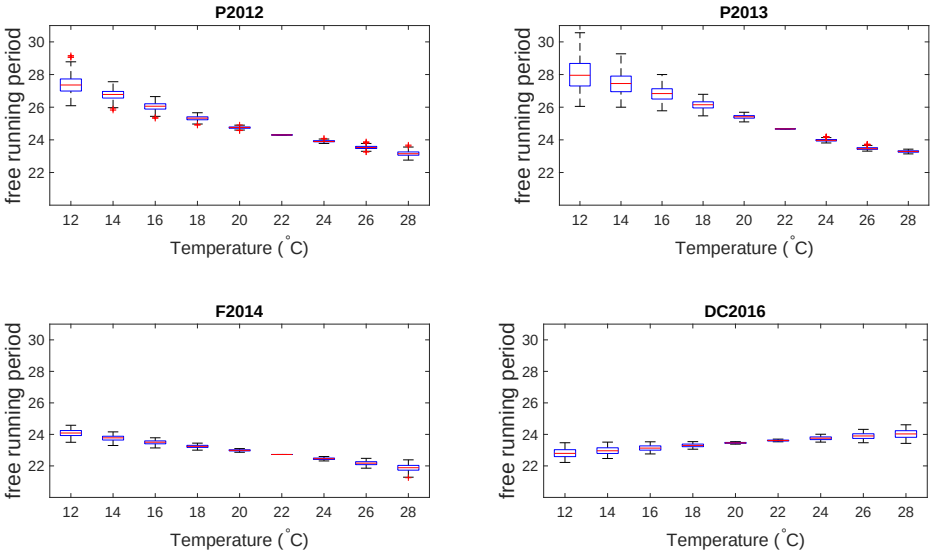

Figure 4.6: **The models P2012, P2013, F2014 and DC2016 exhibit temperature compensation**. Simulations were carried out following experimental protocols of [4] and [82]. Results show the distribution of the free-running period when random uniformly distributed activation energy values between 40 kJ mol^{-1} and 60 kJ mol^{-1} were allocated independently to the translation rates of the model. Results support outputs obtained in Figure 4.5, where the influence of temperature was parametrized to be equal.

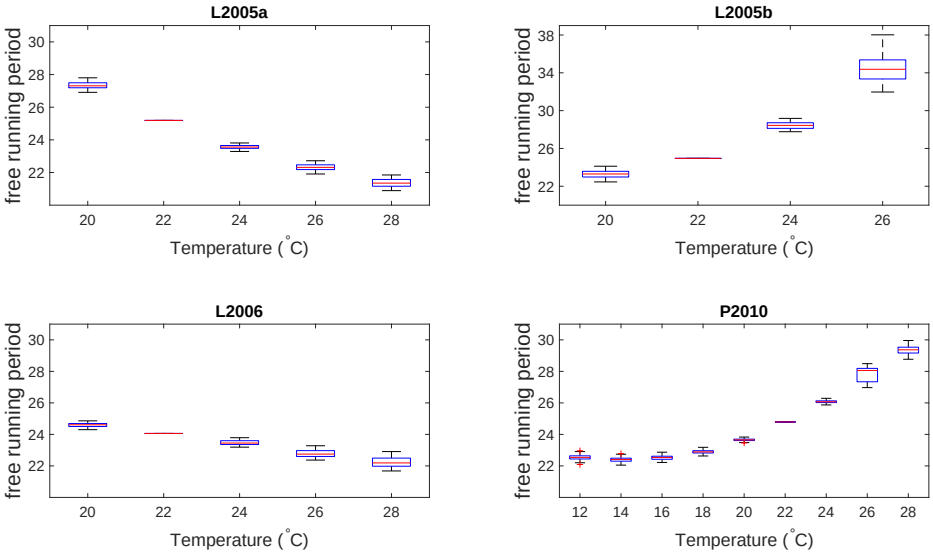

Figure 4.7: **The earliest clock models, L2005a, L2005b, L2006 and P2010 do not exhibit temperature compensation**. Simulations were carried out following experimental protocols of [4] and [82]. Results show the distribution of the free-running period when random uniformly distributed activation energy values between 40 kJ mol^{-1} and 60 kJ mol^{-1} were allocated independently to the translation rates of the model. Results support outputs obtained in Figure 4.5, where the influence of temperature was parametrized to be equal.

Although these results hint that complexity is helpful in facilitating temperature compensation, it is not yet possible to attribute this phenomenon to any network motif in particular. For example, clock models presenting autoregulation motifs displayed robustness against variation in translation rates due to temperature changes and it might be tempting to explain this phenomenon in a causal way. This is not the case that is shown in Figure 4.8, where outputs are presented for both P2012 and DC2016 models in the absence of their autoregulation loops; temperature compensation is maintained. Indeed, repeating investigations similar to these but with changes to feedback and feedforward loops reveals no clear patterns (data not shown), further underlining the differences between plant circadian oscillators and the more general networks of systems biology. Interestingly, when temperature compensation was tested under constant dark condition in DC2016 model (not shown), compensation was still observed; however, the Q_{10} of period was reduced from 0.97 to 0.87. Note that autoregulation coupled with three-node feedback loops are not present in the DC2016 model under dark conditions (see Figure 2.1 in Chapter 2). Putting all these observations together, these results suggest that autoregulation combines with three-node feedback loops to form a highly inhibiting transcription network which might contribute to temperature compensation. These ideas are tested in the following section.

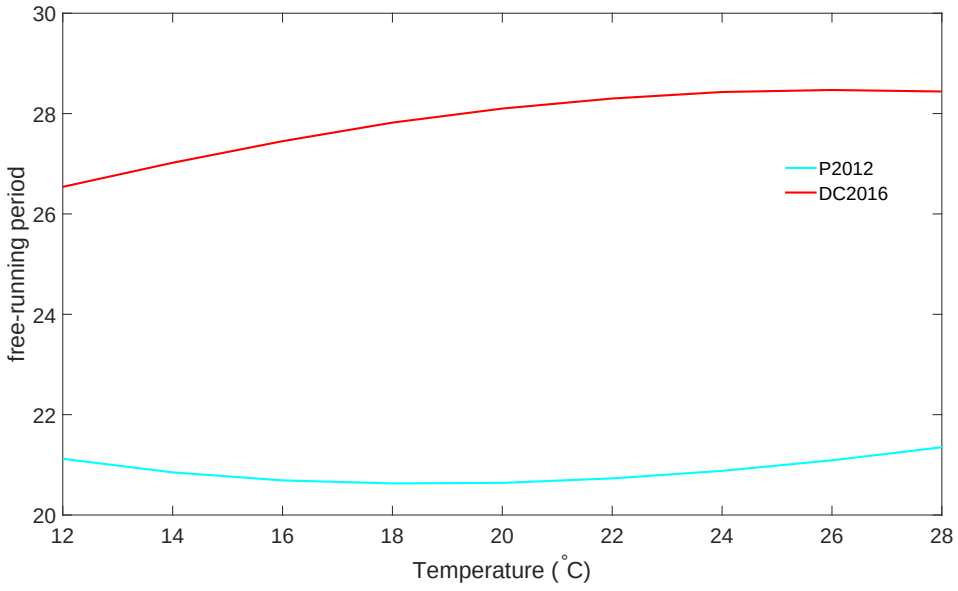

Figure 4.8: **Autoregulation alone is inadequate to explain temperature compensation**. The figure shows outputs from modified P2012 and DC2016 models, where the autoregulation loops have been removed. In both cases, temperature compensation persists in spite of the change to the network structure.

4.3.2 Minimal models via random parameterisation

We defined three minimal structures for numerical investigation (S1, S2 and S3 in Figure 4.4) in order to test whether the inclusion of certain well-defined regulatory patterns may facilitate temperature compensation. Taking into account the previous results, all proposed structures have been modelled to have negative interactions only. Model S1 includes a three-node feedback loop, model S2 is proposed to test the effect of having a three-node feedback together with negative autoregulation loops, and the inclusion of an incoherent feedforward circuit was tested in model S3. That is, model S3 is an extension of S2, and model S2 is an extension of S1. Figure 4.9 depicts the main results when the behaviours of these models are compared, using random parameterisations and the criteria for periodicity and compensation as explained in Section 4.2.4. Surprisingly, across the range of random parameterisations, we found no important differences between the models S1, S2 and S3 in terms of their ability to produce sustained oscillations with the correct ordering of peaks in gene expression (Figure 4.9A). Moreover, all structures presented high hitting rates, indicating that a high percentage of parameter sets met our criteria of oscillatory behaviour and proper order of peak mRNA levels. However, we did find differences when temperature dependence was incorporated into these models. Figure 4.9B shows that the incorporation of autoregulation patterns improves the robustness of the system across an extended temperature range; the model S2 showed a much higher proportion of oscillating parameter sets that tolerated temperatures between 12°C and 28°C compared to the model S1. Note that the models S2 and S3 showed similar results, which suggests that feedforward loop is not required to extend the tolerable temperature range, but that three-node feedback and autoregulation patterns are required together to allow the system to oscillate in extended temperature boundaries.

Figure 4.9C shows the distribution of the Q_{10} of period for each model under random parameterisation. Although model S1 displays robustness against temperature changes with 62% of its parameter sets allowing the system to achieve temperature compensation (Q_{10} lying within the range 0.8-1.2), it is remarkable that adding autoregulation patterns significantly improved this robustness. Outcomes of the model S2 showed that 83% of the parameter sets presented Q_{10} values in the range for compensation. Moreover, the Q_{10} distribution shifted to locating closer to perfect compensation (i.e. $Q_{10} = 1$); the median of the distribution shifted from a Q_{10}=0.83 in model S1 to a Q_{10}=0.90 in model S2. It is also possible to observe a reduction in the dispersion of the distribution; the range of the Q_{10} values is reduced by 14%. However, this improvement was affected when a feedforward

loop was incorporated into the system. In model S3, the percentage of parameter sets resulting in Q_{10} values in the range for compensation dropped to 76% and its distribution was more spread out, the range of the modelled outcomes increased by 43% compared to model S2, and this increased variability is mainly caused by values below the median.

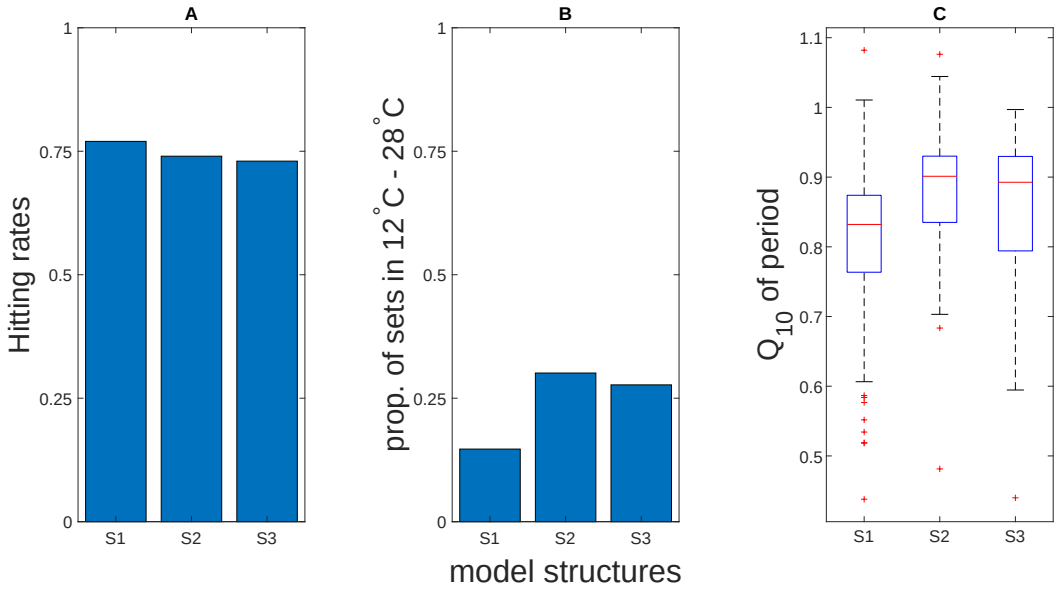

Figure 4.9: **Autoregulation together with three-node feedback structure improves the robustness of the system against temperature changes on translation rates**. Results from random parameterisations of models S1, S2 and S3 in Figure 4.4. A) Normalized proportion of parameter sets that showed sustained oscillations and correct order of peak gene expression. B) Proportion of parameter sets that allowed the system to oscillate across a 12°C - 28°C temperature range with respect to the number of sets obtained after searching (Table 7 in Supplementary Material). C) Distribution of the modelled outputs of the parameter sets selected to show oscillatory behaviour in the range 12°C - 28°C.

4.4 Discussion

Particular subgraphs in transcription networks, called network motifs, have been argued to drive specific tasks and to favour particular behaviours in biochemical systems [108]. The interest in the study of these graph structures is founded on the hypothesis that they are the result of evolutionary selection. We studied whether temperature compensation can be attributable to the function of specific subgraphs of the plant network by exploring the historical structures proposed for the *Arabidopsis* circadian clock and by numerical investigation of three minimal models via random parameterisation. We found that temperature compensation cannot be determined as a function of a particular substructure of the plant network but it involves a global property of this network, where autoregulation together with three-node feedback loops in a transcription network dominated by negative interactions favor the clock to be robust to temperature variability.

Exploring the historical structures for the plant circadian system, we found that only clock models presenting autoregulation patterns displayed robustness against variation in translation rates due to temperature changes. Surprisingly, we also found that although this is observed, it cannot be the cause of temperature robustness; results from modified P2012 and DC2016 models that exclude autoregulation structures showed that these models still present compensated behaviour (Figure 4.8). Similarly, we observed that compensated models have the particular feature of presenting a much higher proportion of negative regulations compared to uncompensated models (Table 3); however, removing the positive interactions or changing them by repressive roles in P2010 model did not change the uncompensated dynamics of this model (results not shown). Additionally, the results (Table 4) also suggest that the three-node feedback loop might favor the robustness of the plant clock against temperature changes, as these patterns occur more often in compensated models. We therefore attempted to understand if the junction of these regulatory patterns rather than each one alone may contribute to temperature compensation. To this end, we proposed three minimal models to analyse the effect of adding new interaction patterns to the plant system. We started with a highly inhibiting transcription network having a three-node feedback loop and in the next two consecutive models we added autoregulation loops and a feedforward circuit, respectively. The results of our models show that the effect of adding autoregulation patterns to a network with a three-node feedback loop improve the temperature tolerance of the plant oscillator; however, adding a feedforward loop reduces the performance of the oscillator to face temperature changes.

Network motif theory has been built using the principle that structures of interactions

observed in natural systems have been maintained over evolutionary time as they grant advantages to the organisms. Under this scenario, one would expect biologically useful motifs to appear more frequently than they would in a random interaction network of the same size. In [108], the authors proposed to detect network motifs by using the Erdos Renyi model to generate random structures sharing the empirical system's size and density, and to assess whether empirically observed networks are significantly different. They provided mathematical expressions to calculate the expected number of occurrences and used the *E. coli* network as an example of a transcription network for calculations. Additionally, they claimed that the transcription networks they study are sparse, the out degree distribution has a long tail describing that very few transcription factors regulate a large number of genes and the distribution of the incoming edges is compact; furthermore, transcription networks have an average clustering coefficient higher than random networks, among other characteristics.

In this research, we have applied these ideas as the basis of an exploratory analysis of the circadian plant clock by using the hypothesised *Arabidopsis* clock structures as the "real" plant transcription network. We found that autoregulation and feedforward loops, typical regulation patterns of transcription networks defined as network motifs, are not present in the proposed *Arabidopsis* networks with significant difference compared to random networks. However, three-node feedback loops appear slightly more often in the hypothesised transcription networks for *Arabidopsis* from 2012. We also found that the hypothesised networks are not sparse but they are dense. In the context of transcription networks, density values less than 0.001 are common, whereas the historical models of circadian networks do not show densities less than 0.27. Out degree distributions are not long tailed, the degree distributions are compact, and there is no clear pattern to their shapes (data not shown). We also observed that the hypothesised transcription networks for the plant clock are highly clustered (i.e. clustering coefficients much larger than density values), which implies that their average clustering coefficient is larger than those in random graphs. The latter is in agreement with what has been observed in transcription networks of other systems, but it has not proved possible to make a theoretical link from this observation to statements about large scale clock function.

The numerical simulations carried out here use certain necessary assumptions, and these in turn may limit the generality of the results. In particular, temperature dependence is assumed to apply only to translation rates within the model; degradation rates are assumed to remain constant (see Section 4.2.3), yet there is experimental evidence on temperature dependence of degradation rates [56]. This is a reasonable assumption and is consistent with the work in Chapters 1 and 3. It should, however, be noted that in

Chapter 2 and [26], the degradation rates in circadian models are shown to play a large role in determining the ranges of temperature entrainment and compensation. In this sense, the conclusion that increased negative feedback is required for temperature compensation is limited by the assumption of constant degradation rates, and the conclusions may be revisited in future if more reliable data on the temperate dependence of degradation rates become available. An alternative parsimonious assumption, whereby all rates in the model vary according to the same Arrhenius law, would necessarily preclude any temperature compensation for the reasons explained in Chapter 2, Discussion Section (i.e. time scaling increasing the pace of the clock network). On the other hand, negative autoregulation has a speeding up effect on systems [106], then one might suppose an additive acceleration effect, which could limit as well the conclusion that increased negative feedback favors temperature compensation. This support the importance of further investigation from modelling and experiments efforts.

We believe that, although our models necessarily have some limitations, and indeed they are highly oversimplified systems to represent complex plant dynamics, our theoretical approach provides helpful insights into what design principles of the *Arabidopsis* transcription network have an important role in the ability of the plant system to bear temperature changes. The observations presented here hint that mathematical and graph-theoretic approaches may become useful in the analysis of the plant clock as a whole system, but the full story is as yet unclear. The importance of forcing, whether of light, temperature, or both, has the effect of enforcing dynamic networks of interaction on the plant clock, a fact not taken into account in the traditional systems biology theories ([108]), and this is likely to limit the applicability of the theory in general.

4.5 Supplementary Material

$$\textbf{L2005a} \rightarrow \begin{array}{c} \\ CL \\ TOC1 \end{array} \begin{array}{c} \begin{array}{cc} CL & TOC1 \end{array} \\ \begin{pmatrix} & - \\ + & \end{pmatrix} \end{array}$$

$$\textbf{L2005b} \rightarrow \begin{array}{c} \\ CL \\ TOC1 \\ X \\ Y \end{array} \begin{array}{c} \begin{array}{cccc} CL & TOC1 & X & Y \end{array} \\ \begin{pmatrix} & - & & - \\ & & + & - \\ + & & & \\ & + & & \end{pmatrix} \end{array}$$

$$\textbf{L2006} \rightarrow \begin{array}{c} \\ CL \\ TOC1 \\ X \\ Y \\ PRR9/7 \end{array} \begin{array}{c} \begin{array}{ccccc} CL & TOC1 & X & Y & PRR9/7 \end{array} \\ \begin{pmatrix} & - & & - & + \\ & & + & - & \\ + & & & & \\ & + & & & \\ - & & & & \end{pmatrix} \end{array}$$

$$\mathbf{P2010} \rightarrow \begin{array}{c} \\ CL \\ TOC1 \\ Y \\ PRR9 \\ PRR7 \\ PRR5 \end{array} \begin{array}{c} \begin{array}{cccccc} CL & TOC1 & Y & PRR9 & PRR7 & PRR5 \end{array} \\ \begin{pmatrix} & - & - & + & + & + \\ + & & - & - & & \\ & + & & & & \\ - & & & & + & \\ - & & & & & + \\ - & & & & & \end{pmatrix} \end{array}$$

$$\mathbf{P2012} \rightarrow \begin{array}{c} \\ CL \\ PRR9 \\ PRR7 \\ PRR5 \\ TOC1 \\ E34L \end{array} \begin{array}{c} \begin{array}{cccccccc} CL & PRR9 & PRR7 & PRR5 & TOC1 & ELF4 & ELF3 & LUX \end{array} \\ \begin{pmatrix} & + & + & + & - & - & - & - \\ - & & + & & & & & \\ - & & & + & & & & \\ - & & & & & & & \\ - & & & & & & & \\ & - & & & - & - & & - \end{pmatrix} \end{array}$$

$$\mathbf{P2013} \rightarrow \begin{array}{c} \\ CL \\ PRR9 \\ PRR7 \\ PRR5 \\ TOC1 \\ E34L \end{array} \begin{array}{c} \begin{array}{cccccccc} CL & PRR9 & PRR7 & PRR5 & TOC1 & ELF4 & ELF3 & LUX \end{array} \\ \begin{pmatrix} & + & + & + & - & - & - & - \\ - & & + & & & & & \\ - & & & + & & & & \\ - & & & & & & & \\ - & - & - & - & & - & & - \\ & - & & & - & - & & - \end{pmatrix} \end{array}$$

$$
\begin{array}{c}
 \\
 \\
 \\
 \\
 \\
 \\
 \\
 \\
\mathbf{F2014} \rightarrow \\
 \\
 \\
 \\
 \\
 \\
 \\
 \\
\end{array}
\begin{array}{c}
\begin{array}{cccccccccc}
CCA1 & LHY & PRR9 & PRR7 & PRR5 & TOC1 & ELF4 & ELF3 & LUX & RVE8
\end{array} \\
\left(\begin{array}{cccccccccc}
CCA1 & - & - & - & - & - & - & - & - & \\
LHY & - & - & - & - & - & - & - & - & \\
PRR9 & - & - & & & & & & & - \\
PRR7 & - & - & & & & & & & - \\
PRR5 & - & - & - & & & & & & - \\
TOC1 & - & - & - & - & - & - & & - & \\
E34L & & - & - & - & - & - & & - & \\
RVE8 & & + & & + & + & + & & + &
\end{array}\right)
\end{array}
$$

$$\begin{array}{c} \\ \textbf{DC2016} \rightarrow \end{array} \begin{array}{c} \begin{array}{cccc} CL & P97 & P51 & EL \end{array} \\ \begin{pmatrix} & + & - & - \\ - & & & \\ - & - & - & - \\ & - & & - \end{pmatrix} \end{array} \begin{array}{l} CL \\ P97 \\ P51 \\ EL \end{array}$$

ODE model	Rate constants of translation
L2005a	p_1, p_2
L2005b	p_1, p_2, p_3, p_4
L2006	p_1, p_2, p_3, p_4, p_6
P2010	p_1, p_2, p_4, p_6, p_8, p_9, p_{10}
P2012	p_1, p_2, p_4, p_8, p_9, p_{10}, p_{23}, p_{27}
P2013	p_1, p_2, p_4, p_8, p_9, p_{10}, p_{23}, p_{27}
F2014	p_1, p_2, p_3, p_4, p_5, p_{16}, p_{23}, p_{30}, p_{31}, p_{32}
DC2016	p_1, p_{1L}, p_2, p_3, p_4

Table 5: Parameters of the models affected by temperature.

The S1 model

$$\frac{d[CL]_m}{dt} = \beta_1 * \frac{1}{1 + (\frac{[P97]_p}{K_1})^n + (\frac{[P51]_p}{K_2})^n} - d_1 * [CL]_m$$
$$\frac{d[CL]_p}{dt} = p_1 * [CL]_m - d_2 * [CL]_p$$
$$\frac{d[P97]_m}{dt} = \beta_2 * \frac{1}{1 + (\frac{[CL]_p}{K_3})^n + (\frac{[EL]_p}{K_4})^n} - d_3 * [P97]_m$$
$$\frac{d[P97]_p}{dt} = p_2 * [P97]_m - d_4 * [P97]_p$$
$$\frac{d[P51]_m}{dt} = \beta_3 * \frac{1}{1 + (\frac{[CL]_p}{K_5})^n} - d_5 * [P51]_m$$
$$\frac{d[P51]_p}{dt} = p_3 * [P51]_m - d_6 * [P51]_p$$
$$\frac{d[EL]_m}{dt} = \beta_4 * \frac{1}{1 + (\frac{[CL]_p}{K_6})^n} - d_7 * [EL]_m$$
$$\frac{d[EL]_p}{dt} = p_4 * [EL]_m - d_8 * [EL]_p$$

The S2 model

$$\frac{d[CL]_m}{dt} = \beta_1 * \frac{1}{1 + (\frac{[P97]_p}{K_1})^n + (\frac{[P51]_p}{K_2})^n} - d_1 * [CL]_m$$
$$\frac{d[CL]_p}{dt} = p_1 * [CL]_m - d_2 * [CL]_p$$
$$\frac{d[P97]_m}{dt} = \beta_2 * \frac{1}{1 + (\frac{[CL]_p}{K_3})^n + (\frac{[EL]_p}{K_4})^n} - d_3 * [P97]_m$$
$$\frac{d[P97]_p}{dt} = p_2 * [P97]_m - d_4 * [P97]_p$$
$$\frac{d[P51]_m}{dt} = \beta_3 * \frac{1}{1 + (\frac{[CL]_p}{K_5})^n + (\frac{[P51]_p}{K_7})^n} - d_5 * [P51]_m$$
$$\frac{d[P51]_p}{dt} = p_3 * [P51]_m - d_6 * [P51]_p$$
$$\frac{d[EL]_m}{dt} = \beta_4 * \frac{1}{1 + (\frac{[CL]_p}{K_6})^n + (\frac{[EL]_p}{K_8})^n} - d_7 * [EL]_m$$
$$\frac{d[EL]_p}{dt} = p_4 * [EL]_m - d_8 * [EL]_p$$

The S3 model

$$\frac{d[CL]_m}{dt} = \beta_1 * \frac{1}{1 + (\frac{[P97]_p}{K_1})^n + (\frac{[P51]_p}{K_2})^n} - d_1 * [CL]_m$$
$$\frac{d[CL]_p}{dt} = p_1 * [CL]_m - d_2 * [CL]_p$$
$$\frac{d[P97]_m}{dt} = \beta_2 * \frac{1}{1 + (\frac{[CL]_p}{K_3})^n + (\frac{[EL]_p}{K_4})^n} - d_3 * [P97]_m$$
$$\frac{d[P97]_p}{dt} = p_2 * [P97]_m - d_4 * [P97]_p$$
$$\frac{d[P51]_m}{dt} = \beta_3 * \frac{1}{1 + (\frac{[CL]_p}{K_5})^n + (\frac{[P51]_p}{K_7})^n} - d_5 * [P51]_m$$
$$\frac{d[P51]_p}{dt} = p_3 * [P51]_m - d_6 * [P51]_p$$
$$\frac{d[EL]_m}{dt} = \beta_4 * \frac{1}{1 + (\frac{[CL]_p}{K_6})^n + (\frac{[EL]_p}{K_8})^n + (\frac{[P51]_p}{K_9})^n} - d_7 * [EL]_m$$
$$\frac{d[EL]_p}{dt} = p_4 * [EL]_m - d_8 * [EL]_p$$

Models	number of parameters	sets searched	sets oscillating	oscillating and phase
S1	23	500,000	2,114 (0.42%)	1,281 (0.26%)
S2	25	500,000	1,870 (0.37%)	239 (0.05%)
S3	26	500,000	1,880 (0.38%)	137 (0.03%)

Table 6: Selecting parameter sets for the clock structures in Figure 4.4. Percentages in brackets were calculated over the number of parameter sets searched (third column). Last column shows the number of sets including the parameters to be applied Arrhenius equations.

Models	sets selected	sets in [12°C ; 28°C]	% obtained
S1	1,281	188	14.7
S2	239	72	30.1
S3	137	38	27.7

Table 7: Parameter sets producing sustained oscillations on a range of 12°C to 28°C. Third column shows the number of modelled inputs for Figure 4.9C.

Conclusion

This thesis aimed to provide the basis for modelling temperature dependence in the plant circadian clock in order to elucidate the mechanisms of entrainment and compensation, and to point out the elementary design principles of the plant network to drive both processes. Overall, by numerical investigation this work contributes to the understanding of the plant system along with mathematical modelling strategies to the plant circadian community with the following key findings:

1. Thermal sensitivity of degradation rates is a key factor involved in temperature mechanisms.

2. The combined effect of light and temperature forcing extends the entrainment range of the clock.

3. HSP90 is required for correct temperature entrainment through interaction with the morning loop.

4. The highly inhibiting feature of the transcription plant network, together with autoregulation patterns and three-node feedback loops, favour the robustness of the plant clock to variation in temperature.

Firstly, in Chapter 1, we presented a recent ODE-based model and developed a foundation scheme to incorporate temperature dependence into this model by applying Arrhenius equations on the parameters of translation rates. We started exploring the robustness of the De Caluwé model by analysing the behaviour of the model when the original square wave light forcing is replaced by a *tanh* and a *sin* function to allow more realistic smooth transitions between light and dark phases. We then made this clock model responsive to temperature and examined whether the temperature dependence of translation rates via the Arrhenius law was adequate to entrain the system. Numerical outputs showed that this simple model was able to display circadian periodicity, a stable phase and sustained oscillations in free-running conditions. Additionally, we simulated several time scales for data collection in order to evaluate whether a change in periodicity may be observed as a consequence of the timing of the sampling.

In Chapter 2, we extended the framework given in Chapter 1 by hypothesizing temperature sensitivity on all rates of the model, which characterize transcription, translation, and mRNA and protein degradation processes of the plant system. More importantly, we analysed the combined effect of thermal and photic forcing by varying the hours of exposure to light and warm and dark and cold phases in a 24 h cycle. This chapter provided

novel and helpful insights into what processes may play important roles in temperature entrainment and compensation. We concluded that compensation depends on the way in which each element of the plant clock interacts, and that it is particularly sensitive to temperature-dependent degradation in the context of observed Q_{10} values. Moreover, we presented a theoretical climatic tolerance range, which highlights the need of studying how the clock adapts to changing environmental conditions in an ecological context.

In Chapter 3, motivated by the experimental observations of the Davis Lab (Department of Biology, University of York), we developed a modelling approach to elucidate the role of HSP90 in entrainment. We adapted the De Caluwé model to exhibit *PRR9* and *PRR7* as functionally independent according to those observations and assumed temperature-dependent translation rates changes. From a range of eight possible models, we proposed a clock functional structure where *CCA1/LHY* inhibits *PRR9* and activates *PRR7* and we simulated the effect of Geldanamacyn for both light and thermal entrainment on this clock model. We hypothesised that HSP90 acts in thermal entrainment via the morning loop. Moreover, our model predicted that HSP90 is required for temperature entrainment and not for light entrainment, consistent with the empirical observations of the Davis group. This chapter highlights the importance of interactive work between modelling and experiments to explain the complex clock responses and adds emphasis to the need for future collaborative investigation to reveal the design principles of the *Arabidopsis* circadian clock.

In Chapter 4, we asked whether particular subgraphs that have been argued to carry out specific tasks in biological networks, which could in principle explain the dynamics of biochemical systems, are found in the *Arabidopsis* transcription network, and whether they can be related to functions that would be responsible for the dynamics of the plant clock in response to temperature variation. We performed this analysis by two theoretical approaches: 1) presenting a framework of the historical proposed transcription networks for the plant clock and, 2) proposing three minimal models parameterised by random searches for qualitative insights. We found that no autoregulation loops (neither feedforward nor three-node feedback circuits) can alone explain temperature compensation. However, our results suggested that a transcription network governed by negative interactions together with those structural loops, rather than being considered in isolation, has to be part of the design of a temperature-robust oscillator.

In short, this research provides a range of practical insights which can guide future investigation into how circadian rhythms are altered by temperature forcing, and it emphasises how important it is to study the temporal adjustment of those rhythms in a scenario where both light and temperature forcing are considered simultaneously. Fur-

thermore, it has shed light on the relationship between clock function and transcriptional network clock structure. Although no clear simple causal relationships emerge, these results in general support the need to consider new modelling approaches to better describe plant dynamics in our attempt to understand how this clock assimilates external cues with internal interactions.

With this aim, it may therefore be useful to turn our attention into network analysis of ecological systems in order to profit from the advances developed in that field. For example, in behavioral ecology, analyzing social network activity over time gives valuable information about the causes and consequences of animal sociality [109, 110]. Thus, animal sampling is carried out to collect social data in order to construct an underlying social network. After collecting animal social data, temporal interactions between animals are represented by mainly two types of networks: 1) time-ordered networks, where the duration of the interactions is considered, and 2) time-aggregated networks (a simplification of the time-ordered approach), where a sequence of static networks are analysed [111, 112]. In the construction of these temporal network representations, association indices are used to quantify the strength of the interaction between animals so that define the edges of the social network [113]. This is a classic method designed to correct the inherent bias due to sampling; other statistical approaches to estimate edge weights and their uncertainty involve boostrapping methods and Bayesian inference [114]. It is also worth noting that the emergent outcomes of simulating ecological dynamics on dynamically evolving networks can give new insight into the robustness of systems [115]; the dynamical system may be resilient to change in circumstances were an equivalent static time-averaged network would not.

This network sampling approach can, in principle, be translated to the plant circadian network context. Indeed, we have shown in chapter 2 that the De Caluwe model is in fact a representation of a dynamic plant network governed by two different network structures depending on the phases of light and dark (rather than one static clock structure). Thus, the question that naturally arises is, is it possible to find other underlying structures which potentially could explain the mechanisms of the plant clock to synchronise with the external environment? This could be investigated numerically, for example, by considering the Hill function as a threshold to define a temporal dynamics edge in the 24 h cycle, as this function quantifies the interaction strength between transcription factors and genes. Perhaps the answer of this question might help to characterize the dynamical plasticity mentioned in [116]. This computational approach could also help, for example, to corroborate experimental observations from phase-response-curve assays. Moreover, we have shown in Chapter 2 that the current characterization of the clock model does not allow

the clock to show temperature compensation, and this failure comes from the temperature sensitivity of degradation rates. A theoretical temporal approach could help to elucidate the temperature input pathway driving clock entrainment, and eventually to clarify the time scales governing the relationship between production and degradation of gene products which might explain the temperature compensation mechanism. Additionally, the analysis of Chapter 4 could be expanded in future studies; for example, if we observed a series of time-specific snapshots of this clock, can the clock still be regarded as a dense highly clustered network structure as is typically hypothesised? Finally, a analysis of a series of temporal networks representing the dynamic plasticity of the plant clock might help to deal with other big questions of importance to the plant circadian community; for example, is temperature compensation an emergent property of thermal entrainment?

References

[1] Hotta CT, Gardner MJ, Hubbard KE, Baek SJ, Dalchau N, Suhita D, et al. Modulation of environmental responses of plants by circadian clocks. Plant, Cell & Environment. 2007;30:333–349.

[2] Johnson CH, Elliott JA, Foster R. Entrainment of circadian programs. Chronobiology International. 2003;20:741–774.

[3] Whitelam GC, Millar AJ. 10. In: Light Regulation and Biological Clocks. American Cancer Society; 2018. p. 349–378.

[4] Salomé PA, Weigel D, McClung CR. The role of the Arabidopsis morning loop components CCA1, LHY, PRR7, and PRR9 in temperature compensation. The Plant Cell. 2010;22:3650–61.

[5] Johnson CH, Zhao C, Xu Y, Mori T. Timing the day: what makes bacterial clocks tick? Nature reviews Microbiology. 2017;15:232242.

[6] Cohen SE, Golden SS. Circadian Rhythms in Cyanobacteria. Microbiology and Molecular Biology Reviews. 2015;79:373–385.

[7] Lowrey PL, Takahashi JS. Genetics of Circadian Rhythms in Mammalian Model Organisms. 2011;74:175 – 230.

[8] Hevia MA, Canessa P, Larrondo LF. Circadian clocks and the regulation of virulence in fungi: Getting up to speed. Seminars in Cell & Developmental Biology. 2016;57:147–155.

[9] Bell-Pedersen D, Cassone VM, Earnest DJ, Golden SS, Hardin PE, Thomas TL, et al. Circadian rhythms from multiple oscillators: Lessons from diverse organisms. Nature Reviews Genetics. 2005;6:544–556.

[10] Gerstner JR, Yin JCP. Circadian rhythms and memory formation. Nature Reviews Neuroscience. 2010;11:577–588.

[11] Dodd AN. Plant Circadian Clocks Increase Photosynthesis, Growth, Survival, and Competitive Advantage. Science. 2005;309:630–633.

[12] Schmelling NM, Axmann IM. Computational modelling unravels the precise clockwork of cyanobacteria. Interface Focus. 2018;8.

[13] Podkolodnaya OA, Tverdokhleb NN, Podkolodnyy NL. Computational modeling of the cell-autonomous mammalian circadian oscillator. BMC Systems Biology. 2017;11:27–42.

[14] Fathallah-Shaykh HM, Bona JL, Kadener S. Mathematical model of the Drosophila circadian clock: loop regulation and transcriptional integration. Biophysical journal. 2009;97:2399–408.

[15] Rand DA, Shulgin BV, Salazar D, Millar AJ. Design principles underlying circadian clocks. Journal of The Royal Society Interface. 2004;1:119–130.

[16] Rand DA, Shulgin B, Salazar D, Millar A. Uncovering the design principles of circadian clocks: Mathematical analysis of flexibility and evolutionary goals. Journal of Theoretical Biology. 2006;238:616–35.

[17] Troein C, Locke JCW, Turner MS, Millar AJ. Weather and Seasons Together Demand Complex Biological Clocks. Current Biology. 2009;19:1961 – 1964.

[18] Locke JCW, Millar AJ, Turner MS. Modelling genetic networks with noisy and varied experimental data: the circadian clock in Arabidopsis thaliana. Journal of Theoretical Biology. 2005;234:383 – 393.

[19] Bujdoso N, Davis SJ. Mathematical modeling of an oscillating gene circuit to unravel the circadian clock network of Arabidopsis thaliana. Frontiers in Plant Science. 2013;4:1–8.

[20] Akman OE, Watterson S, Parton A, Binns N, Millar AJ, Ghazal P. Digital clocks: simple Boolean models can quantitatively describe circadian systems. Journal of The Royal Society Interface. 2012;9:2365–2382.

[21] Mombaerts L, Carignano A, Robertson FC, Hearn TJ, Junyang J, Hayden D, et al. Dynamical differential expression (DyDE) reveals the period control mechanisms of the Arabidopsis circadian oscillator. PLOS Computational Biology. 2019;15:1–26.

[22] Herrero E, Kolmos E, Bujdoso N, Yuan Y, Wang M, Berns MC, et al. EARLY FLOWERING4 recruitment of EARLY FLOWERING3 in the nucleus sustains the Arabidopsis circadian clock. The Plant cell. 2012;24:428–43.

[23] Dalchau N. Understanding biological timing using mechanistic and black-box models. New Phytologist. 2012;193:852–858.

[24] De Caluwé J, Xiao Q, Hermans C, Verbruggen N, Leloup JC, Gonze D. A Compact Model for the Complex Plant Circadian Clock. Frontiers in Plant Science. 2016;7:1–15.

[25] Ohara T, Hearn TJ, Webb AAR, Satake A. Gene regulatory network models in response to sugars in the plant circadian system. Journal of Theoretical Biology. 2018;457:137–151.

[26] Avello PA, Davis SJ, Ronald J, Pitchford JW. Heat the Clock: Entrainment and Compensation in Arabidopsis Circadian Rhythms. Journal of Circadian Rhythms. 2019;17:5.

[27] Tokuda IT, Akman OE, Locke JCW. Reducing the complexity of mathematical models for the plant circadian clock by distributed delays. Journal of Theoretical Biology. 2019;463:155 – 166.

[28] Ignasius Joanito SHW Jhih-Wei Chu, Hsu CP. An incoherent feed-forward loop switches the Arabidopsis clock rapidly between two hysteretic states. Scientific Reports;8(13944).

[29] Minas G, Rand DA. Long-time analytic approximation of large stochastic oscillators: Simulation, analysis and inference. PLOS Computational Biology. 2017;13:1–23.

[30] Ruoff P, Zakhartsev M, Westerhoff HV. Temperature compensation through systems biology. FEBS Journal. 2007;274:940–950.

[31] Ruoff P, Vinsjevik M, Rensing L. Temperature compensation in biological oscillators: a challenge for joint experimental and theoretical analysis. Comments Theor Biol. 2000;5:361–382.

[32] Akman OE, Locke JCW, Tang S, Carré I, Millar AJ, Rand DA. Isoform switching facilitates period control in the Neurospora crassa circadian clock. Molecular Systems Biology. 2008;4:164.

[33] Gould PD, Ugarte N, Domijan M, Costa M, Foreman J, MacGregor D, et al. Network balance via CRY signalling controls the Arabidopsis circadian clock over ambient temperatures. Molecular Systems Biology. 2013;9:650.

[34] Roenneberg T, Merrow M. The Circadian Clock and Human Health. Current Biology. 2016;26:R432 – R443.

[35] Seo PJ, Mas P. STRESSing the role of the plant circadian clock. Trends in Plant Science. 2015;20:230 – 237.

[36] Covington MF, Maloof JN, Straume M, Kay SA, Harmer SL. Global transcriptome analysis reveals circadian regulation of key pathways in plant growth and development. Genome Biology. 2008;9:R130.

[37] Fonseca Costa SS, Ripperger JA. Impact of the Circadian Clock on the Aging Process. Frontiers in Neurology. 2015;6:43.

[38] Bonney S, Hughes K, Harter PN, Mittelbronn M, Walker L, Eckle T. Cardiac Period 2 in myocardial ischemia: Clinical implications of a light dependent protein. The International Journal of Biochemistry & Cell Biology. 2013;45:667 – 671.

[39] Alabadi D. Reciprocal Regulation Between TOC1 and LHY/CCA1 Within the Arabidopsis Circadian Clock. Science. 2001;293:880–883.

[40] Locke JCW, Kozma-Bognár L, Gould PD, Fehér B, Kevei É, Nagy F, et al. Experimental validation of a predicted feedback loop in the multi-oscillator clock of Arabidopsis thaliana. Molecular Systems Biology. 2006;2:59.

[41] Pokhilko A, Fernández AP, Edwards KD, Southern MM, Halliday KJ, Millar AJ. The clock gene circuit in Arabidopsis includes a repressilator with additional feedback loops. Molecular Systems Biology. 2012;8:574.

[42] Fogelmark K, Troein C. Rethinking Transcriptional Activation in the Arabidopsis Circadian Clock. PLoS Computational Biology. 2014;10:e1003705.

[43] Gil KE, Park CM. Thermal adaptation and plasticity of the plant circadian clock. New Phytologist. 2019;221:1215–1229.

[44] Somers DE, Webb AA, Pearson M, Kay SA. The short-period mutant, toc1-1, alters circadian clock regulation of multiple outputs throughout development in Arabidopsis thaliana. 1998;125:485–494.

[45] Ruoff P. Introducing temperature-compensation in any reaction kinetic oscillator model. Journal of Interdisiplinary Cycle Research. 1992;23:92–99.

[46] Leloup JC, Goldbeter A. Temperature Compensation of Circadian Rhythms: Control of the Period in a Model for Circadian Oscillations of the Per Protein in Drosophila. Chronobiology International. 1997;14:511–520.

[47] Nagao R, Epstein IR, Gonzalez ER, Varela H. Temperature (over)compensation in an oscillatory surface reaction. Journal of Physical Chemistry A. 2008;112:4617–4624.

[48] Ruoff P, Loros JJ, Dunlap JC. The relationship between FRQ-protein stability and temperature compensation in the Neurospora circadian clock. Proceedings of the National Academy of Sciences of the United States of America. 2005;102:17681–17686.

[49] Heiland I, Bodenstein C, Hinze T, Weisheit O, Ebenhoeh O, Mittag M, et al. Modeling temperature entrainment of circadian clocks using the Arrhenius equation and a reconstructed model from Chlamydomonas reinhardtii. Journal of Biological Physics. 2012;38:449–464.

[50] Kidd PB, Young MW, Siggia ED. Temperature compensation and temperature sensation in the circadian clock. Proceedings of the National Academy of Sciences of the United States of America. 2015;112:E6284–E6292.

[51] Hastings JW, Sweeney BM. On the Mechanism of Temperature Independence in a Biological Clock. Proceedings of the National Academy of Sciences of the United States of America. 1957;43:804–811.

[52] Ruoff P, Rensing L. The temperature-compensated Goodwin model simulates many circadian clock properties. Journal of Theoretical Biology. 1996;179:275–285.

[53] Goodwin BC. Oscillatory behavior in enzymatic control processes. Advances in Enzyme Regulation. 1965;3:425 – 437.

[54] Pokhilko A, Hodge SK, Stratford K, Knox K, Edwards KD, Thomson AW, et al. Data assimilation constrains new connections and components in a complex, eukaryotic circadian clock model. Molecular Systems Biology. 2010;6:416.

[55] Caluwé JD, de Melo JRF, Tosenberger A, Hermans C, Verbruggen N, Leloup JC, et al. Modeling the photoperiodic entrainment of the plant circadian clock. Journal of Theoretical Biology. 2017;420:220 – 231.

[56] Sidaway-Lee K, Costa MJ, Rand DA, Finkenstadt B, Penfield S. Direct measurement of transcription rates reveals multiple mechanisms for configuration of the Arabidopsis ambient temperature response. Genome Biology. 2014;15:R45.

[57] Dodd AN, Belbin FE, Frank A, Webb AAR. Interactions between circadian clocks and photosynthesis for the temporal and spatial coordination of metabolism. Frontiers in Plant Science. 2015;6:245.

[58] Grundy J, Stoker C, Carré IA. Circadian regulation of abiotic stress tolerance in plants. Frontiers in Plant Science. 2015;6:1–15.

[59] Yazdanbakhsh N, Sulpice R, Graf A, Stitt M, Fisahn J. Circadian control of root elongation and C partitioning in Arabidopsis thaliana. Plant, Cell and Environment. 2011;34:877–894.

[60] Green RM, Tingay S, Wang ZY, Tobin EM. Circadian rhythms confer a higher level of fitness to Arabidopsis plants. Plant physiology. 2002;129:576–584.

[61] Davis SJ, Millar aJ. Watching the hands of the Arabidopsis biological clock. Genome biology. 2001;2:1008.1–1008.4.

[62] Turek FW, Joshu C, Kohsaka A, Lin E, Ivanova G, Mcdearmon E, et al. Obesity and Metabolic Syndrome in Circadian Clock Mutant Mice. Science. 2005;308:1043–1045.

[63] Bell-Pedersen D, Shinohara ML, Loros JJ, Dunlap JC. Circadian clock-controlled genes isolated from Neurospora crassa are late night- to early morning-specific. Proceedings of the National Academy of Sciences. 1996;93:13096–13101.

[64] Guo F, Yu J, Jung HJ, Abruzzi KC, Luo W, Griffith LC, et al. Circadian neuron feedback controls the Drosophila sleep-activity profile. Nature. 2016;536:292–297.

[65] Welkie DG, Rubin BE, Chang YG, Diamond S, Rifkin SA, LiWang A, et al. Genome-wide fitness assessment during diurnal growth reveals an expanded role of the cyanobacterial circadian clock protein KaiA. Proceedings of the National Academy of Sciences of the United States of America. 2018;115:E7174–E7183.

[66] Pokhilko A, Mas P, Millar AJ. Modelling the widespread effects of TOC1 signalling on the plant circadian clock and its outputs. BMC Systems Biology. 2013;7:23.

[67] Rust MJ, Markson JS, Lane WS, Fisher DS, O'Shea EK. Ordered phosphorylation governs oscillation of a three-protein circadian clock. Science (New York, NY). 2007;318:809–12.

[68] Kurosawa G, Aihara K, Iwasa Y. A Model for the Circadian Rhythm of Cyanobacteria that Maintains Oscillation without Gene Expression. Biophysical Journal. 2006;91:2015–2023.

[69] Lerner I, Bartok O, Wolfson V, Menet JS, Weissbein U, Afik S, et al. Clk post-transcriptional control denoises circadian transcription both temporally and spatially. Nature Communications. 2015;6:7056.

[70] Bellman J, Kim JK, Lim S, Hong CI. Modeling Reveals a Key Mechanism for Light-Dependent Phase Shifts of Neurospora Circadian Rhythms. Biophysical Journal. 2018;115:1093–1102.

[71] Crosthwaite SK, Loros JJ, Dunlap JC. Light-Induced Resetting of a Circadian Clock Is Mediated by a Rapid Increase in frequency Transcript. Cell. 1995;81:1003–1012.

[72] Reló Gio A, Westermark PO, Wallach T, Schellenberg K, Kramer A. Tuning the Mammalian Circadian Clock: Robust Synergy of Two Loops. PLoS Comput Biol. 2011;7:e1002309.

[73] Geier F, Becker-Weimann S, Kramer A, Herzel H. Entrainment in a Model of the Mammalian Circadian Oscillator. J Biol Rhythms. 2005;20:83–93.

[74] Hogenesch JB, Ueda HR. Understanding systems-level properties: Timely stories from the study of clocks. Nature Reviews Genetics. 2011;12:407–416.

[75] Kolmos E, Nowak M, Werner M, Fischer K, Schwarz G, Mathews S, et al. Integrating ELF4 into the circadian system through combined structural and functional studies. HFSP journal. 2009;3:350–66.

[76] Zeilinger MN, Farré EM, Taylor SR, Kay SA, Doyle FJ. A novel computational model of the circadian clock in Arabidopsis that incorporates PRR7 and PRR9. Molecular Systems Biology. 2006;2:58.

[77] Locke JCW, Southern MM, Kozma-Bognár L, Hibberd V, Brown PE, Turner MS, et al. Extension of a genetic network model by iterative experimentation and mathematical analysis. Molecular Systems Biology. 2005;1:0013.

[78] Shin J, Davis SJ. Recent advances in computational modeling as a conduit to understand the plant circadian clock. F1000 biology reports. 2010;2:5–8.

[79] Harmer SL. The Circadian System in Higher Plants. Annual Review of Plant Biology. 2009;60:357–377.

[80] Millar AJ. The Intracellular Dynamics of Circadian Clocks Reach for the Light of Ecology and Evolution. Annual Review of Plant Biology. 2016;67:595–618.

[81] Hsu PY, Harmer SL. Wheels within wheels: The plant circadian system. Trends in Plant Science. 2014;19:240–249.

[82] Gould PD, Locke JCW, Larue C, Southern MM, Davis SJ, Hanano S, et al. The molecular basis of temperature compensation in the Arabidopsis circadian clock. The Plant Cell. 2006;18:1177–1187.

[83] Edwards K, Anderson P, Hall A, Salathia N, Locke J, Lynn J, et al. FLOWERING LOCUS C Mediates Natural Variation in the High-Temperature Response of the Arabidopsis Circadian Clock. The Plant cell. 2006;18:639–650.

[84] Jones MA, Morohashi K, Grotewold E, Harmer SL. Arabidopsis JMJD5/JMJ30 Acts Independently of LUX ARRHYTHMO Within the Plant Circadian Clock to Enable Temperature Compensation. Frontiers in Plant Science. 2019;10:57.

[85] Wigge PA. Ambient temperature signalling in plants. Current Opinion in Plant Biology. 2013;16:661–666.

[86] Kolmos E, Herrero E, Bujdoso N, Millar AJ, Tóth R, Gyula P, et al. A Reduced-Function Allele Reveals That EARLY FLOWERING3 Repressive Action on the Circadian Clock Is Modulated by Phytochrome Signals in Arabidopsis. The Plant Cell. 2011;23:3230–3246.

[87] Blair EJ, Bonnot T, Hummel M, Hay E, Marzolino JM, Quijada IA, et al. Contribution of time of day and the circadian clock to the heat stress responsive transcriptome in Arabidopsis. Scientific Reports. 2019;9:4814.

[88] Ripel L, Wendell M, Rognli OA, Torre S, Lee Y, Olsen JE. Thermoperiodic Control of Floral Induction Involves Modulation of the Diurnal FLOWERING LOCUS T Expression Pattern. Plant and Cell Physiology. 2017;58:466–477.

[89] Bours R, van Zanten M, Pierik R, Bouwmeester H, van der Krol A. Antiphase Light and Temperature Cycles Affect PHYTOCHROME B-Controlled Ethylene Sensitivity and Biosynthesis, Limiting Leaf Movement and Growth of Arabidopsis. 2013;163:882–895.

[90] Davis AM, Ronald J, Ma Z, Wilkinson AJ, Philippou K, Shindo T, et al. HSP90 Contributes to Entrainment of the Arabidopsis Circadian Clock via the Morning Loop. Genetics. 2018;210:1383–1390.

[91] Boikoglou E, Ma Z, von Korff M, Davis AM, Nagy F, Davis SJ. Environmental Memory from a Circadian Oscillator: The Arabidopsis thaliana Clock Differentially Integrates Perception of Photic vs. Thermal Entrainment. 2011;189:655–664.

[92] Salomé PA, McClung CR, Salome PA, McClung CR. PSEUDO-RESPONSE REGULATOR 7 and 9 are partially redundant genes essential for the temperature responsiveness of the Arabidopsis circadian clock. The Plant Cell. 2005;17:791–803.

[93] Salomé PA, McClung CR. What makes the Arabidopsis clock tick on time? A review on entrainment. Plant, Cell & Environment;28:21–38.

[94] Schopf FH, Biebl MM, Buchner J. The HSP90 chaperone machinery. Nature Reviews Molecular Cell Biology. 2017;18:345–360.

[95] Cha JY, Kim J, Kim TS, Zeng Q, Wang L, Lee SY, et al. GIGANTEA is a co-chaperone which facilitates maturation of ZEITLUPE in the Arabidopsis circadian clock. Nature Communications. 2017;8:3.

[96] Gil KE, Kim WY, Lee HJ, Faisal M, Saquib Q, Alatar AA, et al. ZEITLUPE Contributes to a Thermoresponsive Protein Quality Control System in Arabidopsis. The Plant Cell. 2017;29:2882–2894.

[97] Thomas R. On the Relation Between the Logical Structure of Systems and Their Ability to Generate Multiple Steady States or Sustained Oscillations. Springer, Berlin, Heidelberg. 1981;9.

[98] Snoussi EH. Necessary Conditions for Multistationarity and Stable Periodicity. Journal of Biological Systems. 1998;06:3–9.

[99] Gouzé JL. Positive and Negative Circuits in Dynamical Systems. Journal of Biological Systems. 1998;06:11–15.

[100] Kwon YK, Cho KH. Boolean Dynamics of Biological Networks with Multiple Coupled Feedback Loops. Biophysical Journal. 2007;92:2975 – 2981.

[101] Sontag E, Veliz-Cuba A, Laubenbacher R, Jarrah AS. The Effect of Negative Feedback Loops on the Dynamics of Boolean Networks. Biophysical Journal. 2008;95:518 – 526.

[102] Kamioka M, Takao S, Suzuki T, Taki K, Higashiyama T, Kinoshita T, et al. Direct Repression of Evening Genes by CIRCADIAN CLOCK-ASSOCIATED1 in the Arabidopsis Circadian Clock. The Plant Cell. 2016;28:696–711.

[103] Adams S, Manfield I, Stockley P, Carré IA. Revised Morning Loops of the Arabidopsis Circadian Clock Based on Analyses of Direct Regulatory Interactions. PLOS ONE. 2015;10:1–11.

[104] Novák B, Tyson JJ. Design principles of biochemical oscillators. Nature Reviews Molecular Cell Biology. 2008;9:981 – 991.

[105] Tsai TYC, Choi YS, Ma W, Pomerening JR, Tang C, Ferrell JE. Robust, Tunable Biological Oscillations from Interlinked Positive and Negative Feedback Loops. Science. 2008;321:126–129.

[106] Alon U. Network motifs: Theory and experimental approaches. Nature Reviews Genetics. 2007;8:450–461.

[107] Mangan S, Alon U. Structure and function of the feed-forward loop network motif. Proceedings of the National Academy of Sciences of the United States of America. 2003;100:11980–11985.

[108] Alon U. An Introduction to Systems Biology: Design Principles of Biological Circuits. Taylor & Francis; 2006.

[109] Farine DR, Whitehead H. Constructing, conducting and interpreting animal social network analysis. Journal of Animal Ecology. 2015;84:1144–1163.

[110] Pinter-Wollman N, Hobson EA, Smith JE, Edelman AJ, Shizuka D, de Silva S, et al. The dynamics of animal social networks: analytical, conceptual, and theoretical advances. Behavioral Ecology. 2013;25:242–255.

[111] Blonder B, Wey TW, Dornhaus A, James R, Sih A. Temporal dynamics and network analysis. Methods in Ecology and Evolution. 2012;3:958–972.

[112] Blonder B, Dornhaus A. Time-Ordered Networks Reveal Limitations to Information Flow in Ant Colonies. PLOS ONE. 2011;6:1–8.

[113] Cairns SJ, Schwager SJ. A comparison of association indices. Animal Behaviour. 1987;35:1454 – 1469.

[114] Farine DR, Strandburg-Peshkin A. Estimating uncertainty and reliability of social network data using Bayesian inference. Royal Society Open Science. 2015;2:150367.

[115] Burns D, Pitchford JW, Parr CL, Franks DW, Robinson EJH. The costs and benefits of decentralization and centralization of ant colonies. Behavioral Ecology. 2019;30:1700–1706.

[116] Webb AAR, Seki M, Satake A, Caldana C. Continuous dynamic adjustment of the plant circadian oscillator. Nature Communications. 2019;10:550.